DECISION-MAKING UNDER THE UNCERTAINTY OF ELECTRICITY MARKET FOR SCHEDULING AND PLANNING

Sachin Gangwar

UNIVERSITAT ROVIRA i VIRGILI

Decision-making under the uncertainty of electricity market for scheduling and planning

Sachin Gangwar

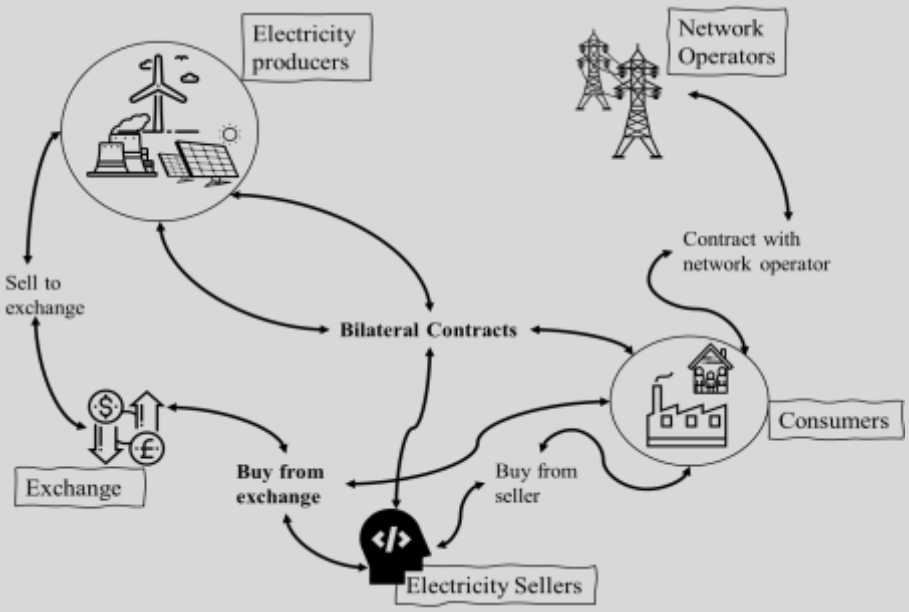

DOCTORAL THESIS
2023

Sachin Gangwar

Decision making under the uncertainty of electricity market for scheduling and planning

Doctoral Thesis

Supervised by

Dr Thomas Dieter Boer

Dr. Laureano Jiménez Esteller

Dr. Carlos Pozo Fernández

Departament d'Enginyeria Mecànica

Departament d'Enginyeria Química

Tarragona

2023

Universitat Rovira i Virgili
Department of Chemical Engineering
Av. Països Catalans, 26
43007 Tarragona, Spain
Phone +34 977 55 80 21

We STATE that the present study, entitled "Decision-making under the uncertainty of electricity market for scheduling and planning", presented by Sachin Gangwar for the award of the degree of Doctor, has been carried out under our supervision at the Chemical Engineering Department of the University Rovira i Virgili.

Tarragona, 3rd May 2023.

Laureano Jiménez Esteller
Firmado digitalmente por Laureano Jiménez Esteller
Fecha: 2023.05.03 15:25:17 +02'00'

Dr. Laureano Jiménez Esteller

BOER DIETER THOMAS - X1992293X
Digitally signed by BOER DIETER THOMAS - X1992293X
Date: 2023.05.03 17:35:23 +02'00'

Dr. Dieter Thomas Boer

Firmado por POZO FERNANDEZ CARLOS - ***1486** el día 03/05/2023 con un

Dr. Carlos Pozo Fernández

Summary

The process of decision making is the most important aspect of human evolution on Earth. From the *homo sapiens* to *Neanderthals* to *homo erectus*, all used decision making to reach the point we are now. We all employ this process consciously or subconsciously in our daily life. Our decision-making process is supported by our past experience and information. If the upcoming problem is similar to what was faced in the past, we can make a decision with utmost certainty to plan our future action based on our experience and proven method to tackle the problem. If the upcoming problem is novel and has not been dealt in past, we roll back to our decision-making process where we analyze the variables at hand and find a statistically efficient solution to plan our future actions in order to tackle the unforeseen problem. This statistically efficient solution comes with a risk and reward situation. Therefore, there is uncertainty about reaching the goal provided by the statistically efficient solution but depending upon the problem at hand the nature of uncertainty is changed and, hence, changes the approach to deal with the uncertainty. If we can identify the nature of the uncertainty and measure or limit the uncertainty to incorporate it in our decision-making process, we can improve our chances of reaching the estimated goal even under uncertain events.

In the era of technology, use of electricity is imperative and thus electricity market has a huge impact on our daily lives both directly and indirectly. The deregulated electricity market is highly unpredictable due to the nature of its participants (consumer, producers and prosumers). While domestic electricity consumption is highly subjective, industrial energy consumption has been

categorized ("Energy Use in Industry - Energy Explained, Your Guide To Understanding Energy - Energy Information Administration," n.d.) and is declared as the largest energy consumer with one-third of global energy demand. Therefore, large energy intensive industries are hit by the uncertainty of electricity market. Thus, the need of scheduling and planning of energy intensive industries is well emphasized (Merkert et al., 2015).

Energy efficiency in the residential building sector is another area which is emphasized by the United Nations under the 17 sustainable goals. To achieve this, long term planning of net zero energy buildings has been the focus of research (Li and Nord, 2018). Planning of future net zero energy buildings involves inclusion of renewable energy technologies, smart energy networks (district heating and electricity grid), energy policies and many other initiatives. Inclusion of multiple decision variables in the long-term planning brings a lot of uncertainty. In this line decision making under uncertainty brings alternative solutions to increase the economic and environmental benefits.

The contributions that are derived from this thesis are the proposed methodologies to facilitate decision making for the long- and short-term planning to achieve economic and environmental efficiency. These methodologies required the development of quantitative tools using mathematical modelling which are generic and can be utilized for similar problems in their respective field.

Contents

Chapter 2.

Discrete scenarios, and risk analysis

2. Discrete scenarios, and risk analysis

Scheduling optimization and risk analysis for energy-intensive industries under uncertain electricity market to facilitate financial planning

*Sachin Gangwar[1], David Fernández[2], Carlos Pozo[3], Rubén Folgado[2], Laureano Jiménez[3], Dieter Boer[1, *]*

[1] Departament d'Enginyeria Mecànica, Universitat Rovira i Virgili, Av. Països Catalans 26, 43007 Tarragona, Spain, Phone: 34-97-7559631, e-mail: dieter.boer@urv.cat

[2] Messer Ibérica de Gases S.A.U, Autovía Tarragona-Salou, km. 3.8, 43480 Vilaseca, Tarragona, Spain

[3] Departament d'Enginyeria Química, Universitat Rovira i Virgili, Av. Països Catalans 26, 43007 Tarragona, Spain

Keywords. Uncertainty; optimization; scheduling; spot market forecast; risk analysis, energy-intensive industry

2.1 Introduction

The industrial sector requires a considerable amount of energy to manufacture ready-to-use products. Indeed, for energy-intensive industries (EIIs), the cost of electricity is the major factor in the operational costs and product pricing. EIIs represent an important share of the industrial sector (U.S. Energy Information Administration, 2016), with a direct impact on our daily life (e.g., chemical, refining, cement or mining). Among EIIs, the bulk chemical is the largest industry, representing over 27% of the energy consumption in the whole industrial sector ("Energy Use in Industry - Energy Explained, Your Guide To Understanding Energy - Energy Information Administration," n.d.).

One of the bulk chemical industries whose profit is greatly affected by the electricity prices is the air separation sector. Cryogenic air separation is the state-of-the-art technology for obtaining purified industrial gases (e.g., liquid oxygen, liquid nitrogen, and liquid argon) at large scale (Smith and Klosek, 2001). In these processes, electricity constitutes 31% of the total cost, evidencing the significance to obtain low-cost electricity (Ierapetritou et al., 2002).

Electricity prices are dictated by the regional/national electricity market, which is partly deregulated in most parts of the world. In deregulated markets, electricity is traded as a commodity for future and spot electricity consumption (Scharfhausen, 2009).

In the context of cryogenic air separation, some authors (Fernández et al., 2017) have optimized plant operations deterministically using their experience to

predict future electricity prices and maximizing the expected profit. A similar approach has also been used for a variety of process industries such as cement production (Mitra et al., 2012), paper and pulp industry or metallurgy (Associates, 2005, Todd et al., 2009). Most works follow a deterministic approach (Sahinidis, 2004, Grossmann et al., 1999, Misra et al., 2017, Ierapetritou et al., 2002) and only to a limited extent include uncertainty (Charitopoulos and Dua, 2017, Finn and Fitzpatrick, 2014).

Due to the inherent fluctuations in electricity prices, all energy intensive plants operate under uncertainty and are susceptible to financial risks in practice. Uncertainties can be mainly due to exogenous and endogenous factors (Castro et al., 2018). For instance, the uncertainty generated from the electricity price fluctuation is an exogenous uncertainty, while uncertainty generated within the operation due to wear and tear of apparatus or intrinsic nature of the process/apparatus affecting the expected output presents endogenous uncertainty.

An inappropriate production scheduling can lead to financial depreciation with a negative effect on product pricing. Such negative effects can be counterbalanced to some extent by resorting to mathematical modelling and programming (Gebreslassie et al., 2009) considering uncertainty aspects. There are several approaches to incorporate different types of uncertainties into mathematical models: two-stage stochastic programming (Weskamp et al., 2019, Chen et al., 2020, Li et al., 2021a), parametric programming (Oberdieck et al., 2016), fuzzy programming (Wang et al., 2020), chance constraint programming (Wu et al., 2015),

robust optimization techniques (Cao et al., 2020), and conditional value-at-risk (Rezaei et al., 2020) are some of the most used frameworks. Dynamic Response scheduling technique is another method which has been recently used in many case studies (Kelley et al., 2018, Kelley et al., 2020, Kelley et al., 2022) related to ASU and chemical plants. Cao et al (2015) applied a framework in which they addressed the plant design limitation by optimizing the system performance under the electricity price fluctuation and demand uncertainty and concluded that the best achievable optimal solution is subjected to plant constraints. Building on the DR framework Cao et al (2016) also addressed the problem of storage and excess production during the low peak hours of electricity pricing. In a similar approach Dias et al (2018) focused on the model predictive control method to accommodate the scheduling changes based on DR feedback. A simulation-optimization methodology was used to predict the scheduling operation and a closed loop feedback tracking system was used later to integrate the required changes in previously optimized scheduling. Their methodology could not provide optimal solutions for discrete changes in the scheduling problem.

A detailed review of planning and scheduling under uncertainty for several sectors can be found in Verderame et al. (2010). All the above methodologies use random function to incorporate uncertainty. This typically provides an acceptable approximation for the real uncertainty, yet it fails to capture the temporal trend (i.e., rise *vs* decline) of electricity prices. On the other hand, and regardless of the approach followed, the inclusion of uncertainty in the problem formulation increases the model complexity and the computational effort required to solve it. For stochastic problems,

in the area of planning and scheduling operations, the rolling horizon approach has been used to deal with this complexity (Mitra et al., 2012, Merkert et al., 2015, Zamarripa et al., 2016, Zhang et al., 2018). Analogously, Pattinson *et al* (2017) used a moving horizon optimal scheduling approach for the scheduling of ASU with multiple assumptions of economic data forecasts and processes. They proposed multiple scheduling calculations over the scheduling time horizon and proposed changing the schedule if deemed necessary for optimal operation. In rolling horizon and moving horizon approach, the production targets and other internal variables change continuously after each rescheduling e.g. in rolling/moving horizon approach the horizon (Total time 'T') remains the same and this time 'T' (e.g. T = 7 days) is divided into 7 discrete time blocks i.e. t1, t2, …, t7 each representing one day. Now, at 't1', the forecasting and scheduling is done for total time 'T'. Then, at the end of day 1 i.e. 't1', the forecasting of the electricity prices performed again but this time the unknown variables corresponding to 't1' are known and are treated at as system constraints while the forecasting and scheduling is repeated again for the remaining period (T - t1). This process is repeated till the end of time horizon is met. Many process industries require short term scheduling (i.e., time horizons from 3 days to one week) and conventional approaches are not practically feasible due to the associated large computational time (Acevedot and Pistikopoulos, 1998). Hence, for complex problems where fluctuations of uncertain parameters can change on a daily to hourly basis, there is a need to adopt an approach trading-off the comprehensive analysis of all possible scenarios and the computational effort required to address it.

To that end, here, we develop a methodology to provide with optimized scheduling plan under electricity price uncertainty, for the given product demand and respective production period, to maximize the profit. Namely, we propose a tool combining mathematical modelling, time-series prediction, Monte-Carlo simulation and risk metrices, to facilitate the decision-making process for the management. The developed tool can handle the multi-period model simulation and the complexity involved in the prediction of electricity prices, with computational efforts that allow providing a timely response to varying electricity prices. The prediction accuracy of the model is found to be as high as 95%. The tool also presents a set of discrete electricity price scenarios for planning and scheduling strategies with estimated profit and associated risk. The applied methodology would reduce the over/under-estimation of the profit, intrinsic to any deterministic approach, while providing more realistic estimations.

As a test bed, we have demonstrated this methodology in an existing cryogenic air separation facility situated in Catalonia (Spain), where we maximize the profit under the volatility of electricity prices. Despite this, the methodology is general enough to be valid for any other energy-intensive sector. With this methodology, complex problems for short-term scheduling (e.g., 1 week for a 24×7 process industry) under uncertain electricity prices can be solved with little computational and programming effort allowing for a rapid response to changes in electricity prices. In this methodology we studied 100 different electricity price scenarios to assess the impact of uncertainty associated with electricity market and electricity price forecasting. We obtained a set of profit values for these scenarios which were then

used to perform risk analysis in a similar manner as portfolio optimization in financial markets.

2.2 Problem statement

Energy intensive industries (EIIs) have a common functional framework as shown in figure 1. All EIIs are subjected to electricity price uncertainty and the demand uncertainty in general. The introduction of the uncertainty presents a planning dilemma for the management of these industries. The uncertainty of electricity prices is common to the EIIs while demand uncertainty can be managed by proper order book in most cases. Thus, the main uncertainty common to all EIIs is electricity price which affects the optimal planning. We are attempting to address this planning (scheduling and financial) problem through our methodology with real time data of an existing EII in the Tarragona region of Spain as a test bed.

We are given the technical data of a cryogenic ASU (Air Separation Unit) located in the petrochemical complex of Tarragona (Spain). The plant (2,adapted from Fernández et al. (2017)) includes a pre-treatment unit (PTU), where impurities are removed from the atmospheric air input. After the PTU, the filtered air goes to the distillation column unit (DCU) where the air is split, under cryogenic conditions, into N_2, O_2, and Ar. Then, each component is either sent to their respective compressor (CUs) and to the customers via pipeline or, alternatively, liquefied and stored in tanks T1 – T4. Further details on the plant's topology and operation are provided elsewhere (Fernández et al., 2017).

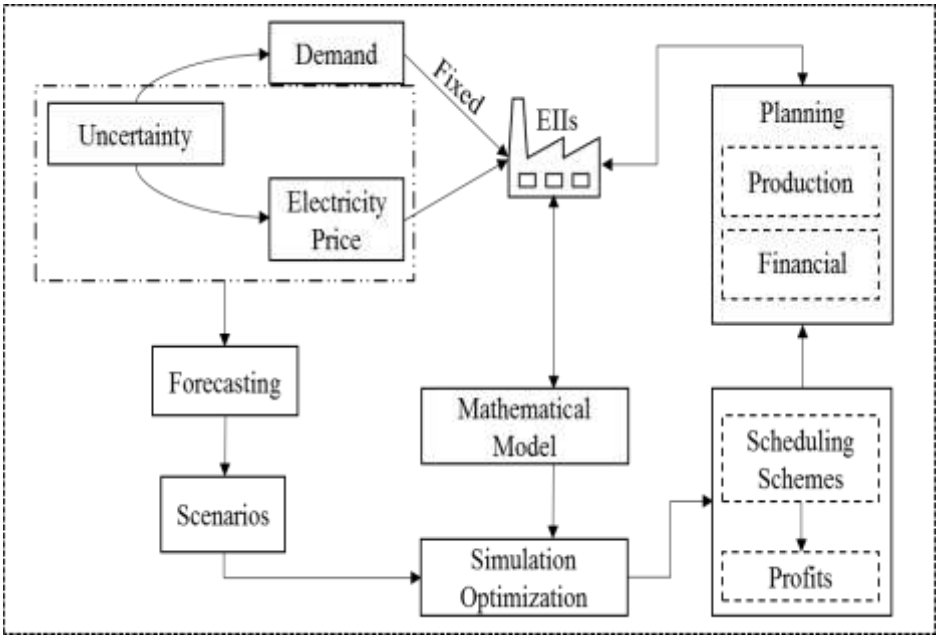

Figure 2.1. Framework to facilitate financial planning of EIIs under uncertainty.

Fernández et al.(2017) optimized the plant operation deterministically using single scenario forecast approach leaving it susceptible to suffer from the financial risks associated with the uncertain electricity price market. In this contribution, we also assume that liquid and gas demands are deterministic as they are known by the sales department one week in advance, whereas unexpected orders entailing large gas consumptions (i.e., deviating from average consumption or contracts) must be notified by the customers with sufficient anticipation.

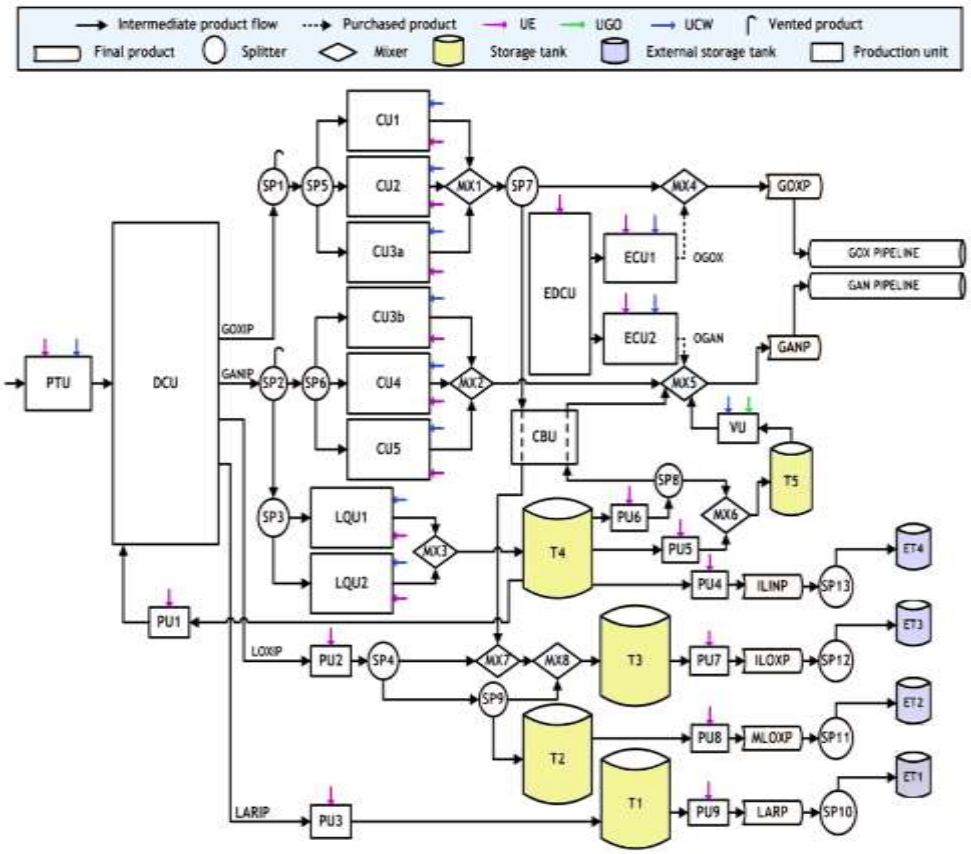

Figure 2.2. Process network configuration of the air separation unit adapted from Fernández *et.al.*(Fernández et al., 2017), PTU: pretreatment unit; DCU: distillation column unit; PU_i: pump units;, SP_i: splitter; CU_i: compressor units; MX_i: mixer units; T_i: tanks; LQU_i: liquefier; CBU: conversion unit; EDCU: external distillation column unit; ET_i: external tanks; VU: vaporizer unit. LOX: liquid Oxygen; GOX: gaseous Oxygen; LAN; liquid Nitrogen; GAN: gaseous Nitrogen; LAR: liquid Argon.

We are also given the price and the amount of electricity that has been bought from the futures market for (typically covering around 60% of the requirements). The remaining electricity (~40%) must be bought from the spot market, for which we

consider the hourly variability of electricity prices and which represents the uncertainty source in this work. The aim is to develop a methodology that first predicts electricity prices in the spot market with accuracy and then optimizes the complex uncertainty scheduling problem in relatively low computational time, otherwise the solution will not be ready before the decision-makers need to make their decisions. To address this issue, we perform optimization for scheduling of the plant under electricity price uncertainty. Optimized scheduling plan for upcoming (next week's) production cycle provides us with speculated profit by calculating the expected incurring production cost and total sale (calculated by the preplaced orders). Then we calculate the associated risk of a shortfall for the optimized scheduling plan.

In this context, the objective is to determine the optimal operation of the plant (e.g., startup and shutdown times for process units, mass flow rates, product purchases from external manufacturers, etc.) under electricity price uncertainty that maximizes the expected profit while simultaneously provides a quantitative measure of the risk associated with this operation. To achieve this objective, we have also added the flexibility of selling the excess electricity back to the grid, provided by the market maker, in case we have surplus of contracted electricity for the contracted period (day, weekdays or weekend for Spanish electricity market) based on scheduling of plant.

2.3 Methodology

We have developed a hybrid two-step approach, as shown in figure 2.3. First, we use Monte-Carlo scenario generator (MCSG) for generating future electricity

prices scenarios. MCSG uses ARIMA (Auto regressive integrated moving averages) to forecast the electricity prices and then it generates plausible scenarios for future electricity prices. In the second step, we introduce electricity price uncertainty by feeding the modified model for the ASU facility (Fernández et al., 2017) with the generated scenarios to calculate the potential outputs for each of the plausible forecasted electricity price scenarios independently. To some extent, even the most efficient forecasting models have prediction errors that can propagate through the model and lead to over or underestimation of the different variables, including the objective function. Therefore, with the aim of minimizing the risk of adopting an economically inefficient scheduling plan, we perform risk analysis for the obtained profit values to analyze the risk of deviating from the obtained profit values in each scenario. Thus, we have considered each scenario as a separate optimization problem and have used MILP to solve it. These steps are described in detail in the ensuing subsections.

2.3.1 Scheduling time horizon

The scheduling period (also known as time horizon) of a 24×7 operational plant is of utmost importance in scheduling problems. The production under the scheduling time horizon must match the customers' demand, and the operation and implementation aspects of the plant. Hence, as per the need in our case, we analyzed hourly electricity price data for a period of one year to find a suitable time horizon for prediction and plant scheduling. To this end, we plot hourly electricity price data

retrieved from Spanish electricity market operator OMIE for the year 2017 (figures 2.4 & A.3.1).

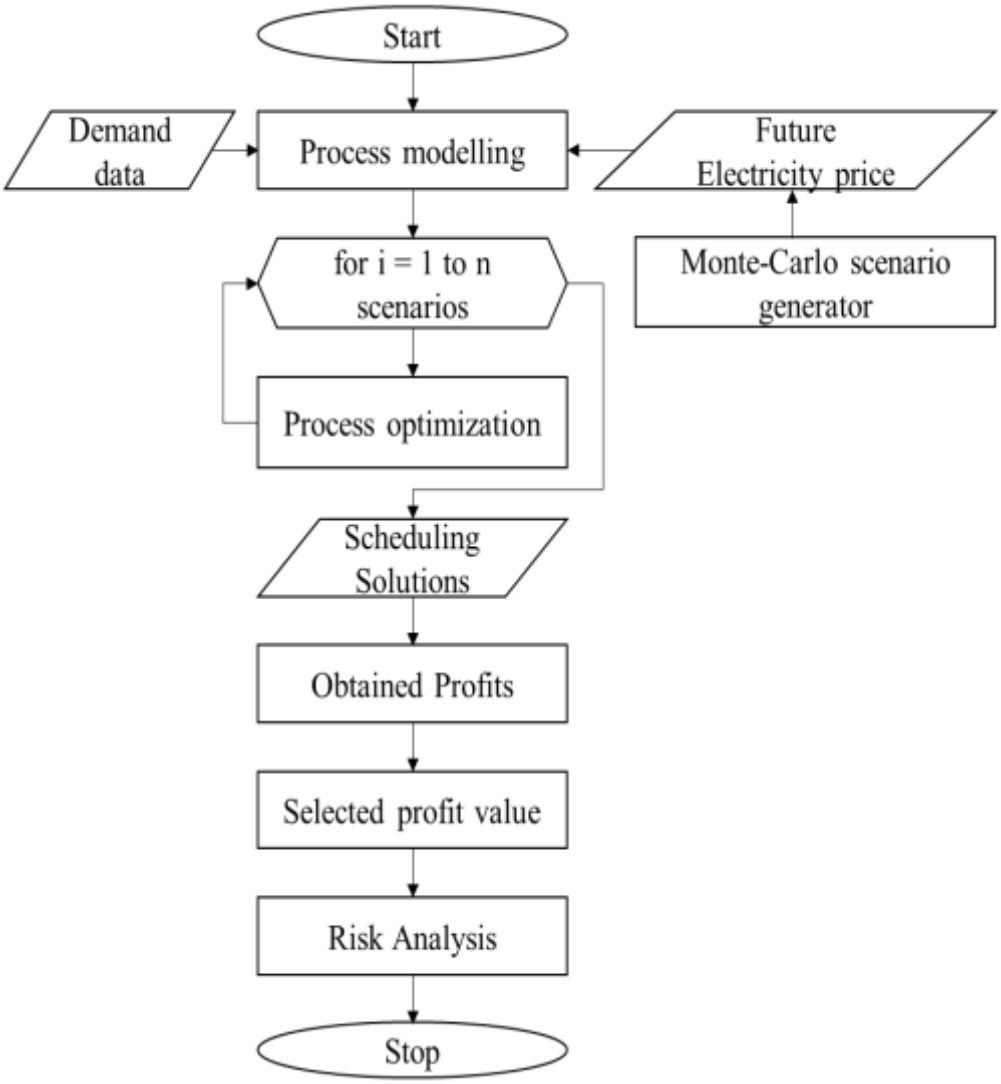

Figure 2.3. Overview of the proposed methodology.

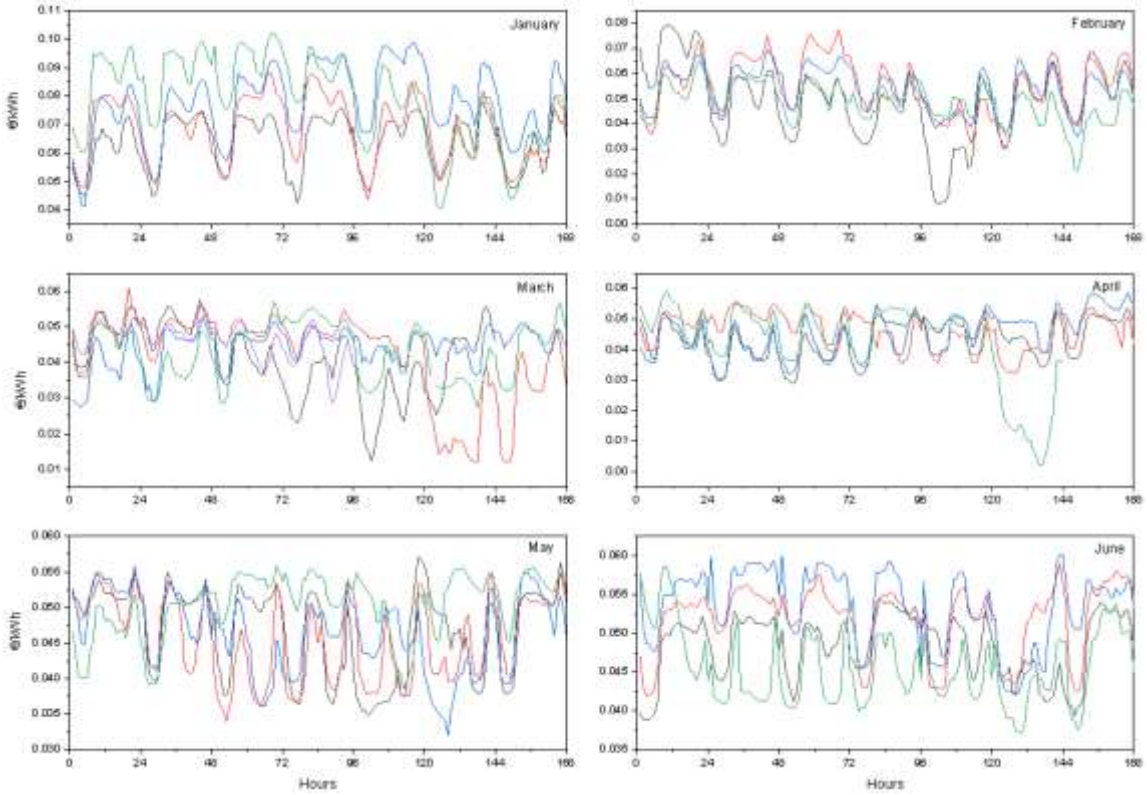

Figure 2.4 Hourly electricity price data for weeks one to four from January to June (week 1 ■, week 2 ■, week 3 ■ , week 4 ■)

2.3.2 Scenario generation model

The mathematical model (explained in detail in section 2.3.3) for the air separation plant is a multi-period model that requires hourly electricity price data. These data are first forecasted deterministically using a statistical model, and then, probable scenarios are generated using Monte-Carlo sampling based on the average error of the forecasting model. The scenarios generated are discrete in nature and each generated scenario is an independent time series data set for the planning horizon.

The nature of energy market is very complex. It is complexly correlated and intertwined with the movement of fossil fuel market and renewable energy market. The nature of USA's energy market was studied by Dowling et al. (2017), who presented the revenue opportunities available in real time energy market and concluded that there is always tradeoff between risk and revenue while trading the energy markets. Gao et al (2022) also studied the impact of multi-source integrated energy system on the electricity market. In a similar study Sorourifar et al. (2020) studied the impact of battery energy storage system on the energy market and cost of operation for the energy producer. In extension of the energy market study, Elmore et al. (2021) analyzed economic opportunities available for large industrial facilities by frequency regulation market, demonstrating that frequency regulation participation in industry has major limitations from the aspect of implementation. Dowling et al. (2018) developed an augmented dynamic mode decomposition method for the forecasting of electricity prices in the day ahead market in the state of California, USA.

Forecasting electricity prices is a particular instance of the more general problem of forecasting time series data (Conejo et al., 2005). Weron (2014) categorized the electricity price forecasting methods according to their modelling approach: multiagent, fundamental, reduced form, statistical and computational intelligence. Weron(2014) found that statistical models were preferred due to readiness for physical interpretation. In the context of the electricity market, a plethora of statistical models have been developed. Mazengia *et al.*(2008) compared Auto-regressive Moving Average, ARIMA (Auto-Regressive Integrated Moving Average), Transfer

Function and Regression Analysis for time series of hourly electricity price forecast, finding that, for weekly predictions of the Spanish electricity market ARIMA provided acceptable errors (4.78%-11.27%). Conejo *et al.*(2005) and Jakaša *et al.*(2011) also used ARIMA to predict the Spanish and the European energy markets, respectively.

ARIMA is a forecasting model for time-series data prediction based on historical data, that incorporates seasonality. It has been widely used by Jakaša et al. (2011), Conejo et al. (2005), and Ierapetritou et al. (2002) to name a few. In our case, where time-series consist of hourly electricity prices, the forecasted electricity price for a future hour *t*+1 is given by Eq 2.1:

$$\text{price}(t') = f(\text{price}(t), p) + \varepsilon(t') \qquad t' > t \tag{2.1}$$

where, $f(price(t), p)$ is the ARIMA function framework used to forecast prices in future periods t'. Price(t') is based on electricity prices in past periods *t*, i.e., price(t) and a set of framework parameters *p* cumulatively representing autoregressive terms, moving average order, differencing and seasonality. Then, $\varepsilon(t')$ provides the stochastic term sampled from the distribution of model residuals (i.e., error). Due to its autoregressive nature, ARIMA can incorporate the unprecedented increase in electricity prices very early in its future forecast, thus, making it a robust time series forecasting model. In this work, ARIMA has been implemented to generate hourly electricity forecast using the historical electricity price data obtained from the Spanish electricity market operator OMIE for a week ahead using software EViews10 SV("EViews.com," n.d.).

For scenario generation approach, we have preferred discrete scenarios approach over the scenario tree approach. The reason is that the latter is used for moving/rolling horizon method, which would cause multiple forecasting instances with frequent scheduling changes during the production period, which would be difficult to implement for a 24×7 operation for a short time horizon.

To obtain discreet electricity price scenarios, we developed a Monte-Carlo scenario generator (MCSG) following the flowchart shown in figure 2.5. MCSG is an appropriate technique to generate scenarios that has been successfully applied for time-series forecasting (Breeden and Ingram, 2010). To generate scenarios, first, prices are (deterministically) forecasted for a period whose prices we know historically (i.e., week 1). Then, the forecasted price is compared with the actual price and the mean average percentage error (MAPE) is calculated. If MAPE is more than the accepted value (15% in this case), the forecasting process is repeated until the MAPE value falls under the accepted limit. Then, we generate a normal distribution of the MAPE with σ = 5% (i.e., MAPE$\sim N(\mu = 0, \sigma = 0.05 \cdot \text{forecasted price})$). Then, the electricity price scenarios are generated by multiplying the obtained MAPE values with the forecasted electricity price scenario and then adding the forecasted electricity price scenario to this multiplication result, e.g. if 'x' is the MAPE error and P is the forecasted electricity price then probable electricity price is obtained as $P + P \times x$. The method follows the Monte Carlo simulation approach and thus, we call this tool Monte Carlo Scenario Generator. At that point, we forecast the electricity price for the future (unknown) time horizon (i.e., week 2 onwards) using the Monte-Carlo scenario generator.

We assume that the realization probability is same for all the scenarios generates. Note, however, that, since scenarios are sampled from a normal distribution, central scenarios are more likely to be sampled than extreme scenarios. As an example, if an infinite number of scenarios were sampled, 95.45% of these scenarios would be expected to fall within $\mu \pm 2\sigma$. This assumption would later allow us to follow the worst-case approach for risk analysis which in real time would provide us with extra cushion against the uncertainty of electricity market making the solution reliable.

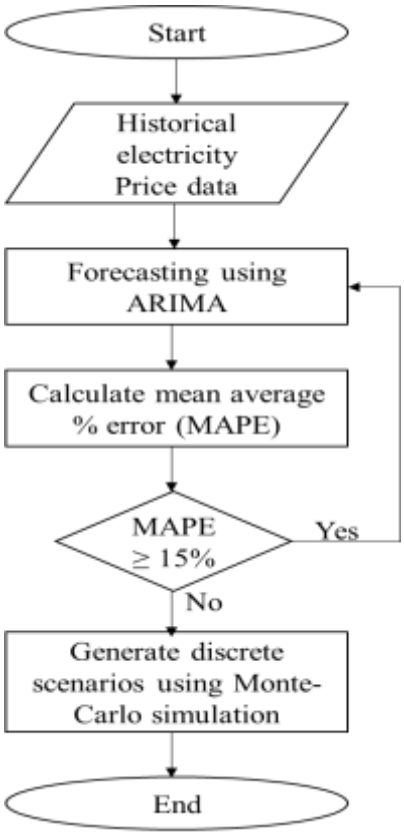

Figure 2.5. Flowchart for the Monte-Carlo scenario generator using ARIMA. MAPE: mean average percentage error.

2.3.3 Multi-period stochastic model

The operation of the air separation unit is optimized for maximum profit using model M-ASUOPT, explained in detail in this section. This model is a modification of the ASUOPT model presented by Fernández el al.(2017), which is enhanced here to consider, not only a single deterministic scenario, but every generated scenario for electricity prices.

Mass balance constraints

Mass balances are demarcated for every process units and time interval. A sketch of generic units and the sets defined around it is shown in figure (2.2). Here, SIi and SOi are the input and output streams of unit 'i', respectively. For processes having more than one input and output streams, another set MSi (MOi) have been defined for these units. Knowing that most units do not accumulate material, eq (2.2) applies,

$$\sum_{s\in SO_i} F_{s,t,sn} = \sum_{s'\in SI_i} F_{s',t,sn} \qquad \forall\, t, sn$$
$$i \in VU, ECU1, ECU2, CBU, PTU, CU1-CU5, SP1-SP14, MX1 \qquad (2.2)$$
$$-MX8, PU1-PU9$$

Here, $F_{s,t,sn}$ denotes volumetric flow rate of stream *s* in time period *t* for scenario *sn.* Note that these are expressed in [Nm^3], therefore, the constraint of mass balance holds even. For the DCU, the output flows are determined by

$$F_{s,t.sn} = \sum_{s' \in MS_i} F_{s',t,sn}\, YIELDVOL_{i,s,sn} + \sum_{s'' \in SI_i \setminus MS_i} F_{s'',t}\, YVC_{i,s,sn} \qquad \forall\, t, s, sn \in SO_i, i = DCU \tag{2.3}$$

where, $YIELDVOL_{i,s,sn}$ is a parameter denoting volumetric yield of stream *s* in unit *i* for scenario *sn* and $YVC_{i,s}$ is a correction coefficient for the volumetric yield if there is a recycle (*i.e.*, stream from T4) into the DCU. For CBU unit, mass balance is computed separately for oxygen and nitrogen stream as they flow separately inside the unit. CF parameter provides the appropriate ratio between nitrogen and oxygen for the unit.

$$\sum_{s \in MO_i} F_{s,t,sn} = \sum_{s' \in MS_i} F_{s',t,sn} \qquad \forall\, t, i, sn = CBU \tag{2.4}$$

$$\sum_{s \in SO_i \setminus MO_i} F_{s,t,sn} = \sum_{s' \in SI_i \setminus MI_i} F_{s',t,sn} \qquad \forall t, i, sn = CBU \tag{2.5}$$

$$CF \sum_{s \in MS_i} F_{s,t,sn} = \sum_{s' \in SI_i \setminus MS_i} F_{s',t,sn} \qquad \forall t, i, sn = CBU \tag{2.6}$$

To consider the accumulation in the storage tanks (T1 – T5) we include equations 7 and 8:

$$INVini_i + TIME\left(\sum_{s \in SI_i} F_{s,t,sn} - \sum_{s' \in SO_i} F_{s',t,sn}\right) = INV_{i,t,sn} \qquad \forall\, i \in ST, t, sn = 1 \tag{2.7}$$

$$INV_{i,t-1,sn} + TIME\left(\sum_{s \in SI_i} F_{s,t,sn} - \sum_{s' \in SO_i} F_{s',t,sn} = INV_{i,t,sn}\right) \tag{2.8}$$

$$\forall\, i, sn \in ST, t > 1$$

Here, $INV_{i,t,sn}$ represents the inventory of storage tank *i* in time period t for scenario *sn*, *TIME* is the duration of time period, and ST is the set of storage tank units (T1 – T5). Parameter *INVini* provides the initial inventory of tank *i*.

To model the real operation, the system has the possibility of purchasing two external streams OGOX and OGAN. The price is equal to the price of electricity consumed in the EDCU, ECU1 and ECU2 to produce them. It is then linked to the demand flow network through contractual arrangements. Again, EDCU has limitation of producing OGAN, which is related to the amount of OGOX, due to the air composition and the process itself. To model this, the *CF2* parameter is used.

$$\sum_{s\prime \in SO_i \setminus MO_i} F_{s',t} \leq CF2 \sum_{s \in MO_i} F_{s,t} \qquad \forall\, t, i \in EDCU \tag{2.9}$$

Capacity constraints

Due to unit's size limitations, we have capacity constraints in the model. For instance, the storage tanks' level must lie between a lower and upper level bound. Parameters $MININV_i$ and $MAXINV_i$ indicate the minimum and maximum inventory level for unit i of set ST (storage tanks), whereas, $INVCAP_i$ represents the 100% capacity of the tank. These bounds are imposed as:

$$MININV_i INVCAP_i \leq INV_{i,t,sn} \leq MAXINV_i INVCAP_i \tag{2.10}$$

$$yi_{i,t,sn}\, MINCAPVOL_i \leq \sum_{s \in MS_i} F_{s,t,sn} \qquad \forall\, t, i, sn \in MINCAP \tag{2.11}$$

$$\sum_{s \in MS_i} F_{s,t,sn} \leq yi_{i,t,sn}\, CAPVOL_i \qquad \forall\, t, i, sn \tag{2.12}$$

where, $yi_{i,t,sn}$ is a binary variable which corresponds to on and off condition of the operating unit at a particular time. $MINCAP$ is a set that contains the minimum input flow rates of all the units (PTU, PU1, PU3, LQU1, LQU2, CBU, ECU1 and ECU2). Limits on EDCU output streams are applied through the input streams of compressors ECU1 and ECU2.

Process units LQU1 and LQU2, have a characteristic delay between the start and the moment they start producing. This idle period of starting is modelled via:

$$\begin{bmatrix} YON_{i,t,sn} \\ \sum_{z \in MS_i} F_{s,t,sn} \leq DT.CAPVOL_i \end{bmatrix} \bigvee \begin{bmatrix} -YON_{i,t,sn} \\ \sum_{z \in MS_i} F_{s,t,sn} \leq DT.CAPVOL_i \\ YON_{i,t} \in \{True, False\} \end{bmatrix} \quad \forall t, i = LQU1, LQU2 \tag{2.13}$$

Here, *DT* is a parameter which computes the effect of idle time (limiting the amount of product produced from the moment it is on; $DT \leq 1$). The model uses parameter $YON_{i,t}$ (true if the unit is on; false otherwise) to model this time-delay. Convex hull reformulation has been used to transform this disjunction in a mathematical equation. The simplified equations imposing lower bound on the capacities of input flows:

$$\begin{aligned} T.MINCAPVOL_i YON_{i,t,sn} \leq FD^1_{s,t,sn} \\ \leq DT.CAPVOL_i YON_{i,t,sn} \\ \forall i, t, sn = LQU1, LQU2, s \in MS_i \end{aligned} \tag{2.14}$$

$$\begin{aligned} MINCAPVOL_i\left(YI_{i,t,sn} - YON_{i,t,sn}\right) \leq FD^2_{s,t} \\ \leq CAPVOL_i\left(YI_{i,t,sn} - YON_{i,t,sn}\right) \end{aligned} \tag{2.15}$$

$$\forall\, t, i, sn = LQU1, LQU2, s \quad \in MS_i$$

$$FD^1_{s,t,sn} + FD^2_{s,t,sn} = F_{s,t,sn} \qquad \forall t, i, sn \in LQU1, LQU2, s \quad \in MS_i \tag{2.16}$$

Here, $FD^1_{s,t,sn}$ and $FD^2_{s,t,sn}$ are disaggregated variables. Equations (2.14) and (2.15) will force both $FD^1_{s,t,sn}$ and $FD^2_{s,t,sn}$ variables to be 0 if the unit *i* is inactive. On the other hand, an active unit *i* (*i.e.*, $YI_{i,t,sn} = YON_{i,t,sn} = 1$) will let $FD^1_{s,t,sn}$ to take any value from $DT.MINCAPVOL_i$to $DT.CAPVOL_i YON_{i,t,sn}$.

The value of $YON_{i,t.sn}$ corresponds to the value of $YI_{i,t,sn}$ given by the equations (2.17) – (2.19).

$$YON_{i,t,sn} \geq YI_{i,t,sn} - YI_{i,t-1,sn} \qquad \forall i, t, sn > 1 \tag{2.17}$$

$$YON_{i,t,sn} \leq YI_{i,t,sn} \qquad \forall i, t, sn > 1 \tag{2.18}$$

$$YON_{i,t,sn} \leq 1 - YI_{i,t-1,sn} \qquad \forall i, t, sn > 1 \tag{2.19}$$

Further, compressor CU3 is modelled as two separate units CU3a and CU3b as it can operate with two different products (*i.e.*, N_2 and O_2). However, maintenance work is required before it can handle the other product. This is shown via equations (2.20) – (2.22).

$$Y_{i,d,t,sn} + Y_{i',d,t,sn} \geq 1 \qquad \forall t, i, sn = CU3a, i' = CU3b, d = 1 \tag{2.20}$$

$$YI_{i,t,sn} \leq 1 - YI_{i',t',sn} \qquad i = CU3a, i' = CU3b, \forall t, t' | t > t' > (t - PCHT) \tag{2.21}$$

$$YI_{i,t,sn} \leq 1 - YI_{i't',sn} \qquad i = CU3b, i' = CU3a, \forall t, t' | t > t' > (t - PCHT) \tag{2.22}$$

Here, parameter *PCHT* indicates the time required to change the product in the compressor. Equation (2.22) checks that unit CU3 cannot be used simultaneously to process both products.

To avoid failure, due to big step changes in flow rate, the operation is kept smooth by imposing a limit MFC_s on the changes in flow rates over consecutive time periods (eqs. 2.23 – 2.25).

$$F_{s,t,sn} - F_{s,t-1,sn} \leq AV_{s,t,sn} \qquad \forall\, t > 1, s \in FCL \qquad (2.23)$$

$$F_{s,t-1,sn} - F_{s,t,sn} \leq AV_{s,t,sn} \qquad \forall\, t > 1, s \in FCL \qquad (2.24)$$

$$AV_{s,t,sn} \leq YFC_{s,t,sn} MFC_{s,t,sn} \qquad \forall\, t > 1, s \in FCL \qquad (2.25)$$

Here, $AV_{s,t,sn}$ represent the absolute value of the increment or decrement in the flow rate of stream in consecutive time periods. Whereas, *FCL* comprises the set of streams on which the limitation is put on. $YFC_{s,t,sn}$ is a binary variable that equals 1 if there is a change in the flow rate of stream *s* in time interval *t*; 0 otherwise.

If a storage tank has reached its upper limit during the production, there is an option to partially empty the tank by filling the road tankers and sending them to nearby additional storage plant that belongs to the same company. This is done by using splitters (SP10-SP13) which also act as a switch for these situations. Sometimes these road tankers are also used to sell the product. To differentiate between these two operations, a set MO_i is used containing the streams of the product to be sold. Therefore, a lower bound is imposed on the streams not contained in MO_i, which allows other flows to be constrained by demand. This is modelled as:

$$YW_{i,t,sn} SMINCAP_s \leq F_{s,t,sn} \leq YW_{i,t,sn} SMAXCAP_s \qquad (2.26)$$

$$\forall\, t, i, sn \in SPW, s \in SO_i \backslash MO_i$$

$$F_{s,t.sn} \leq \left(1 - YW_{i,t.sn}\right) GSCAP \qquad \forall\, t, i, sn \in SPW, s \in MO_i \tag{2.27}$$

where, the binary variable $YW_{i,t,sn}$ is '1' if splitter i is sending the product to the outside storage, otherwise '0'. $SMINCAP_s$ and $SMAXCAP_s$ are lower and upper limits on the flow requirements of stream *s*. *SPW* and *GSCAP* represent a set containing the splitters (responsible for sending the tankers to storage plants) and a generic limit on the stream's flowrate respectively.

Tanks are used for this purpose only if the level in the tank (represented by $INV_{i,t-1,sn}$) of (t-1) time interval is higher than the threshold value ($VSINV_i$). To model this:

$$\begin{bmatrix} YINV_{i,t}, sn \\ VSINV_i INVCAP_i \leq INV_{i,t,sn} \leq MAXINV_i INVCAP_i \end{bmatrix} \bigvee \begin{bmatrix} -YINV_{i,t}, sn \\ MININV_i INVCAP_i \leq INV_{i,t,sn} \leq VSINV_i INVCAP_i \end{bmatrix} \tag{2.28}$$

$$\forall\, t, i \in TVS \;\&\; YINV_{i,t} \in \{True, False\}$$

Here, set *TVS* consists of units of tanks which are sending the product to the storage plant. In eq (2.28) $YINV_{i,t,sn}$ is the binary variable with value '1' if the tank level is between the maximum and the threshold value; '0' otherwise. The above disjunction leads to:

$$VSINV_i INVCAP_i YINV_{i,t} \leq INVD^1_{i,t} \leq MAXINV_i INVCAP_i YINV_{i,t} \tag{2.29}$$

$$\forall\, t, i, sn \in TVS$$

$$MININV_i INVCAP_i \left(1 - YINV_{i,,snt}\right) \leq INVD^2_{i,t,sn} \tag{2.30}$$

$$\leq VSINV_i INVCAp_i\left(1 - YINV_{i,t,sn}\right) \quad \forall\, t, i \in TVS$$

$$INV_{i,t,sn} = INVD^1_{i,t,sn} + INVD^2_{i,t,sn} \qquad \forall\, t, i.sn \in TVS \qquad (2.31)$$

In eqs (2.29) – (2.31), $INVD^1_{i,t}$ & $INVD^2_{i,t}$ are disaggregated variables from the convex hull reformulation. Further, eq (2.32) prevents the tank discharge when the level is below the threshold value.

$$YW_{i',t,sn} \leq YINV_{i,t-1,sn} \qquad \forall\, t > 1, i \in TVS, i' \in SPTI_i \qquad (2.32)$$

Here, the set $SPTI_i$ contains the splitters associated with tank i. In the case of period 1, the value of $YW_{i',t}$ is '0'. Splitter SP8 has only one pump and therefore can only handle one output stream. So, to distinguish the output streams going to unit CBU or to tank T5, we use binary variable $YI_{i,t}$ in following equations.

$$\sum\nolimits_{s \in SI_i \setminus MS_i} F_{s,t} \leq YI_{i,t} GSCAP \qquad \forall\, t, i = CBU \qquad (2.33)$$

$$\sum\nolimits_{s \in SO_{i'} \setminus SI_i} F_{s,t} \leq (1 - YI_{i,t}) GSCAP \qquad \forall\, t, i = CBU\,, i' = SP8 \qquad (2.34)$$

where GSCAP is the generic limit on the stream flow rates.

The production unit is set to satisfy the demand which varies from one time interval to another and is denoted by $DEM_{s,t}$ (demand has to be satisfied with all products and time periods).

$$F_{s,t,sn} = DEM_{s,t,sn} \qquad \forall\, t, s, sn \in FP \qquad (2.35)$$

where *FP* is a set of streams containing final products.

A final inventory level is defined and enforced for the last time interval of the production using parameter $INVfin_i$:

$$INV_{i,t,sn} + \partial^{+}_{i,t,sn} + \partial^{-}_{i,t,sn} = INVfin_i \qquad \forall\, t = tfin, i \in ST \qquad (2.36)$$

$$0 \leq \partial^{+}_{i,t,sn} \leq UB_i \qquad \forall\, t = tfin, i \in ST \qquad (2.37)$$

$$-UB_i \leq \partial^{+}_{i,t,sn} \leq 0 \qquad \forall\, t = tfin, i \in ST \qquad (2.38)$$

where, $\partial^{+}_{i,t,sn}$ and $\partial^{-}_{i,t,sn}$ are slack variables to accommodate the deficit or excess of final product compared to $INVfin_i$, and UB_i is imposed as an upper bound on both slack variables.

Utility consumption

Only two utilities, electricity and gasoil, are considered here.

There are two types of electricity consuming units:

1) Consumption does not depend upon the stream flow rate, contained by set *EC* {LQU1, LQU2, P1-P9}.
2) Consumption depends upon the stream flow rate, contained by set *EV* {CU1-CU5, ECU1, ECU2, PTU}.

For (1)

$$UTCONS_{i,u,t,sn} = YI_{i,t,sn} UTRATE_{i,u} \qquad \forall\, t, i, sn \in EC, u = UE \qquad (2.39)$$

where, $UTCONS_{i,u,t,sn}$ is a variable accounting the consumption of utility *u* in unit *i* in time period *t* for scenario *sn*. $UTRATE_{i,u}$ denotes the rate of consumption of utility *u* by unit *i* during operation.

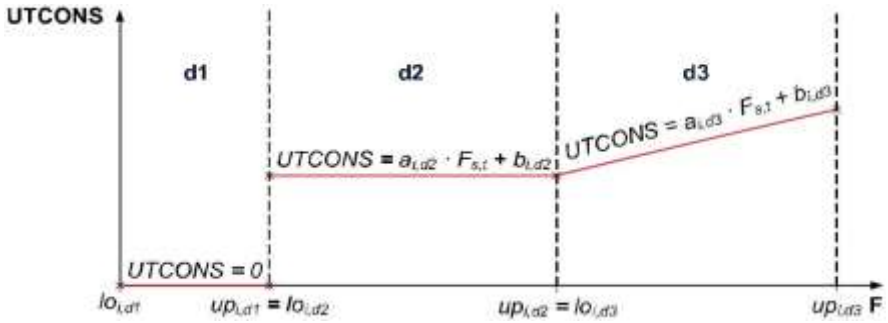

Figure 2.6. Linear approximation of electricity consumption as a function of flow rate processed. d1 is oversized for visualization. Gathered from (Fernández et al., 2017)

For units which consumption depends upon the stream flow rate, a piecewise linear function is defined as depicted in figure 6. Sector 'd1' indicates when there is no operation, sector 'd2' presents a region where electricity consumption is constant, while sector 'd3' shows the part where electricity consumption is proportional to the flow rate. Also, the upper limit ($up_{i,d1}$) of 'd1' is very small (≈0).

$$V_d \begin{bmatrix} Y_{i,d,t,sn} \\ a_{i,d}F_{s,t,sn} + b_{i,d} = UTCONS_{i,u,t,sn} \\ lo_{i,d} \le F_{s,t,sn} \le up_{i,d} \end{bmatrix} \qquad (2.40)$$

$$\forall\, t, i, sn \in EV, u = EC, Y_{i,d,t,sn} \in \{True, False\}$$

Here, $a_{i,d}$ and $b_{i,d}$ are parameters of linear function denoting the consumption of electricity of unit *i* sector d. This disjunction gives rise to the equations:

$$\sum_d \left(\left(a_{i,d} Z_{i,d,t.sn} + b_{i,d} Y_{i,d,t,sn} \right) \right) = UTCONS_{i,u,t,sn} \qquad (2.41)$$

$$\forall\, t, i, sn \in EV, u = UE$$

$$\sum_d Z_{i,d,t,sn} = \sum_{s \in SI_i} F_{s,t,sn} \qquad \forall\, t, i, sn \in EV \qquad (2.42)$$

$$lo_{i,d}y_{i,d,t,sn} \leq Z_{i,d,t,sn} \leq up_{i,d}y_{i,d,t,sn} \qquad \forall\, d,t,i,sn \in EV \qquad (2.43)$$

$$\sum\nolimits_{d} y_{i,d,t,sn} = 1 \qquad \forall\, t,i,sn \in EV \qquad (2.44)$$

where, $Z_{i,d,t,sn}$ is a disaggregated variable for the convex hull reformulation. The value of the binary variable $Y_{i,d,t}$ is enforced, for the internal units with variable electricity consumption, by:

$$1 - Y_{i,d,t} \leq YI_{i,t} \leq 1 - Y_{i,d,t} \qquad \forall\, t,i \in EV, d = d1 \qquad (2.45)$$

Please, note that the external compressors are embedded in the set EV, while the external distillation column EDCU is not included, as it needs a different treatment and has been modelled as:

$$\sum\nolimits_{d} Z_{i,d,t,sn} = \sum\nolimits_{s \in MO_i} F_{s,t,sn} \qquad \forall\, t,i,sn = EDCU \qquad (2.46)$$

$$lo_{i,d}y_{i,d,t,sn} \leq Z_{i,d,t,sn} \leq up_{i,d}y_{i,d,t}, sn \qquad \forall\, d,t,i,sn \in EDCU \qquad (2.47)$$

$$MINCAPVOL_{i'}\left(1 - Y_{i,d,t,sn}\right) \leq \sum\nolimits_{s \in SO_i \setminus MO_i} F_{s,t,sn} \leq CAPVOL_{i'}\left(1 - Y_{i,d,t,sn}\right) \qquad \forall\, t,i,sn = EDCU, i' = ECU1 \qquad (2.48)$$

$$\sum\nolimits_{d} Y_{i,d,t,sn} = 1 \qquad \forall\, t,i,sn = EDCU \qquad (2.49)$$

$$1 - Y_{i,d,t} \leq YI_{i,t} \leq 1 - Y_{i,d,t} \qquad \forall\, t,i \in EO, d = d1 \qquad (2.50)$$

where, *EO* contains the external units (*e.g.*, {EDCU}).

The total energy consumed by the process is restricted in a given time interval due to contract requirements with energy suppliers. The breach of these contracts gives rise to penalties.

$$\sum_{i \in UPRI} UTCONS_{i,u,t,sn} + PHTR_{t,sn} + PLQ3_{t,sn} \leq MAXPR1_{t,sn} + MAXPR2_{t,sn} \qquad \forall\, t,u,sn \qquad (2.51)$$
$$= UE$$

Here, the limits on the power consumed by the process networks are given by $MAXPR1_{t,sn}$ and $MAXPR2_{t,sn}$ including the units of the main process (*UPR1*) and the units of external supplier (*UPR2*). Parameters $PHTR_{t,sn}$ and $PLQ3_{t,sn}$ consider the power consumed by the machines working in discontinuous mode. Thus, to calculate the total electricity over the simulated time (*ECONS)*:

$$ECONS = TIME \sum_{t} \sum_{i} UTCONS_{i,u,t} \qquad u = UE \qquad (2.52)$$

where *TIME* is a parameter representing the simulated time consisting of every time period of operation of every length of every time interval.

Only unit VU consumes gasoil. The fuel used during time interval *t*, is modelled by the continuous variable $UTCONS_{i,u,t,sn}$, which is proportionally related by the parameter $UTRATE_{i,u}$ to the flow rate $F_{s,t,sn}$ processed in that time interval in unit *i*.

$$UTCONS_{i,u,t,sn} = \sum_{s \in MS_i} F_{s,t,sn} UTRATE_{i,u} \qquad \forall\, t,i,sn = VU,u \qquad (2.53)$$
$$= UGO$$

The value of $UTRATE_{VU,}$ *UGO*, is calculated using the lower heating value of the gasoil assuming a thermal efficiency (η) of 0.75. Hence, total utility *UGO* consumed over the complete simulated time (*GOCONS)* is calculated from $UTCONS_{I,u,t,sn}$ for the time length of the time interval (*TIME*):

$$GOCONS = TIME \sum_t \sum_i UTCONS_{i,u,t,sn} \qquad u = UGO \tag{2.54}$$

Also, VU and the corresponding tank T5 are only used if EDCU is not operated. This is modelled as:

$$YI_{i,t,sn} \leq Y_{i',t,sn} \qquad \forall\, t, i, sn = VU, i' = EDCU \tag{2.55}$$

Objective function

We seek to maximize the profit of the plant denoted by the continuous variable *PROFIT*, which is computed as in eq. (2.56)

$$PROFIT = SALES + DISC - EEC - GOC - MAINTENANCE\ COST \tag{2.56}$$

Here, *SALES* is the revenue generated from the product produced and is computed as in equation (2.57), *DISC* is the discount obtained from the external supplier when products are purchased from EDCU and is calculated as shown in equation (2.58), *EEC*, computed in equation (2.59), and *GOC*, computed in equation (2.60), are electricity and gas utility costs, respectively, and *MAINTENANCECOST* is the cost involved in the maintenance of compressors.

$$SALES = TIME \sum_t \sum_{s \in FP} F_{s,t}\, PRICE_s \tag{2.57}$$

$$DISC = TIME.DRATE \sum_t \sum_{s \in MO_i} F_{s,t} \qquad i = EDCU \tag{2.58}$$

$$EEC = TIME \sum_t (PCON_t ECONCOST_t + (\sum_t UTCONS_{i,u,t} - PCON_t).ECOST_t \qquad ,u = UE \tag{2.59}$$

$$GOC = GOCONS.GOCOST \tag{2.60}$$

Where, DRATE is parameter relating the amount of product obtained through EDCU.

In the objective function (OF), several types of PENALTIES are deducted from the profit to prevent the model from incurring in abnormal schedules from a practical point of view (e.g., penalty associated with number of startup and shutoff of equipment, penalties associated with not meeting the required inventory for a particular storage tank at a particular instance of time etc.). Penalties help to make the operation more realistic. Thus, the value of *OF* provides the expected net profit.

$$OF = PROFIT - PENALTIES \tag{2.61}$$

Thus, M-ASUOPT is formulated from eq (2.2) – eq (2.61). The adopted methodology allows solving M-ASUOPT for all the uncertain but plausible scenarios in a decoupled manner which enables the model flexibility for making changes in the first and second stage variables if required under any scenario. First stage variables correspond to input variables while second stage variables correspond to on/off decisions, operational settings etc. In this case we are considering uncertainty only in electricity price which is a first stage variable for this model. The second stage variables are unaffected with respect to electricity price scenarios with this methodology.

2.3.4 Risk analysis metrices

Model M-ASUOPT is solved for every plausible scenario, as described in section 3.3, thus providing multiple solutions. Since scenarios are uncertain, there is a risk that the estimated profit is not achieved, which can affect the financial planning of decision makers. Therefore, we compute some risk metrics to deal with the risk

associated with equally probable scenarios. All the risk metrics are described in detail by Knopf *et al* (2015) and Medina-gonzález et al.(2017) , yet a brief mathematical explanation follows. If the estimated profit value is denoted by 'Ω', then the risk metrics associated to this 'Ω' are calculated as follows:

a) $Risk_{\Omega}$: It calculates the probability of not achieving an estimated value (Ω) of the profit, and it is calculated by using Eq. (2.68):

$$Risk_{\Omega} = \sum_{sn} prob_{sn} Z_{\Omega sn} \qquad (2.68)$$

where,

$$Z_{\Omega sn} = \begin{cases} 1, & Profit_{sn} \leq \Omega \\ 0, & otherwise \end{cases} \qquad (2.69)$$

b) Downside Risk (DR_{Ω}) represents the positive deviation of the expected profit from an estimated profit value, Ω, for different scenarios (represented by index *sn*). It is mathematically expressed as:

$$DR_{\Omega} = E\{\delta_{\Omega sn}\} = \sum_{sn} prob_{sn}\, \delta_{\Omega sn} \qquad (2.70)$$

where,

$$\delta_{\Omega \mathrm{sn}} = \begin{cases} \Omega - Profit_{sn}\,, & Profit_{sn} < \Omega \\ 0\,, & otherwise \end{cases} \qquad (2.71)$$

Further, it is also important to gauge the performance of a solution (i.e., profit realization of the optimized scheduling plan) for any plausible scenario in terms of the statistical confidence level of achieving a defined target value. In this context, two

risk management metrices are widely used by portfolio management institutions to reduce the expected losses and optimize the profit: VaR (Value at Risk) and CVaR (conditional value at Risk) (Sarykalin et al., 2008). Calculation of these risk metrices for our estimated profit provides us with a quantitative value of shortfall in the estimated profit, where a higher CVaR and VaR values indicate greater shortfall and vice versa. A detailed explanation and comparison of these metrices has been given by Rockafellar and Uryasev (2002). Use of these metrices, for similar case study, has also been performed by Li *et al* (2021b). Therefore, these metrics can help the management team to choose for a low or high-risk scheduling strategy based on the risk-taking capacities.

2.4 Results

Model capabilities were tested using real-time data from an existing industrial facility located in Tarragona (Spain). Also, comparison of the forecasting techniques revealed that even though the Spanish electricity market has tariff periods and empirical relations to compute electricity prices for those periods, forecasting techniques for time-series data are better suited to compute the electricity prices. A detailed analysis of the findings is provided in ensuing subsections.

To achieve this, we used modified ASUOPT (Fernández et al., 2017) (M-ASUOPT) model and optimized in GAMS 25.0.1 (General Algebraic Modelling System)(“GAMS software,” n.d.) using the solver XPRESS v33.01 (“XPRESS Solver,” n.d.) on a 64 bit/MS Windows 10 computer with Intel® Core™ i5-7500 CPU @ 3.4 GHz processor and 16 GB RAM. The model used 6.24 CPU-hours to solve for

100 scenarios in series. Note that this amount of time is already long enough considering that electricity prices change on a daily basis. If a traditional stochastic programming model, considering the 100 scenarios simultaneously, were to be solved, there is a significant risk that its solution will not arrive on time to provide a proper reaction to updated prices. In addition, the proposed methodology could be further expedited by parallelizing calculations, since scenarios are independent from each other.

2.4.1 Tariff periods and electricity price scenarios

To schedule the air separation plant, we need hourly electricity price values in advance for the selected time horizon. In the Spanish system, there are six different electricity tariff periods depending on the hour and on the typology of the day (i.e., working, weekend, vacation and not-working), which dictate the cost of the spot electricity prices. Specifically, electricity prices are calculated daily using the following relation:

$$P_i = A_i \times B_i + C_i \tag{2.72}$$

where P represents the electricity price, *'i'* represents the index for the tariff period, *A* is the base electricity price; *B* is a cofactor corresponding to tariff period and *C* represents additional costs. Hence, even for the same type of day and tariff period in a given month, hourly variations on the values of parameters A, B and C result in different electricity prices in the spot market (see figure 2.7a).

Historical electricity prices can be fed to the ARIMA method to forecast electricity prices for the different tariff periods in the future (figure 2.7b). However, there is always the possibility that the hourly electricity prices differ from the average price of their respective tariff periods. Indeed, a close comparison of figures 2.7a and 2.7b reveals that the electricity price forecasted using empirical relations in low tariff periods is higher than in some higher tariff periods (and vice versa) on multiple occasions (47% price predictions higher than the actual price and 23% price predictions lower than the actual price, with 30% price predictions matching the actual price). This translates in an average relative error of ~70% which means that the deterministic approach (Fernández et al., 2017) might lead to high error in profit calculation under uncertain scenarios.

To overcome this limitation, we incorporate uncertainty into the electricity prices forecasted by means of ARIMA. For ARIMA, the average forecasting error is 15% in our case, which demonstrates that ARIMA prediction considering uncertainty can reduce the error in forecasting electricity prices if compared with the method previously used in Fernández et al.(2017) (15% vs 70%). This proves that scheduling of an energy-intensive plant based on ARIMA, which includes seasonality and weekly variation, leads to more realistic assumptions than those based only in tariff periods.

Therefore, MCSG is used to generate 100 discrete plausible scenarios for electricity prices of the subsequent week. The historical data for electricity prices was provided by the OMIE (Spanish electricity market regulator) for the years 2015,2016 and 2017. We used 3 months (12 weeks) of historical data to generate the scenarios

for the upcoming week using our MCSG tool. A wide distribution of the generated scenario is shown in figure 2.8.

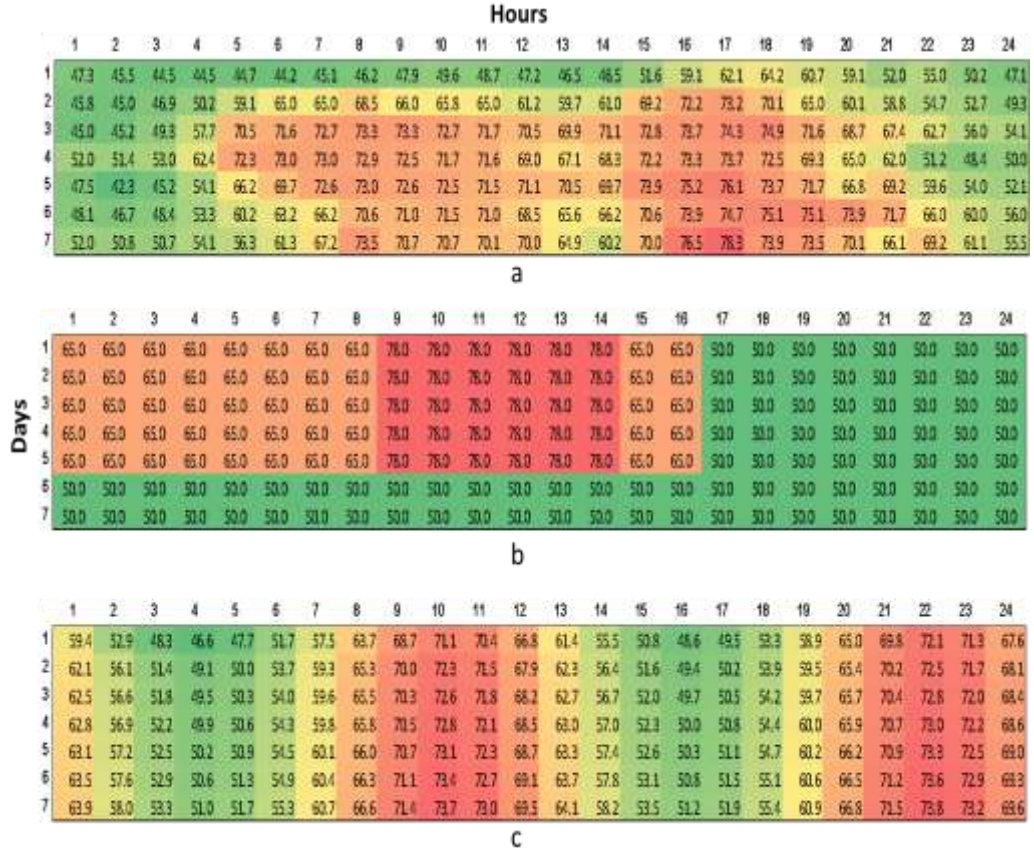

Figure 2.7 (a) Heat map for actual electricity prices during the first week of the year 2017, (b) Heat map for the electricity prices forecasted in the deterministic case, (c) Heat map for the electricity prices forecasted incorporating uncertainty in ARIMA.

To validate the forecasting model and its output, a validation test for the similarity of historical and forecasted scenarios is first performed (Breeden and Ingram, 2010). Figure 8 represents the forecasted 100 scenarios generated using MCSG for the second week of January 2017, where pattern similarity can be

identified. Also, Kandell test for coefficient correlation is used to assess the degree of similarity between the two datasets ("Artificial Intelligence and Expert Systems," 2012). The range of Kandell test for similarity varies from [-1, 1] where '-1' indicates a complete dissimilarity while '+1' denotes a complete similarity (Brossart et al., 2018). The average value for Kandell test for the predicted electricity price scenarios is 0.68. This means that the pattern of predicted electricity price scenarios has a strong resemblance to the pattern of historical electricity prices.

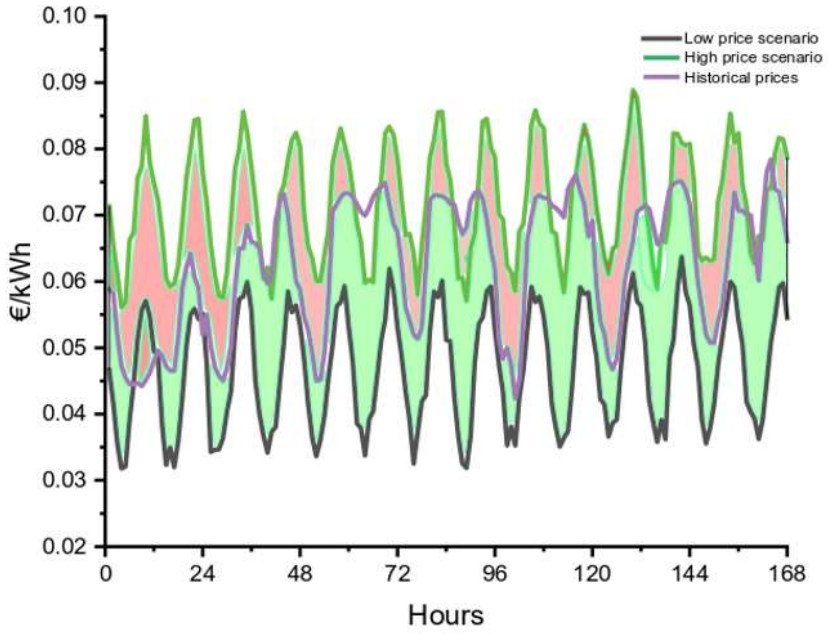

Figure 2.8. Forecasted scenarios for the electricity cost during the first week of January using ARIMA and Monte Carlo scenario generation.

2.4.2 Scheduling

The modified ASUOPT model was executed for all the generated scenarios separately for the upcoming week (i.e., the model optimized the plant scheduling for each scenario for week 2). We observed that the scheduling plan changes in every

scenario and is exclusive to its corresponding scenario, which also translates into the discreet profit value in each scenario. Thus, at the end, when all scenarios have been optimized, we get a profit distribution. For the ease of understanding the scheduling change, we plotted the operational and shut down hours of liquefiers of the plant during the whole scheduling horizon. As liquefiers are the units with the highest energy consumption, their operation has the largest impact on the optimal scheduling, with a tendency to determine the scheduling of other lesser energy-consuming units. The optimal schedule for the liquefiers' operation is illustrated in figure 2.9, with figure 2.9a providing the optimal scheduling scheme for the deterministic case using nominal forecasted electricity prices, while figures 2.9b and 2.9c correspond to the optimal schedules for the scenarios achieving the lower and upper quartile of the profit distribution, respectively. As expected, both liquefiers are not fully utilized despite the demand is satisfied in all periods (Figures 2.9b and 2.9c). Hence, the model selects the most economical units based on power consumption, start-up time and production rate collectively. The reason for this is that startup of any energy consuming device causes a power surge on the system in turn consuming even more energy. Therefore, in our model we introduced penalties for frequent startup/shutdown of the plant units and, thus, the model tries to reduce the penalties incurred due to the number of start-ups and shut down of each unit. Hence, some units are over-utilized under economically optimized scheduling. From figures 9b and 9c, it can be observed that, despite their similarities, the optimal scheduling schemes tend to reduce the implementation of alternative units as we move towards higher price scenarios (i.e., low-profit values). This reduces the penalties incurred for multiple

start-ups and shutdowns. For example, in this case, the lower quartile scheduling scheme (in figure 2.9b) uses LQ1 for fewer hours compared to upper quartile scheduling scheme (in figure 2.9c).

Figure 2.9. Optimal scheduling schemes for (a) deterministic forecast of electricity prices (b) scenario corresponding to the lower quartile the profit distribution (c) scenario corresponding to the upper quartile of the profit distribution.

2.4.3 Risk-analysis

The deterministic optimization by Fernández et al (2017) obtained a profit of 547323 €, but as mentioned in section 2.3.3, electricity prices vary on an hourly basis

for spot market and cannot be forecasted with utmost certainty. Thus, a deterministic plant scheduling based on a single scenario will not capture the essence of the problem. To deal with the uncertainty, the methodology explained in section 2.3.1 has been used to generate multiple scenarios for one week. For scenario-based approaches, a common practice is to compare base, best and worst case, although depending upon the level of uncertainty the number of scenarios required to achieve a certain confidence level in the predictions may be as high as 50, or even higher (Mohamed and Bouhania, 2014). In our case, we generated 100 scenarios for analysis to incorporate a wide spectrum of different possible realization within the feasible range. The result of this optimization of scenarios provides with multiple scheduling plans and a distribution of profit values which allows us to evaluate risk metrices corresponding to the scenario. Risk metrics provide the decision-makers with insight on the associated risk with the expected profit target in a particular scenario. For example, CVaR allows to evaluate the likelihood that a specific loss will exceed a certain value at risk (VaR) for a given confidence level (Vieira et al., 2018). Therefore, if a decision-maker chose the best case scenario for profit, they would be open to approximately 32000 (= Ω x % deviation from $\Omega_{Average}$) € of value loss (over a one week period) with a 95% confidence level of achieving the calculated profit in this case.

Table 2.1. Statistics summary of the different risk metrics evaluated with a 95% confidence. Lq: lower quartile profit; Uq: upper quartile profit.

Targeted profit	Ω (€)	$Risk_{\Omega}$	VAR(95)	CvaR(95)	DR_{Ω}	% deviation from $\Omega_{Average}$
$\Omega_{Worst\ case}$	440644	-	-	-	-	6.305
$\Omega_{Average}$	477312	0.566	-0.040	-0.052	0.560	0
Ω_{Median}	476849	0.500	-0.039	-0.051	0.500	0.097
Ω_{Lq}	470301	0.253	-0.025	-0.038	0.750	1.469
Ω_{Uq}	480479	0.750	-0.046	-0.058	0.220	-0.664
$\Omega_{Best\ case}$	509922	0.990	-0.101	-0.113	0.100	-6.940
$\Omega_{Deterministic}$	547323	-	-	-	-	-14.079

Table 1shows the results for four representative cases: average, median, lower quartile and upper quartile profit values. Table 1indicates that all scenarios obtain profit (from +6.9% in the best scenario to –6.3% in the worst-case when compared to the average profit value of 477312 €). The last column of Table 1shows the deviation from the expected profit in the different scenarios while the RISK value in the second column gives a fair idea about the selection of the scenario (the higher the target value, the higher the potential shortfall). The negative sign '- 'in CVaR/VaR indicates shortfalls. Table 1indicates that the deterministic profit has a positive deviation from the $\Omega_{Average}$ by a fair margin (~14.1%) but is more exposed to any

variation in the electricity cost due to its different prediction model as depicted in figure 7 using heatmap.

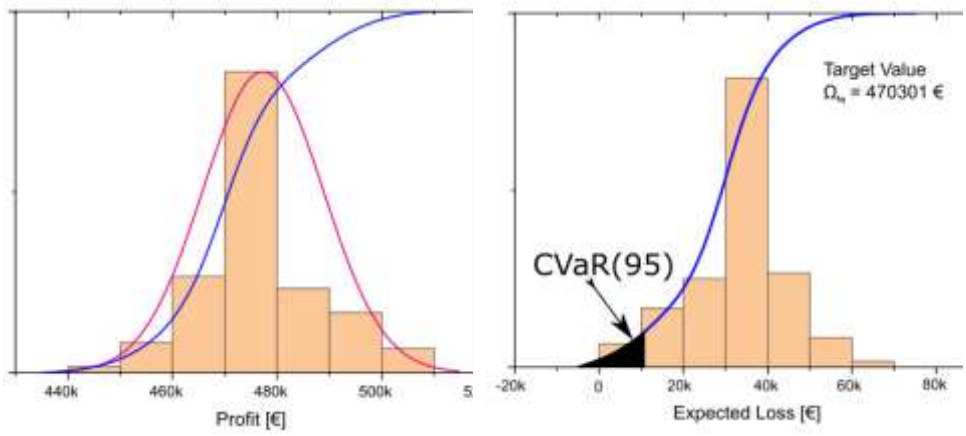

(a) (b)

Figure 2.10. (a) profit and (b) shortfall of the calculated profit value for lower quartile scenario.

A conservative decision-maker choosing the scheduling corresponding to the optimal solution with the lower quartile or worst case profit, has the possibility of deviating from attainable average profit value by positive ~1.5% and ~7% respectively, while a risk-taking decision-maker (i.e. preferring upper quartile or best case scenario) would have a possibility of overshooting the average profit target value by negative ~0.6% and ~6.9%, respectively, and would also be exposed to the risk of falling short of the calculated profit (Ω_{Uq}) by 5.8% of Ω_{Uq}. For the worst-case scenario (where the profit is virtually uninfluenced by uncertainty) we are undershooting by 6.3 % the expected average profit. This can also be seen in figures

10a and 10b, which depict the distribution of simulated expected profits. The spread of calculated profits distribution fits the normal curve which is expected as the MCSG uses normal distribution for generating the electricity price scenarios. Figure 10b shows the expected shortfall in the case of choosing the scheduling from the lower quartile scenario, where CVaR(95) is 0.025 and the expected shortfall corresponds to 11,758 € from the targeted profit value.

2.4.4 Correlation among operational variables

In the cryogenic air separation plant, variation in profit is also correlated with the electricity sold back to the grid after having been bought from the futures market in the past. The Spanish electricity market maker has a derivative product called 'SWAP' (OMIE, n.d.) which allows the electricity consumer to sell back the unused contracted power in the futures market or in real time market. The market maker applies a penalty for breach of power contract and takes a commission for enabling the 'SWAP' to sell back the unused contracted power. In figure 2.11 we have presented a scenario in which how the contracted power can be surplus. For low spot market prices, the model schedule the plant for maximum production in those hours thus it becomes possible by the end of scheduling period some contracted power is unused and swapping back of this power presents with a better economic solution then then letting the contract expire without use.

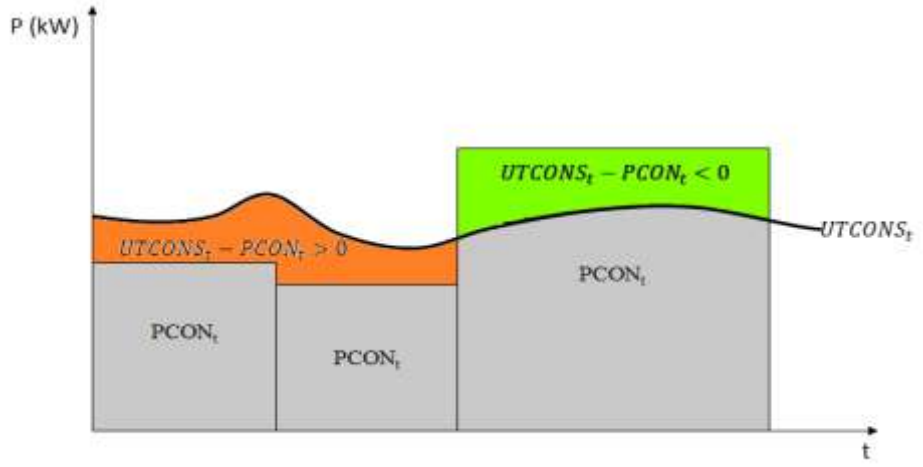

Figure 2.11. An example of electricity consumed depending upon power contracted.

Energy blocks from futures market are purchased in two categories: weekday blocks and weekend block. Thus, we calculate the credits received from the electricity company for electricity sold back to the grid (Eliq) using:

$$Eliq = (TCP - TCC)_{Weekday} + (TCP - TCC)_{Weekend} \qquad (2.73)$$

where TCP is total cost of energy block purchased and TCC is total cost of energy consumed.

Figure2.12 shows the values of output variables (i.e. profit, cost of electricity consumed, and revenues from electricity sold back to the grid) corresponding to the different targeted profit values.

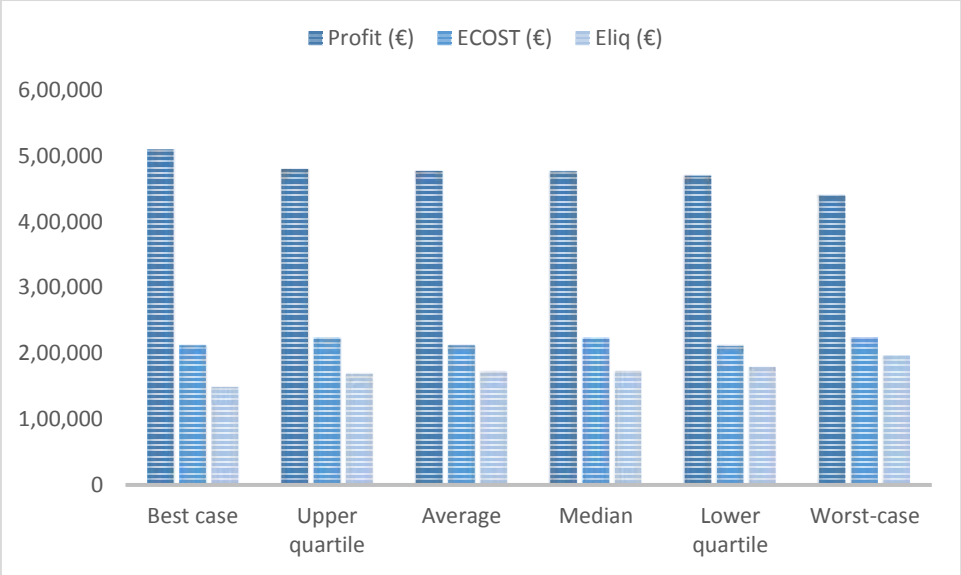

Fig 2.12. Output variable values for scenarios considered for risk analysis.

Analysis of fig. 2.13 suggests that expected profit has a reverse behavior with the electricity sold back to the grid: the lower the 'Eliq', the higher the expected profit, which clearly indicates the importance of a good match of the ratio for the energy blocks to be purchased and the amount energy to be consumed from Spot market. Figure 12 shows this behavior for all the 100 scenarios.

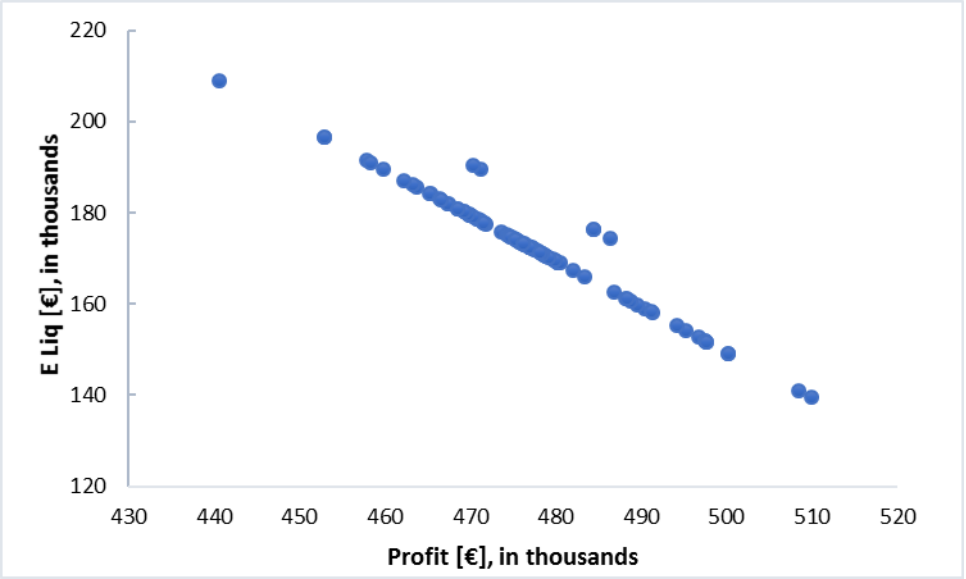

Figure 2.13. Expected profit vs electricity liquidation correlation. 'Eliq' is the credit received for the electricity sold back to the grid. This process is implied under the assumption that the consumer is selling all the surplus contracted power at the spot price in real time market.

2.5 Conclusions

We have developed a methodology to address the scheduling problem of energy intensive industries under the uncertainty of energy market operating 24x7 and applied it to optimally operate a cryogenic air separation plant under electricity price uncertainty for short term scheduling. The case study presented in this contribution corresponds to an installed ASU facility located in Tarragona, Spain. All the model parameters and the ARIMA method for forecasting electricity prices have been tuned to accurately represent the reality of this specific unit. We have used a discrete scenario approach due to the weekly pattern in the spot electricity prices and

in the purchase orders. Further, we hybridized deterministic simulation optimization approach with the discrete scenarios, which resulted in the simplicity of deterministic optimization while incorporating the effectiveness of stochastic considerations by covering a wide range of electricity price scenarios while keeping calculations to a minimum. To develop this approach, we have used a MILP formulation, time series forecasting with ARIMA, and Monte-Carlo scenario generator. The MILP effectively copes with changing electricity prices while maximizing the plant performance. To this end, decisions on flow rates, starts-up and shutdowns of unit operations, and purchase orders are optimized according to the market needs of the existing industrial facility (*i.e.*, demand of liquid N_2, O_2 and Ar and gaseous N_2 and O_2). To forecast hourly electricity prices (*e.g.*, spot market electricity prices) ARIMA model is used with a forecasting accuracy of 85%. The demonstrated approach is computationally affordable and easy to implement. Realistic process scenarios were analyzed to exhibit and establish the usefulness of this methodology. The computational time for this scenario-based analysis was 6.24 CPU-hours for 100 scenarios (in series computation) with a 7-day (168 hours) horizon period. The methodology uses a discrete scenarios approach, and thus can easily be used under the paradigm of parallel computing to significantly reduce the computational time by a factor of number of processors used. The optimization using 100 scenarios entailing different electricity prices shows how these prices affect the plant profit. In the situation of power limitations, the model adjusts the operation to fulfil contractual and demand liabilities, hence avoiding economic penalties. Expected profit values obtained (440644€ - 509922€) provides decision-makers with a wide range of probable values

of the profit. Risk analysis facilitates the decision making of stakeholders in choosing a probable scenario for optimizing the scheduling of the plant with the risk involved for respective scenario by providing values of risk metrices associated (i.e. 0.566 for $\Omega_{average}$) and expected shortfall (i.e. 0.052 for $\Omega_{average}$) for each scheduling. Overall, the model identifies the most profitable ways to operate the plant under the uncertainty of electricity prices in near future. It assists managers to select one probable scenario (based on risk taking capacities) and help them plan their daily activities by effectively optimizing production planning, energy rules, sales and product stocks, at the same time considering external constraints and dynamic market conditions. The output of the methodology also helps financial planning of the organization in a subsequent manner from the insights of risk analysis. Thus, our method provides an encouraging alternative that can be extended to other energy-intensive industrial processes.

In general, the developed methodology is generic and can be easily implemented for the scheduling of any energy intensive industry operating 24x7 under the uncertainty of electricity price market. Also, the computational time can further be reduced by considering a fewer number of scenarios pertaining to statistically significant values while sampling the scenarios for simulation and optimization and using parallel computing.

The scope of this work can be extended in future by implementing the optimization of contracted power based on the prediction of spot electricity market and planning the scheduling under the scenarios of different power contracts and spot electricity

price scenarios to reduce the losses incurring because of the breach of the power contract.

- Acknowledgements

The Universitat Rovira i Virgili authors would like to thank the the "Ministerio de Ciencia, Innovación y Universidades" of Spain [PID2021-127713OA-I00, PID2021-123511OB-C33, PID2021-124139NB-C22 MCIN/AEI/10.13039/501100011033/FEDER, UE & TED2021-129851B-I00] for their financial support to carry out this work.

2.6 Nomenclature

Process Units/Products

CBU	conversion unit
CU	compression unit
DCU	distillation column unit
ECU	external compression unit
EDCU	external distillation column unit
FP	final products

GANIP	gas nitrogen intermediate product
GANP	gas nitrogen product
GOXIP	gas oxygen intermediate product
GOXP	gas oxygen product
ILOXP	industrial liquid oxygen product
LOXIP	liquid oxygen intermediate product
LARIP	liquid argon intermediate product
LARP	liquid argon product
LINP	liquid nitrogen product
LQU	liquefaction unit
MILP	mixed-integer linear programming
MLOXP	medical liquid oxygen product
MX	mixers
OGAN	purchased gas nitrogen
OGOX	purchased gas oxygen
PU	pump unit

PTU	pretreatment unit
SP	splitters
T	storage tank
U	utility
VU	vaporizer unit

Sets/indices

i	set of process units indexed by i
p	set of stream properties indexed by p
s	set of streams indexed by s
t	set of time intervals indexed by t
u	set of utilities indexed by u
sn	set of scenarios

Subsets

EC	set of units i whose electricity consumption is constant

EE	set of units i with electrical consumption
EO	set of external units i whose electricity consumption is accounted for
EV	set of units i whose electricity consumption is variable
FCL	set of streams s with maximum switch flow limitations in a time period
FP	set of streams s which are final products
GP	set of units i whose gasoil consumption is proportional to the input flow
MINCAP	set of units i with a minimum input flow requirement
MO_i	main output stream s of unit i
MS_i	main input stream s of unit i
SI_i	set of input streams s of unit i
SO_i	set of output streams s of unit i
$SPTI_i$	set of units i which are splitters in which one output stream can only be used if the inventory level of the associated tank i is over VSINVi
SPW	set of units i which are binary splitters (i.e., which cannot use more than one output stream simultaneously)
ST	set of units i which are tanks
TVS	set of tanks i which can send tankers to an associated storage plant

UPR2	set of units i which belong to supply process (i.e., downstream the main process)
UPR1	set of units i which belong to the main process
VS	set of streams s which are tankers to a storage plant
GOCONS	total gasoil consumption, L
$INV_{i,t}$	inventory of unit i in time period t, N m^3
$INVD_{i,t}$	disaggregated variable for inventory at level at which it can be depleted by means of tankers (inventory of unit i in time period t), N m^3
PROFIT	profit, €
SALES	sales, €
$UTCONS_{i,u,t}$	consumption of utility u in unit i in time period t, kWh
$Z_{i,d,t}$	auxiliary variable for Fs in interval d of piecewise equation for electricity consumption of unit i in time period t

Binary variables

$y_{i,d,t}$	binary variable (1 if interval d in piecewise equation for electricity consumption of unit i is active in time period t, 0 otherwise)

$yfc_{s,t}$	binary variable (1 if the flow of stream s is switched in binary variable (1 if the flow of stream s is switched in time period t, 0 otherwise)
$yi_{i,t}$	binary variable (1 if unit i is working in time period t, 0 otherwise)
$yinv_{i,t}$	binary variable (1 if inventory of tank i in time period t surpasses the minimum required for it to be depleted by means of tankers, 0 otherwise)
$yon_{i,t}$	binary variable (1 if unit i is switched on in time period t, 0 otherwise)
$yw_{i,t}$	binary variable that equals 1 or 0 depending on which output stream s is used in i in time period t

Parameters

η	vaporizer efficiency
$a_{i,d}$	the slope of a straight-line equation in interval *d* of piecewise linear approximation for electricity consumption of unit i
$b_{i,d}$	independent term of a straight-line equation in interval *d* of piecewise approximation for electricity consumption of unit i
$CAPVOL_i$	maximum capacity allowed for input stream of unit i, N m^3/h
CF	corrective factor between input and output streams in any unit

CF2	corrective factor between OGOX and OGAN in EDCU
$DEM_{s,t}$	demand for a product in stream *s* in time period *t*, N m^3/h
DISC	supplier discount on outsourcing cost, €
DT	idle time in liquefiers, h
$ECONCOST_t$	cost of electricity bought in advance for time period *t*, €/kWh
$ECOST_t$	electricity cost in time period *t*, €/kWh
GOCOST	gasoil cost, €/L
GSCAP	maximum flow allowed for a given stream, N m^3/h
HVAPN2	heat of vaporization of N_2, kJ/N m^3
$INVCAP_i$	capacity of unit i, N m^3
$INVini_i$	inventory of tank *I* at the beginning of the period scheduled, N m^3
$INVfin_i$	inventory of tank *i* requested for the end of the period scheduled, N m^3
LHVGO	lower heating value of gasoil, MJ/L
$lo_{i,d}$	lower bound of interval *d* of piecewise equation for electricity consumption of unit i
MAINTCOST	cost of maintenance applied in unit *i* when it is working in time period t, €/h

$MAXINV_i$	maximum inventory allowed for unit *i*, %
$MAXPR2_t$	maximum electricity that can be consumed in time period t by supply process, kW
$MAXPR1_t$	maximum electricity that can be consumed in time period t by main process, kW
MFCs	maximum flow change allowed in stream *s* in between two consecutive time periods, N m^3/h
$MINCAPVOL_i$	minimum flow rate required for input stream of unit i, N m^3/h
PCHT	product change time, h
MININVi	minimum inventory allowed for unit *i*, %
PCONt	Electricity purchased in advance for time period *t*, kW
PENINV	penalty for the deficit or excess of stored product in the last period time
PENYFC	penalty for changes in the flowrate of streams
PENYON	penalty for the numbers of times a unit is started
PENYW	penalty for the number of times external storage plant is used
PENMB	penalty for the breach of mass balances constraints
$PHTR_t$	electricity consumption in PTU heater in time period t, kWh

PLQ3t	electricity consumption limitation in time period t, kWh
$PRICE_s$	price of product in stream *s*, €/N m^3
PRODISC	unitary price discounted related with EDCU production, €/N m^3
RELATION	amount of product obtained by EDCU to apply the price discount
$SMINCAP_s$	minimum flowrate required for stream *s*, N m^3/h

2.6 References

Acevedot, J., Pistikopoulos, E.N., 1998. Stochastic optimization based algorithms for process synthesis under uncertainty, Computers chem. Engng.

Artificial Intelligence and Expert Systems, 2012. , in: Lees' Loss Prevention in the Process Industries. Elsevier, pp. 2201–2312. https://doi.org/10.1016/b978-0-12-397189-0.00030-6

Associates, C.R., 2005. Prime on Demand Side Management 2017-Janua, 71.

Breeden, J.L., Ingram, D., 2010. Monte Carlo scenario generation for retail loan portfolios Monte Carlo simulation 399–410. https://doi.org/10.1057/jors.2009.105

Brossart, D.F., Laird, V.C., Armstrong, T.W., 2018. Interpreting Kendall's Tau and Tau-U for single-case experimental designs. Cogent Psychol. 5, 1–26. https://doi.org/10.1080/23311908.2018.1518687

Cao, Y., Huang, L., Li, Y., Jermsittiparsert, K., Ahmadi-Nezamabad, H., Nojavan,

S., 2020. Optimal scheduling of electric vehicles aggregator under market price uncertainty using robust optimization technique. Int. J. Electr. Power Energy Syst. 117, 105628. https://doi.org/10.1016/j.ijepes.2019.105628

Cao, Y., Swartz, C.L.E., Baldea, M., Blouin, S., 2015. Optimization-based assessment of design limitations to air separation plant agility in demand response scenarios. J. Process Control 33, 37–48. https://doi.org/10.1016/j.jprocont.2015.05.002

Cao, Y., Swartz, C.L.E., Flores-cerrillo, J., 2016. Optimal Dynamic Operation of a High-Purity Air Separation Plant under Varying Market Conditions. https://doi.org/10.1021/acs.iecr.6b02090

Castro, P.M., Grossmann, I.E., Zhang, Q., 2018. Expanding scope and computational challenges in process scheduling. Comput. Chem. Eng. https://doi.org/10.1016/j.compchemeng.2018.01.020

Charitopoulos, V.M., Dua, V., 2017. A unified framework for model-based multi-objective linear process and energy optimisation under uncertainty. Appl. Energy 186, 539–548. https://doi.org/10.1016/j.apenergy.2016.05.082

Chen, Y., Feng, X., Li, Z., Xu, Y., Miragha, A., 2020. Multi-stage coordinated operation of a multi-energy microgrid with residential demand response under diverse uncertainties. Energy Convers. Econ. 1, 20–33. https://doi.org/10.1049/enc2.12002

Conejo, A.J., Plazas, M.A., Espinola, R., Molina, A.B., 2005. Day-Ahead

Electricity Price Forecasting Using the Wavelet Transform and ARIMA Models. IEEE Trans. Power Syst. 20, 1035–1042. https://doi.org/10.1109/TPWRS.2005.846054

Dias, L.S., Pattison, R.C., Tsay, C., Baldea, M., Ierapetritou, M.G., 2018. A simulation-based optimization framework for integrating scheduling and model predictive control , and its application to air separation units. Comput. Chem. Eng. 113, 139–151. https://doi.org/10.1016/j.compchemeng.2018.03.009

Dowling, A.W., Kumar, R., Zavala, V.M., 2017. A multi-scale optimization framework for electricity market participation. Appl. Energy 190, 147–164. https://doi.org/10.1016/j.apenergy.2016.12.081

Dowling, A.W., Zavala, V.M., 2018. Economic opportunities for industrial systems from frequency regulation markets. Comput. Chem. Eng. 114, 254–264. https://doi.org/10.1016/j.compchemeng.2017.09.018

Elmore, C.T., Dowling, A.W., 2021. Learning spatiotemporal dynamics in wholesale energy markets with dynamic mode decomposition. Energy 232, 121013. https://doi.org/10.1016/j.energy.2021.121013

Energy Use in Industry - Energy Explained, Your Guide To Understanding Energy - Energy Information Administration [WWW Document], n.d. URL https://www.eia.gov/energyexplained/index.php?page=us_energy_industry#tab1 (accessed 6.21.19).

EViews.com [WWW Document], n.d. URL http://www.eviews.com/home.html (accessed 7.29.20).

Fernández, D., Pozo, C., Folgado, R., Guillén-Gosálbez, G., Jiménez, L., 2017. Multiperiod model for the optimal production planning in the industrial gases sector. Appl. Energy 206, 667–682. https://doi.org/10.1016/j.apenergy.2017.08.064

Finn, P., Fitzpatrick, C., 2014. Demand side management of industrial electricity consumption: Promoting the use of renewable energy through real-time pricing. Appl. Energy 113. https://doi.org/10.1016/j.apenergy.2013.07.003

GAMS software [WWW Document], n.d. URL https://www.gams.com/products/gams/gams-language/

Gao, X., Knueven, B., Siirola, J.D., Miller, D.C., Dowling, A.W., 2022. Multiscale simulation of integrated energy system and electricity market interactions. Appl. Energy 316, 119017. https://doi.org/10.1016/j.apenergy.2022.119017

Gebreslassie, B.H., Guillén-Gosálbez, G., Jiménez, L., Boer, D., 2009. Economic performance optimization of an absorption cooling system under uncertainty. Appl. Therm. Eng. 29, 3491–3500. https://doi.org/10.1016/j.applthermaleng.2009.06.002

Grossmann, I.E.I., Caballero, J.A.J., Yeomans, H., 1999. Mathematical programming approaches to the synthesis of chemical process systems. Korean J. Chem. Eng. 16, 407–426. https://doi.org/10.1007/BF02698263

Ierapetritou, M.G., Wu, D., Vin, J., Sweeney, P., Chigirinskiy, M., 2002. Cost Minimization in an Energy-Intensive Plant Using Mathematical Programming Approaches. Ind. Eng. Chem. Res. 41, 5262–5277. https://doi.org/10.1021/ie011012b

Jakaša, T., Andročec, I., Sprčić, P., 2011. Electricity price forecasting ARIMA model approach. 2011 8th Int. Conf. Eur. Energy Mark. EEM 11 222–225. https://doi.org/10.1109/EEM.2011.5953012

Kelley, M.T., Baldick, R., Baldea, M., 2020. Demand response scheduling under uncertainty: Chance-constrained framework and application to an air separation unit. AIChE J. 66. https://doi.org/10.1002/aic.16273

Kelley, M.T., Pattison, R.C., Baldick, R., Baldea, M., 2018. An MILP framework for optimizing demand response operation of air separation units. Appl. Energy 222, 951–966. https://doi.org/10.1016/j.apenergy.2017.12.127

Kelley, M.T., Tsay, C., Cao, Y., Wang, Y., Flores-cerrillo, J., Baldea, M., 2022. A data-driven linear formulation of the optimal demand response scheduling problem for an industrial air separation unit. Chem. Eng. Sci. 252, 117468. https://doi.org/10.1016/j.ces.2022.117468

Knopf, P.M., Teall, J.L., 2015. Risk neutral pricing and financial mathematics: A primer, Risk Neutral Pricing and Financial Mathematics: A Primer. Elsevier Inc. https://doi.org/10.1016/C2014-0-00295-X

Li, Z., Xu, Y., Feng, X., Wu, Q., 2021a. Optimal Stochastic Deployment of

Heterogeneous Energy Storage in a Residential Multienergy Microgrid with Demand-Side Management. IEEE Trans. Ind. Informatics 17, 991–1004. https://doi.org/10.1109/TII.2020.2971227

Li, Z., Xu, Y., Wu, L., Zheng, X., 2021b. A Risk-Averse Adaptively Stochastic Optimization Method for Multi-Energy Ship Operation under Diverse Uncertainties. IEEE Trans. Power Syst. 36, 2149–2161. https://doi.org/10.1109/TPWRS.2020.3039538

Mazengia, D.H., 2008. Forecasting spot electricity market prices using time series models. 2008 IEEE Int. Conf. Sustain. Energy Technol. 1256–1261. https://doi.org/10.1109/ICSET.2008.4747199

Medina-gonzález, S., Pozo, C., Corsano, G., Guillén-gósalbez, G., Espu, A., 2017. Using Pareto filters to support risk management in optimization under uncertainty : Application to the strategic planning of chemical supply chains 98, 236–255. https://doi.org/10.1016/j.compchemeng.2016.10.008

Merkert, L., Harjunkoski, I., Isaksson, A., Säynevirta, S., Saarela, A., Sand, G., 2015. Scheduling and energy - Industrial challenges and opportunities. Comput. Chem. Eng. 72, 183–198. https://doi.org/10.1016/j.compchemeng.2014.05.024

Misra, S., Kapadi, M., Gudi, R.D., Srihari, R., 2017. Energy-Efficient Production Scheduling of a Cryogenic Air Separation Plant. Ind. Eng. Chem. Res. 56, 4399–4414. https://doi.org/10.1021/acs.iecr.6b04585

Mitra, S.., Grossmann, I.E.., Pinto, J.M.., Arora, N.., 2012. Optimal production planning under time-sensitive electricity prices for continuous power-intensive processes. Comput. Chem. Eng. 38, 171–184. https://doi.org/http://dx.doi.org/10.1016/j.compchemeng.2011.09.019

Mohamed, K., Bouhania, G., 2014. Scenario-Based Methods and the Complexity of 04, 157–168.

Oberdieck, R., Diangelakis, N.A., Nascu, I., Papathanasiou, M.M., Sun, M., Avraamidou, S., Pistikopoulos, E.N., 2016. On multi-parametric programming and its applications in process systems engineering. Chem. Eng. Res. Des. 116, 61–82. https://doi.org/10.1016/j.cherd.2016.09.034

OMIE, n.d. No Title [WWW Document]. URL https://www.omip.pt/en/electricity

Pattison, R.C., Touretzky, C.R., Harjunkoski, I., Baldea, M., 2017. Moving horizon closed-loop production scheduling using dynamic process models. AIChE J. 63, 639–651. https://doi.org/10.1002/aic.15408

Rezaei, F., Najafi, A.A., Ramezanian, R., 2020. Mean-conditional value at risk model for the stochastic project scheduling problem. Comput. Ind. Eng. 142, 106356. https://doi.org/10.1016/j.cie.2020.106356

Rockafellar, R.T., Uryasev, S., 2002. Conditional value-at-risk for general loss distributions. J. Bank. Financ. 26, 1443–1471. https://doi.org/10.1016/S0378-4266(02)00271-6

Sahinidis, N. V., 2004. Optimization under uncertainty: State-of-the-art and

opportunities. Comput. Chem. Eng. 28, 971–983. https://doi.org/10.1016/j.compchemeng.2003.09.017

Sarykalin, S., Serraino, G., Uryasev, S., 2008. Value-at-Risk vs. Conditional Value-at-Risk in Risk Management and Optimization. State-of-the-Art Decis. Tools Information-Intensive Age 270–294. https://doi.org/10.1287/educ.1080.0052

Scharfhausen, F.M., 2009. Electricity Tariff Structure : The Spanish case.

Smith, A.R., Klosek, J., 2001. A review of air separation technologies and their integration with energy conversion processes. Fuel Process. Technol. 70, 115–134. https://doi.org/10.1016/S0378-3820(01)00131-X

Sorourifar, F., Zavala, V.M., Dowling, A.W., 2020. Integrated Multiscale Design , Market Participation , and Replacement Strategies for Battery Energy Storage Systems 11, 84–92.

Todd, D., Caufield, M., Helms, B., Starke, M., Kirby, B., Kueck, J., 2009. Providing Reliability Services through Demand Response: A Preliminary Evaluation of the Demand Response Capabilities of Alcoa Inc., Technical report ORNL/TM-2008/233.

Tsay, C., Kumar, A., Flores-cerrillo, J., Baldea, M., 2019. Optimal demand response scheduling of an industrial air separation unit using data-driven dynamic models R. Comput. Chem. Eng. 126, 22–34. https://doi.org/10.1016/j.compchemeng.2019.03.022

U.S. Energy Information Administration, 2016. Chapter 7 : Industrial sector energy

consumption [WWW Document]. Int. Energy Outlook. URL https://www.eia.gov/outlooks/ieo/pdf/industrial.pdf (accessed 10.30.20).

Verderame, P.M., Elia, J.A., Li, J., Floudas, C.A., 2010. Planning and scheduling under uncertainty: A review across multiple sectors. Ind. Eng. Chem. Res. 49, 3993–4017. https://doi.org/10.1021/ie902009k

Vieira, M., Paulo, H., Vilard, C., Pinto-Varela, T., Barbosa-Póvoa, A.P., 2018. Risk assessment for the design and scheduling optimization of periodic multipurpose batch plants under demand uncertainty, Computer Aided Chemical Engineering. Elsevier Masson SAS. https://doi.org/10.1016/B978-0-444-64235-6.50174-1

Wang, Y.C., Chiu, M.C., Chen, T., 2020. A fuzzy nonlinear programming approach for planning energy-efficient wafer fabrication factories. Appl. Soft Comput. J. 95, 106506. https://doi.org/10.1016/j.asoc.2020.106506

Weron, R., 2014. Electricity price forecasting: A review of the state-of-the-art with a look into the future. Int. J. Forecast. 30, 1030–1081. https://doi.org/10.1016/j.ijforecast.2014.08.008

Weskamp, C., Koberstein, A., Schwartz, F., Suhl, L., Voß, S., 2019. A two-stage stochastic programming approach for identifying optimal postponement strategies in supply chains with uncertain demand. Omega (United Kingdom) 83, 123–138. https://doi.org/10.1016/j.omega.2018.02.008

Wu, C.B., Huang, G.H., Li, W., Xie, Y.L., Xu, Y., 2015. Multistage stochastic

inexact chance-constraint programming for an integrated biomass-municipal solid waste power supply management under uncertainty. Renew. Sustain. Energy Rev. https://doi.org/10.1016/j.rser.2014.09.019

XPRESS Solver [WWW Document], n.d. URL https://gams.com/latest/docs/RN_26.html

Zamarripa, M., Marchetti, P.A., Grossmann, I.E., Singh, T., Lotero, I., Gopalakrishnan, A., Besancon, B., André, J., 2016. Rolling Horizon Approach for Production-Distribution Coordination of Industrial Gases Supply Chains. Ind. Eng. Chem. Res. 55, 2646–2660. https://doi.org/10.1021/acs.iecr.6b00271

Zhang, Q., Bremen, A.M., Grossmann, I.E., Pinto, J.M., 2018. Long-Term Electricity Procurement for Large Industrial Consumers under Uncertainty. Ind. Eng. Chem. Res. 57, 3333–3347. https://doi.org/10.1021/acs.iecr.7b04589

Annex 1.

Multi objective optimization, sensitivity analysis and decision making

Annex 1. Multi objective optimization, sensitivity analysis and decision making

---

Sustainable Insights on Emerging Solar District Heating Technologies to Boost the Nearly Zero Energy Building Concept

Mohamed Hany Abokersh [a], Sachin Gangwar [a], Marleen Spiekman [b], Manel Vallès [a], Laureano Jiménez [c], Dieter Boer [a*]

[a] Departament d'Enginyeria Mecànica, Universitat Rovira i Virgili, Av. Països Catalans 26, 43007 Tarragona, Spain

[b] Department of Building Physics and Systems, TNO, Leeghwaterstraat 44, Delft, the Netherlands

[c] Departament d'Enginyeria Química, Universitat Rovira i Virgili, Av. Països Catalans 26, 43007 Tarragona, Spain

Keywords: Solar assist district heating system; Nearly zero energy building; Life cycle assessment; Multi-objective optimization; Multi-criteria decision making; Sustainability targets

A.1.1. Introduction

The world population is expected to consume 50% more energy by 2035 (compared to 1990) due to rapid growth in population, infrastructure, technology, and energy-intensive systems. This aspect has a direct impact on building energy

consumption (Ghosh, 2020). In the European Union (EU), the building sector alone accounts for approximately 40% of total energy consumption and 36% of the total CO_2 emissions (M. Abokersh et al., 2020). Consequently, a more sustainable and climate oriented efficient building stock is needed to achieve climate-neutral Europe's goals by 2050. Corporations in the infrastructure industry face an urgent need to change their traditional practices in terms of energy access and its use to reduce building stocks' energy needs. International bodies set guidelines to follow the nearly/net-zero energy building (NZEB) route. The NZEB concept is vastly interpreted as the utilization of renewable energy to satisfy building energy need. Sustainable energy authority of Ireland defines NZEB as '*a building that has a very high energy performance, and the nearly zero or very low amount of energy required should be covered to a very significant extent by energy from renewable sources, including energy from renewable sources produced on-site or nearby*'("Nearly Zero Energy Building Standard | Business & Public Sector | SEAI," n.d.). However, communities worldwide have not yet reached a consensus on the definition (Luo et al., 2019). National Renewable Energy Laboratory of the United States has classified NZEB as a range of buildings, e.g., from a building that offsets all of its energy needs from renewable energy resources available on-site' to a building that achieves an NZEB status through a combination of on-site renewables and off-site purchases of renewable energy credits (Ely Lecture et al., 2008). The Energy Performance of Building Directive (EPBD) from the EU, requires all new buildings to be NZEB from 2021 and aims to achieve a highly decarbonized building stock by 2050 for existing and new buildings (Directives 2010/31/EU and 2018/844/UE) (Commission, 2020).

Driving forces for the rise of NZEBs have been explained in detail elsewhere (Lai et al., 2017), showing the social, economic and environmental benefits. To achieve this transition, centralized and decentralized renewable energy usage can push net-zero energy buildings. Currently, Europe has 70% of the building stock needed by 2050 and improving the existing building stock's energy efficiency is an effective way to reduce energy demand (Al Dakheel et al., 2020), so this paper focuses on installable renewable energy solutions to satisfy the energy demand on building stock (Hamburg et al., 2020).

The transition of existing building blocks towards NZEB can be achieved by improving the building's energy efficiency, equipping the building block with renewable energy generation sources and connecting the building block with the district heating (DH) network. 4th generation district heating (4GDH) network is a promising concept to reduce high energy losses and installation and maintenance cost of previous generations district heating systems (Lund et al., 2018). The high performance of 4GDH is attributed to its low-operation temperature (50–60°C). However, more research is required for the broad implementation of 4GDH (Li and Nord, 2018). The use of renewable energy technology and DH networks can reduce the building block's carbon footprint and, thus, building blocks with low carbon emission are called Low Carbon Buildings (LCB), building blocks with net-zero carbon emission called Net Zero Energy Building (NZEB). A plethora of research is available on the NZEB with different energy sources and different perspectives. While some of the researchers have used photovoltaics, solar thermal systems, geothermal systems (Gondal, 2020), others have tried to measure the prospects of

conventional smart energy systems and net metering (Li and Nord, 2018). While the research has been catching up to the target of carbon neutrality and the NZEB concept (Grillone et al., 2020), some researchers have also developed positive energy buildings (PEBs). PEB essentially means that the building or the building stock can satisfy its energy demand and be able to produce more energy to supply to the centralized district heating (DH) network (thermal energy) or the grid (electrical energy). Research in PEB is still in its nascent stage, and till now very few researchers have tried to make the transition from low carbon buildings to nearly zero energy buildings to positive energy buildings (Magrini et al., 2020). The concept of integrating smart energy systems to connect the building stock with grid and district heating network has also been studied (Behzadi et al., 2020) and the technical feasibility of the building stock (Behzadi and Arabkoohsar, 2020). The smart energy system is a broader concept which suggests the load reduction on the electrical grid by connecting the demand to the respective energy networks (i.e., electricity demand to the electricity grid, heating demand to district heating networks, etc.). Smart energy system also incorporates the concept of net metering, thereby addressing the component of direct financial benefit to the user for the implementation of such a system. The futuristic vision of high energy performance building stock can be achieved with smart energy system integration, especially in cold regions, by connecting to 4GDH (Abokersh, Mohamed Hany, Kangkana Saikia, Luisa F cabeza, Dieter Boer, 2020). To implement EPBD regulations towards the NZEB transition, the Netherlands set the guidelines for achieving energy efficiency and the building's rating (Commission, 2020). These indicators collectively form “EPC” (energy

performance coefficient), which standardize the process of building energy efficiency rating (Hany et al., 2021).

Netherlands has a high potential for retrofit residential building stock and connects to renewable energy sources to reduce greenhouse gas emissions (GHG) (Majcen et al., 2013). Numerous efforts are being made to satisfy building energy consumption by renewable energy system installation (e.g., rooftop PV (Hong et al., 2017), geothermal heat pumps (Jeong et al., 2018), solar-assisted heat pumps (Rehman et al., 2018), passive heating and cooling (Cao et al., 2016)). Researchers have analyzed from the life cycle perspective (Marszal et al., 2012) building integrated solutions with photovoltaics (PV) (Susan and Wardhani, 2020), increased renewable energy input with multiple systems (Song et al., 2019), comprehensive solar energy solutions with PV and flat plate collectors (Barone et al., 2020) to satisfy the energy demand of the building and to assess the greenhouse gas emission. Extensive research has been done on case studies related to the application of photovoltaics (Ghosh, 2020), solar thermal applications (Li et al., 2020) and technological design option for PV (Kuhn et al., 2020) in NZEBs and low carbon energy buildings. Given the environmental benefits associated with renewable energy utilization in buildings, a global rise has been observed in the area of NZEB and the low-carbon buildings (LCBs) application and research (Luo et al., 2019).

The availability of various green energy solutions has led to the adoption of different approaches by the researchers. In attempts to reach NZEB status, Dawood et al. (Dawood et al., 2013) suggested a framework that includes the integration of

energy simulation tools, national calculation methods and codes for low carbon buildings (LCB) and multi-criteria decision making (MCDM) to support the building design process. However, this framework was specifically addressing the architects for retrofitting. To emphasize the impact of various key areas, researchers have also used MCDM: for energy systems design optimization to encounter load uncertainty (Sun et al., 2015), for building design optimization methods (Mokhtara et al., 2019), for assessment and ranking of renewable energy technology (Laguna Salvad et al., 2019) to point out the key decision-makers. Hang et al.(Chang and Wei, 2021) has summed up the findings of major agencies and researchers to move from low carbon buildings to NZEB: (i) assessing the energy and GHG emissions; (ii) optimizing the on-site and off-site distribution of renewable energy; (iii) answering low carbon buildings (LCB) potentials through high-performance energy end-use devices and occupants' green behavior.

Achieving NZEB or PEB status for a building requires optimization of numerous variables (e.g. selection of an optimal renewable energy technology (Pinamonti and Baggio, 2020), optimizing building energy design (Li and Wang, 2019), optimizing the use of energy-efficient material). (Zhou et al., 2020). Classical and metaheuristic optimization methods are not able to effectively optimize a large number of variables simultaneously as require large computational resources. Optimizing a multivariate objective function is difficult for non-confluent variables with mathematical programming, and some researchers use machine learning (Bengio et al., 2020). With the use of machine learning, Rehman et al. (Rehman et al., 2020) analyzed and optimized a building integrated photovoltaic panel, battery

and use of electric vehicles in central European climatic condition, Han et al. (Han et al., 2020) optimized the fault diagnosis of a building energy system, and Salah et al. (Seyedzadeh et al., 2020) predicted the building energy performance to support deep energy retrofit. The use of machine learning by various researchers has been reviewed by Fathi et al. (Fathi et al., 2020) in urban building energy performance forecasting, by Mishra (Mishra, 2020) for structural health monitoring of heritage buildings, by Sun et al. (Sun et al., 2020) for building structural design and performance assessment, by Ayoub (Ayoub, 2020) to predict daylighting inside buildings and by Hong et al. (Hong et al., 2020) in the area of building life cycle. The use of machine learning in energy systems design, sizing and techno-economic analysis and environmental analysis to achieve NZEB targets is yet to be explored. We have used a machine learning approach based on an artificial neural network (ANN) to optimize a multi-objective function that incorporating economic, environmental, and social variables. The robustness of these optimization approaches can be investigated with a global sensitivity analysis (GSA) against the uncertain parameters. GSA is an extensive tool to identify the major parameters causing uncertainty into an optimization model. Mavromtidis et al. (Mavromatidis et al., 2018) used GSA to determine the major causes of variation in economic and energy performance optimization of a distributed energy system. The use of GSA to provide the cushion against parameter uncertainty in energy system design is extensive (You and Kim, 2020). Zhang et al have used GSA or key parameters identification of net-zero energy buildings for grid interaction optimization (Zhang et al., 2020). Hence, machine

learning in conjugation with GSA is gaining popularity for energy systems optimization under uncertainty for NZEB.

The available literature on NZEB unanimously recommends the integration of renewable energy into building footprints. Therefore, we aim to achieve the PEB targets by retrofitting a building stock situated in North-East Netherlands (Emmen). We are trying to achieve PEB status following the 4GDH principles to satisfy the heating and adding a rooftop PV system to meet the building stock's electricity demand. In addition, we connected the model to the electricity grid and centralized DH network.

Hence, this work's novelty lies in demonstrating the sustainable aspects for integrating 4GDH at various residential community sizes located in the Netherlands to achieve NZEB targets. Additionally, this paper develops a MCDM framework based on optimal scenarios to support the selection of the most sustainable system design at various residential community size. This work suggests a roadmap for a transition from LCBs to PEBs with the integration of seasonal storage, heat pumps, PV, and smart energy systems. The structure of this article is as follows: section A.1.2 shows a complete description of the 4GDH system and neighborhood demand. Section A.1.3 describes the sustainable criteria to evaluate the DH performance. The ANN model's mathematical description and its coupling with a multi-objective optimization framework are presented and discussed in section A.1.4. The post-analysis of the optimal solutions, including the MCDM and GSA, is shown in Section

A.1.5. Section A.1.6 offers the required results and discussion. Finally, the work summary and conclusion are shown in section A.1.7.

A.1.2. System Description

A.1.2.1. Roof-mounted hybrid solar assisted district heating

A typology of solar assisted district heating system (SDHS) combined with heat pump (HP) is designed for a residential neighbourhood in the Netherlands to supply yearly demand of space heating (SH), domestic hot water (DHW) and electricity, as shown in Fig. A.1.1. This system primarily incorporates roof-mounted solar thermal collectors (ST) and photovoltaic panels (PV), a seasonal thermal storage tank (SST), a domestic hot water tank (DHWT), central water to water HP unit, and auxiliary heaters fuelled by natural gas. HP serves as a heat input source for both SST and DHWT. For this arrangement, heat collected via the ST is used to meet SH/DHW demand, where the heat is transferred across the distribution network through heat exchangers using 'Y' valves. Contingent to operational mode, the heat produced by HP is either used for SH or DHW with potential application for SST heat charging. For the winter season, the SST is used to satisfy SH demand, whereas short-term DHWT meets the daily DHW. The heat is supplied at low-temperature (50°C) for space-heating, while the heat to DHW is supplied at higher-temperature (60°C). Lastly, when solar collectors, HP and SST are not able to satisfy the heat load, the disparity is overcome via auxiliary heaters. On the other hand, the electricity demand comprising both the neighbour and SDHS electric equipment is covered by a combination of the on-grid roof-mounted PV panels and the electricity grid.

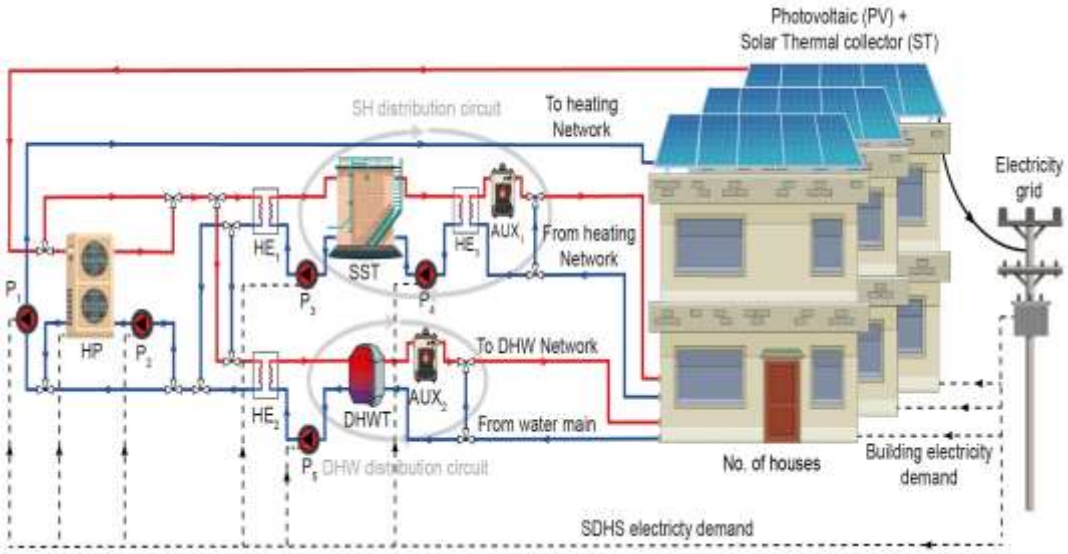

FIG. A.1.1: SCHEMATIC OF ROOF-MOUNTED HYBRID SOLAR ASSISTED DISTRICT HEATING NETWORK

An efficient control strategy is adopted to meet the residential neighbourhood heating demand maximizing the use of solar energy and minimizing the network heat losses. Four modes of operation are planned considering the temperature levels of SDHS, which are enabled via on-off control switches. At the start:

1) In the first operational Mode or DHW operation mode, the heat obtained by solar collectors is transported to the DHWT with the help of P_1, P_2, and P_5 pumps through HE_2. When the solar thermal energy is not enough to satisfy the demand in the DHW network, the auxiliary heater (AUX_2) is enabled. During DHW mode, the HP unit does not operate.
2) In the second mode, the SH gets initiated when a suitable level of temperature in DHWT (T_{DWT}) is reached while the temperature of the collector (T_{COL}) is

at a higher temperature than the bottom of the SST (T_{SST}). In this mode of operation, P_1, P_2, P_3 pumps are used to transfer heat to SST from ST via HE_1.

3) In the third operation mode, a concurrent operation of DHW and SH circuits gets initiated when the criteria of DHW and SH operations are met and $T_{SST} > T_{DHWT}$.

4) In the fourth mode of operation, HP operates if the solar thermal system fails to satisfy the heating demand. Thus, in this mode of operation, the HP is activated when the $T_{COL} < T_{SST}$ which, subsequently is less than the reference turn-on temperature of the heat pump (T_{ref}). Under the HP operation mode, the heat generated is transported to either SST or DHWT depending on the demand. In this case, the uncovered heat demand is met by using the auxiliary heaters as well. In cooperation with the thermal SDHS part, the on-grid PV panels are integrated to reduce the purchased electricity from the supply grid while covering both the neighbourhood electric demand and SDHS electric equipment.

A.1.2.2. Simulation model

To model and analyse the SDHD system behaviour, TRNSYS 18 (Klein, 2004) has been used. This software uses partial differential equations and input constraints as limits for mass and energy conservation with defined boundary conditions. Due to the intrinsic dynamic nature of the system, it offers a realistic simulation of hybrid SDHS (MH Abokersh, M Vallès, LF Cabeza, 2020). In order to reduce the computational cost, the hybrid SDHS model has been simulated for three

benchmarking operational years. The solution is then inferred over the project lifetime, assuming that weather data and demand profiles are constant over the project lifetime (40 years). The SDHS model validation is performed based on the implemented work by Abokersh et al. (Abokersh, Mohamed Hany, Kangkana Saikia, Luisa F cabeza, Dieter Boer, 2020) and Tulus et al. (Tulus et al., n.d.), incorporating the hybrid solar circuits and their control schemes. The information flow diagram is shown in Fig. A.12. (Type – inside TRNSYS GUI).

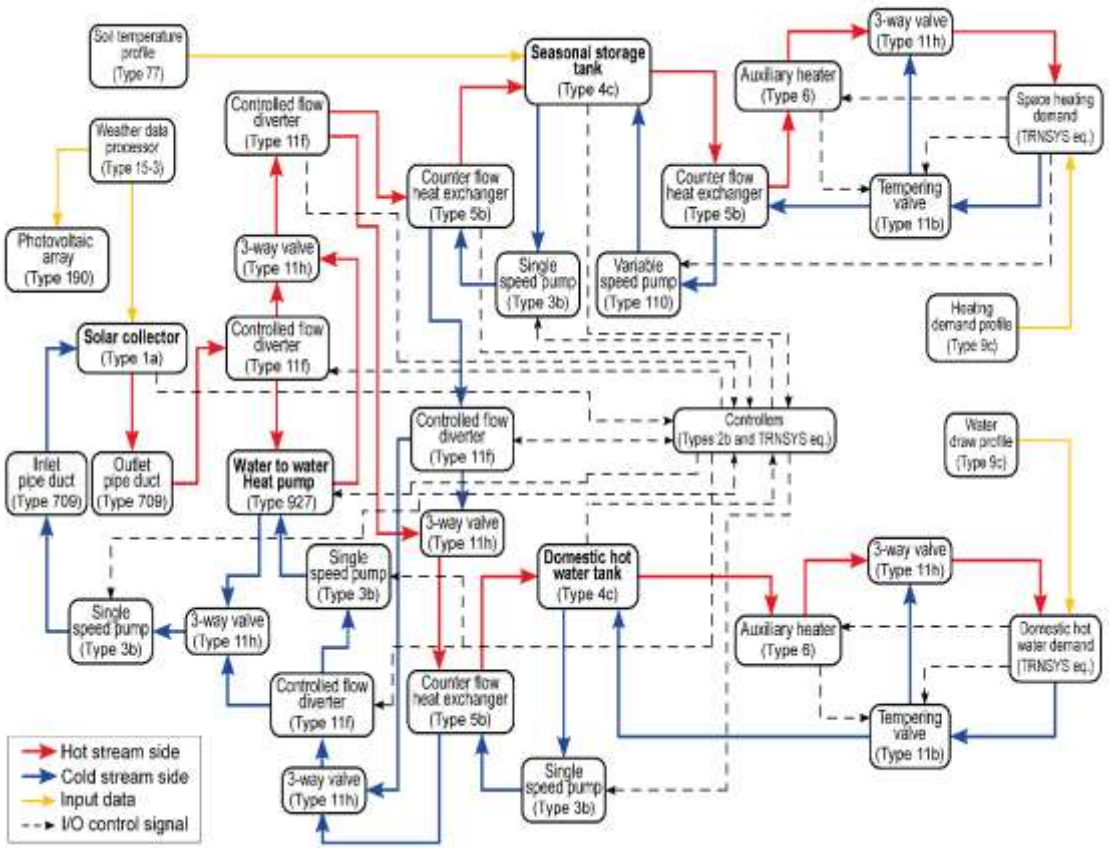

FIG. A.12: FLOW DIAGRAM OF THE SDHS SYSTEM SIMULATED, WITH THE COMPONENTS AND THEIR INTERCONNECTIONS USED TRNSYS 18.

Each component has information boxes for component-specific parameters and input-output variables. Mainly the model includes the following types: flat plate solar collectors (Type 1a) with an optical efficiency of 0.817, heat loss coefficient of 2.205 $W/m^2 \cdot K$; PV panel (Type 190) with a module conversion efficiency of 0.186; water to the water heat pump (Type 927); fully stratified storage tanks (Type 4c) with heat loss coefficient of 0.3125 $W/m^2 \cdot K$ for the DHWT, whereas the SST heat loss coefficient is a function of the selected construction materials; counterflow heat exchangers (Type 5b) with overall heat transfer coefficient of 3.931 $kW/m^2 \cdot K$; and auxiliary heaters (Type 6) with an efficiency of 93%. The secondary units are: single speed centrifugal pumps (Type 3b), inlet and outlet pipe ducts (Type 709), three-way valves (Type 11 h), controlled flow diverters (Type 11f), tempering valves (Type 11b), soil temperature profile for the SST (Type 77), weather data (Type 15-3), time-dependent forcing functions for the heating and DHW demand profiles (Type 9c), and controllers (Type 2b).

The thermal performance of a fluid-filled sensible energy storage tanks (Type 4c), subject to thermal stratification, can be modeled by assuming that the tank consists of N (N <= 100) fully mixed equal volume segments. The degree of stratification is determined by the value of N. If N is equal to 1, the storage tank is modeled as a fully mixed tank, and no stratification effects are possible. At the current work, the storages are divided into 12 nodes for considering the stratification effect. This instance of Type 4 models a stratified tank having variable inlet positions such that entering fluid may be added to the tank at a temperature as nearly equal to its own temperature as

possible. This instance further assumes that losses from each tank node are equal and does not compute losses to the gas flue of the auxiliary heater.

A.1.2.3. Decentralized reference case (Base case)

In this setup, the heating demand (SH&DHW) of each building in the residential neighbourhood is satisfied through an individual air source heat pump (PUHZ-SW50VHA) with a Coefficient of performance equal to 5 (Hany et al., 2021). The heat pump compressor controller managed the required flow temperature based on the weather compensation routine and the zone setpoint (user adjusted). While the dwelling electric demand is met through the national grid. A schematic drawing for this decentralized system is shown in Fig. A.1.3.

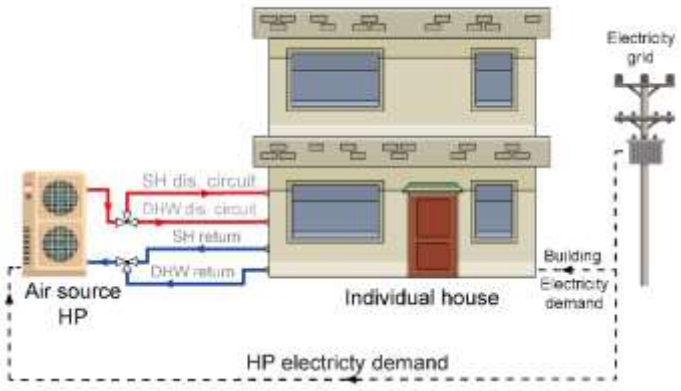

FIG. A.1.3: SCHEMATIC DRAWING FOR THE DECENTRALIZED AIR SOURCE HEAT CONNECTED TO THE SUPPLY GRID TO COVER AN INDIVIDUAL HOUSE DEMAND

A.1.2.4. The neighborhood description and demand profiles

The neighbourhood consists of 10 newly retrofitted houses located in Emmen, Netherlands (Hany et al., 2021). The dwelling layout is shown in Fig. A.1.4, where each floor area is 60 m^2, and the ceiling height is 3 m. The considered dwelling has two external façades with a total area of 33.7 m^2, oriented to the East and West, whereas the opaque part represents 19.6 m^2. The outer walls of each dwelling are made of two primary walls, which are made using hollow bricks coated with plaster and insulation layers. The interior partition walls, made of gypsum boards, are finished with light concrete. The floor is made of two surfaces; the main ground surface comprises layers of insulation material, concrete, and stones, whereas the ground floor's inward surface is made of light concrete with gypsum boards. Moreover, the top roof surface composed of multiple layers of light concrete and plaster with insulation. A summary of the construction material properties is shown in Table A.11.

TABLE A.11: THERMAL PROPERTIES OF THE BUILDING ENVELOPES (HANY ET AL., 2021)

Parameter name	Unit	Value
RC_{roof}	[m^2K/W]	5
RC_{floor}	[m^2K/W]	5
RC_{facade}	[m^2K/W]	4.7
U_{glass}	[W/m^2K]	1.1
G_{value}	-	0.7

To obtain real-time weather data for the dwelling, the climate data are obtained from a KNMI weather station. The nearest KNMI weather station to the dwellings in Emmen is in the Hoogeveen (STN:279, LON(east):6.574, LAT(north):52.750, ALT(m):15.80), which is approximately 25-30 km away from the dwellings. The solar radiation in Emmen (Netherlands) varies from 23 kWh/m^2 in December to 155 kWh/m^2 in May. In summer (May-August), the solar radiation is towards the upper range of solar irradiance range. The heating and electricity demands are extracted from the hourly TNO measurements for these dwellings (Hany et al., 2021). The buildings are heated up through radiators on all levels that are primarily provided by an air source heat pump (PUHZ-SW50VHA) at each building. The heat pump compressor controller managed the required flow rate based on the thermostats and the zone setpoint (user adjusted). Therefore, a variation in the heat pump performance factor (COP) is recognized with the variation in the ambient air temperature. Base on the time-dependent of the COP and its relative heat pump electricity consumption, the thermal heat pump power is estimated.

FIG. A.1.4: GENERAL VIEW FOR THE EMMEN DWELLING

The thermal demand of the neighbourhood consists of an annual DHW demand of 5.29 MWh/house, and SH demand of 4.14 MWh/house. Apart from the heat demand, the annual electricity demand (5.53 MWh/house) is currently supported by the electricity grid. The total energy demand and its monthly variation for the dwelling are plotted in Fig. A.1.5 alongside with monthly solar radiation and average monthly ambient temperature. DHW and electricity demand is decreased in the months of summer due to reduced activities of occupants in these months, while the space heating demand is significantly higher in winter due to low ambient temperatures and increased indoor occupant hours. Energy demand profiles (heat demand load for SH, DHW, and demand load for electricity) are provided as inputs variables for the time-dependent simulations of entire cases.

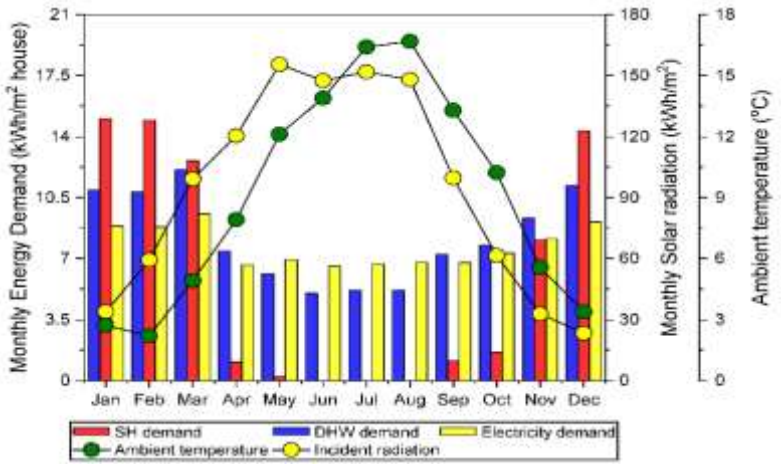

FIG. A.1.5: MONTHLY AVERAGE ENERGY DEMAND PROFILE, SOLAR RADIATION PROFILE AND AMBIENT TEMPERATURE PROFILE

A.1.3. SDHS sustainability assessment

In the context of NZEB, the developed framework assesses proposed SHDS based on four main criteria: energy performance based on established energy efficiency indicators for the dwelling, the social indicator for direct and indirect benefits of society, economic performance and environmental impact throughout the system lifespan.

A.1.3.1 Energy indicators

The SDHS energy performance is evaluated through a couple of indicators to evaluate both its thermal and electric renewable energy equipment.

Firstly, the REF_{th} is the renewable energy fraction calculated for the on-site utilization of solar thermal energy for SH and DHW demand. It can be defined as a ratio between the total solar thermal energy used to the total thermal energy demand, as shown in eq. (A.1.1.0) (Abokersh, Mohamed Hany, Kangkana Saikia, Luisa F cabeza, Dieter Boer, 2020).

$$REF_{th} = 1 - (R_{HP} + R_{fuel}) \quad \text{(A.1.1.0)}$$

where:

$$R_{HP} = \frac{\int_0^t Cap_{heating}}{Q_{SH\ load} + Q_{DHW\ load}} \quad \text{(A.1.1.1)}$$

$$R_{fuel} = \frac{\int_0^t \dot{Q}_{AUX_1} + \int_0^t \dot{Q}_{AUX_2}}{Q_{SH\ load} + Q_{DHW\ load}} \quad \text{(A.1.1.2)}$$

where $Cap_{heating}$ is the energy supplied by the heat pump. While $\dot{Q}_{AUX_1}$ and $\dot{Q}_{AUX_2}$ are the energy provided by the auxiliary heaters to cover the SH load ($Q_{SH\ load}$) and DHW load ($Q_{DHW\ load}$) under the condition of insufficient solar energy.

In addition, solar electric energy is evaluated through the REF_{elec} which represent the energy fraction calculated for the on-site utilization of renewable electrical energy to satisfy the electricity demand of the neighbourhood, and it is calculated as follows:

$$REF_{elec} = \frac{\int_0^t EC_{RE}}{Q_{electric\ load}} \quad \text{(A.1.2)}$$

where EC_{RE} is the generated electricity by the PV array, and $Q_{electric\ load}$ is the total electricity demand.

Since the SST usually presents a significant importance in the SDHS performance (M. Abokersh et al., 2020), the SST performance should be taken into account through, and its efficiency is calculated as follows.

$$\eta_{SST} = 1 - \frac{\int_0^t \dot{Q}_{SST\ loss}}{\int_0^t \dot{Q}_{HE_1}} \tag{A.1.3}$$

Where the $\dot{Q}_{SST\ loss}$ is the heat loss through the SST and $\dot{Q}_{HE_1}$ is the heat transfer through the HE1.

Furthermore, the SST performance depends greatly on the amount of heat losses through the top, sideways and bottom of the storage. Therefore, Eqs. (A.1.4) to (A.1.6) are used to estimate the heat loss coefficients of the SST, as suggested by Hadorn (Hadorn, 1990).

$$U_{Roof} = \frac{1}{\frac{d_{con}}{\lambda_{con}} + \frac{d_{Roof}}{\lambda_{ins}} + \frac{1}{h_{conv}}} \tag{A.1.4}$$

$$U_{Wall} = \frac{1}{\frac{d_{con}}{\lambda_{con}} + \frac{d_{Wall}}{\lambda_{ins}} + \frac{1}{h_{conv}}} \tag{A.1.5}$$

$$U_{Gnd} = \frac{2}{R^2}\left\{ a\left(\frac{\lambda_G}{\pi}\right)^2 . \ln\left[\frac{a}{a - \left(\frac{\pi R}{\lambda_G}\right)}\right] - \frac{R.\lambda_G}{\pi}\right\} \tag{A.1.6}$$

Where: $a = \frac{\pi R}{\lambda_G} + \frac{(d_{con} + d_{Gnd})}{\lambda_G} + \frac{d_{con}}{\lambda_{con}} + \frac{d_{Gnd}}{\lambda_{Gnd}}$

In these above equations U_{Roof}, U_{Wall} , and U_{Gnd} are the relative heat loss coefficients of the top, wall, and bottom of the SST. R is the SST radius, d_{con} represents the construction material thickness, whereas, d_{Roof}, d_{Wall} and d_{Gnd} represent the top, wall, and bottom surfaces insulation thicknesses of the SST, respectively. In addition, λ_{con} represents the thermal conductivity of the construction

material, $\lambda_{ins}$and λ_{Gnd} represent the thermal conductivity of the insulating materials used for the roof, wall, and bottom surfaces of the SST, respectively. Parameter h_{conv} is the convective heat transfer coefficient to the air, and it is assumed to be 10 W/(m^2·K) for equations (A.1.4) to (A.1.6) (Mohamed Hany Abokersh et al., 2020). The thermal conductivity of the ground λ_G is considered to be 3 W/(m·K).

Besides evaluating the SDHS performance, it is important to assess the effect of the proposed SDHS to enhance the building energy performance to achieve a nearly zero energy consumption at both scales: individual buildings and community. In this context, Energy Performance Indicators (EPI) present an estimation for the energy performance of the building. This index is widely used in the Netherlands as '*Dutch energy label for dwellings'* (Majcen et al., 2013), and it is calculated as:

$$EPI = \frac{Q_{total}}{155A_{floor} + 106A_{loss} + 9560} \quad \text{(A.1.7)}$$

Where: $Q_{total} = Q_{SH\ load} + Q_{DHW\ load} + Q_{AUX} + Q_{electric\ load} - \int_0^t EC_{RE} - \int_0^t EG_S$ (A.1.8)

where Q_{total} is the total energy consumption in the building, whereas EG_S is the generated thermal energy covered by the solar thermal energy system and A_{loss} is the area which is not heated up in the dwelling. The values obtained from eq.(A.1.7) are categorized corresponding to Dutch energy labels (from G to A++), as shown in Table A.1.2, where the lowest Value of EPI indicates the highest building energy efficiency.

Table A.1.2: Dutch energy labelling for building's energy performance in 2013

EPI	A++	A+	A	B	C	D	E	F	G
	<0.50	0.51 – 0.70	0.71 - 1.05	1.06 - 1.30	1.31 – 1.60	1.61 – 2.00	2.01- 2.40	2.40 – 2.90	>2.90

A.1.3.2. Economic indicators

The net present cost (NPC) assess the life cycle cost (LCC) to evaluate the SDHS feasibility over the project lifespan (Mohamed Hany Abokersh et al., 2020). The NPC is calculated as a summation of the capital cost (IC), the operational cost (OC), and the replacement cost (RC). A detailed description of NPC calculation is provided in the supplementary information – A.2.1.

$$NPC = IC + OC + RC \quad \text{(A.1.9)}$$

A common alternative approach to evaluate the economic feasibility is the payback period (PBT) which is the payback time of the proposed SDHS model, and it denotes the number of years taken by the proposed system to deliver the total life cycle cost (Mohamed Hany Abokersh et al., 2020). It is calculated as:

$$PBT = \frac{NPC}{Annual\ cost\ saving} \quad \text{(A.1.10)}$$

A.1.3.3 Environmental indicators

The impact on environment of adding HP, SST and PV to the SDHS system is determined using the life cycle approach (LCA) (Gonzalo Guillén-Gosálbez, José

Antonio Caballero, 2007). LCA can be performed using a variety of indicators to determine the environmental impact of any technology. For the developed SDHS system, we use the ReCiPe 2016 (Huijbregts et al., 2017) framework to determine the environmental impact. The ReCiPe is among the widely used environmental indicator due to the methodological perspective (Gursel and Ostertag, 2017). To calculate ReCiPe, Life Cycle Inventory Analysis (LCIA) data is transformed into endpoint scores, which are then categorized into three classes: human health, ecological systems, and resources depletion. Furthermore, theses damage classes are combined as a normalized indicator metric (RCP) for the SDHS conformation. The RCP can be expressed as:

$$RCP = \sum_{d} \delta_d \, \varepsilon_d DAM_d \qquad \forall d \tag{A.1.11}$$

where DAM_d is the endpoint score for damage category d. δ_d is a factor based on the use of extraction of material and use of land in the European setting to normalize endpoint data for different damage categories while ε_d is the weight factor based on values recommended in the ReCiPe 2016 framework. The data and environmental impact of SDHS components can be found in A.2.2.

In addition, the environmental payback period (EPBP) is introduced to estimate the sustainability of the proposed SDHS model (Abokersh, Mohamed Hany, Kangkana Saikia, Luisa F cabeza, Dieter Boer, 2020). This indicator is estimated through calculating the total number of years required by the SDSH to replace the conventional system using the HP.

$$EPBP = \frac{RCP}{Annual\ RCP\ saving} \quad \text{(A.1.12)}$$

A.1.3.4 Social indicators

The proposed SDHS framework with the integration of multiple renewable energy technologies has a greater potential for providing social benefits, improving the quality of life of the residents in the dwellings, providing more and better employment opportunities (EO).This value can be estimated as (Chen et al., 2020):

$$EO = \lambda_{E.grid} E_{nom} + \lambda_{heat} Q_{nom,heat} + \lambda_{PV} Q_{nom,PV} \quad \text{(A.1.13)}$$

Here $\lambda_{E.grid}$ = 0.61 persons/MW is the grid electricity coefficient, λ_{heat} = 0.38 persons/MW is the solar thermal collector coefficient, and λ_{PV} = 0.70 persons/MW is the PV module coefficient; all of them used to calculate the employment coefficients for technologies incorporated in the SDHS system (Cameron and Van Der Zwaan, 2015). E_{nom}, $Q_{nom,heat}$,and $Q_{nom,PV}$ are nominal capacities of the power plant, roof mounted solar thermal collectors and roof mounted PV module, respectively (Chen et al., 2020).

A.1.4. Multi-objective optimization based on a surrogate model

Our objective is to enhance the economic and environmental performance of the proposed SDHS system. We used a surrogate modelling approach to implement multi-objective optimization on the SDHS system. The objective function is to minimize the net present cost and the environmental impact of a SDHS for a residential community while tracking its technical and social performance. In this

work, we used surrogate models, which uses simulation results obtained with the TRNSYS model validated in section 3 to train a neural network to predict the thermal performance of the SDHS. Running the SDHS TRNSYS model with a feasible range of decision variables provides a set of feasible scenarios used as a training data set for the ANN. The trained ANN is then coupled to a genetic algorithm to devise a multi-objective optimization (MOO) function for minimizing NPC and RCP under several technical constraints.

A.1.4.1. Data generation

Dataset development is a key aspect when developing a surrogate model, as a valid dataset obtained from a large number of simulations is used to train the surrogate model. For this work, data generation is performed by identifying the uncertain independent variables (inputs) and providing them to the TRNSYS simulation tool to obtain the dependent variables (outputs). In this work, the independent variables comprising the performance of the solar circuit, the SH distribution circuit and the DHW distribution circuit are used to create a combination of inputs to obtain the sample point. More details regarding the data generation are introduced in Abokersh et al. (Abokersh, Mohamed Hany, Kangkana Saikia, Luisa F cabeza, Dieter Boer, 2020).

A.1.4.2 Surrogate model convergence

The metamodel is built based on a multi-layer feedforward ANN model, where this model contains 14 neurons in the input layer and three hidden layers. The ANN simulations are implemented based on the Bayesian regularization algorithm

with a learning rate and a Momentum mean of 0.001 and 0.004. The model structure is determined through the optimization approach proposed by Abokersh et al. (Mohamed Hany Abokersh et al., 2020) to provide a relatively good convergence. In the ANN model, 21 outputs are considered in the output layer. These outputs include the energy produced in the solar collector field, the energy supplied by the heat pumps, the energy supplied by the storage tanks, and energy covered by the auxiliary heaters. The metamodel is validated using the performance metrics: (i) adjusted R^2 ($R^2-adj.$) and (ii) variation coefficient (CV). Equations (14) to (16) shows the mathematical form of R^2-adj and CV.

$$R^2 = 1 - \frac{\sum_{i=1}^{n}\left(y_{predict,i} - y_{data,i}\right)^2}{\sum_{i=1}^{n}\left(y_{data,i} - \overline{y}_{data}\right)^2} \quad \text{(A.1.14)}$$

$$R^2 - Adj. = 1 - \frac{(1-R^2)(n-1)}{n-k-1} \quad \text{(A.1.15)}$$

$$C.V(\%) = \sqrt{\frac{\sum_{i=1}^{n}\left(y_{predict,i} - y_{data,i}\right)^2}{\overline{y}_{data}}} \times 100 \quad \text{(A.1.16)}$$

Here, $y_{predict,i}$ represents the value estimated at a time 'i', $y_{data,i}$ shows the value of output y at a time 'i', n displays the sample size while k shows the total number of regressors used.

A.1.4.3. Optimization algorithm and surrogate model integration

After developing the surrogate model, the next step is to incorporate the heuristic optimization techniques with the robust ANN model to solve a MOO problem. MOO framework deals with two or more conflicting objectives in the

objective function. In this case study, the energy performance of the system is optimized by adjoining the environmental and economic system requirements. Ultimately, the residential community size's impact is also examined on the SDHS performance in an extended optimization problem. For the proposed SDHS system, the objective function to simultaneously optimize the NPC and RCP is given as:

$$\begin{aligned} & min\,\{f_1(x), f_2(x)\} \\ & s.t.\ h(x) = 0 \\ & \quad g(x) \geq 0 \\ & lb_i \leq x_i \leq ub_i \qquad i \in \{1, \dots, 18\} \end{aligned} \tag{A.1.17}$$

Here, f_1 is NPC, f_2 is RCP, h represents equality constraints corresponding to the physics of physical systems solved in TRNSYS, and g denotes inequality constraints corresponding to technical evaluation of SDHS. These constraints must maintain the annual solar collector efficiency above 60%, whereas SH annual solar fraction and SST efficiency should be maintained above 50% as recommended by Bauer et al. (Bauer et al., 2010) and Solites ("A Multiobjective Simplex Method," 2005).

The solutions of multi-objective functions provide us with a non-dominated solution called Pareto solutions, which represent the optimal trade-off for the economic and environmental targets. To avoid obtaining sub-optimal solutions (which is probable in classical MOO using point by point search), an improved technique called Pareto-ranking (Nö et al., 2018) is utilized to refine the solutions for NPC and RCP. The simulation-based optimization model is obtained by merging the generated robust

metamodel based on ANN and the NSGA-II algorithm. Based on Alajmi et al.(Alajmi and Wright, 2014) recommendation, the MOGA uses the NSGA-II algorithm with 1000 preliminary population due for 300 generations.

The performance for SDHS has been examined for various community sizes (10, 25, 50, 100, and 500 houses) based on the decision variables explained in ensuing section.

A.1.4.4. Decision variables and parameters

In the case study, 18 decision variables are used to formulate an optimization problem, including system components' relative alignment, structure, operating criteria and sizing. To categorize these variables, decision variables are classified into 3 field circuits, namely (i) supply (ii) SH (iii) DHW (Figure A.1.6). These decision variables are linked with mathematical equations to determine the equipment size for SDHS. The solar field circuit has 5 decision variables, i.e., the area of photovoltaic panels (A_{PV}), area of the solar thermal collector (A_{col}), the inclination angle of solar collectors, including the photovoltaic and thermal collectors (β_{col}), number of solar thermal collectors in series (N_{col}), heat pump capacity as a function of the maximum heat demand supplied (FC_{HP}), the turn-on temperature of the heat pump (T_{ref}). The space heating circuit has 9 decision variables, i.e., the volume of SST (V_{SST}), height to diameter ratio for SST (HDR), the thickness of insulation for the wall (d_{wall}), roof (d_{roof}), and ground (d_{Gnd}), insulation material type represented by the conductivity of construction material (λ_{con}), roof and wall (λ_{ins}) and ground ($\lambda_{ins,gnd}$), and auxiliary heating unit capacity as a fraction of the maximum heating demand (FC_{AUX_1}). Finally, the domestic hot water circuit has 3 decision variables, e.g. volume

of DHWT (V_{DHW}), height to diameter ratio of DHWT (HDR_{DHWT}) and the fraction capacity supplied by the auxiliary unit as a percentage of the maximum heating load (FC_{AUX_2}).

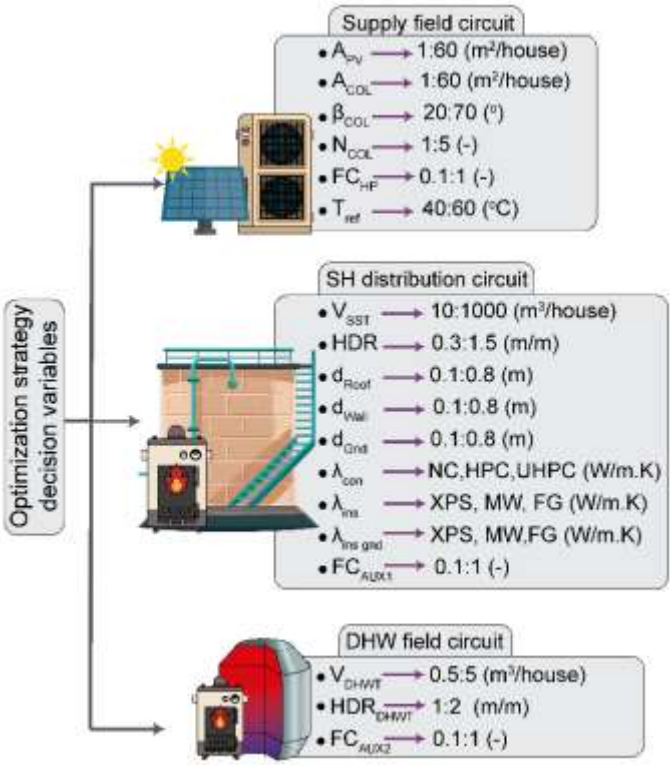

FIG. A.1.6: CLASSIFICATION OF THE DECISION VARIABLES IN THE SDHS OPTIMIZATION PROBLEM

A.1.5. Optimal solutions post analysis

We have proposed a framework for the inclusive sustainability assessment of a solar assisted district heating system. The methodology is outlined in Fig. A.1.7. The framework starts with the simulation of SDHS in TRNSYS 18 and defines the most

suited decision variables, their range and related output to showcase the thermal performance of the SDHS. To reduce the computational cost of the process, the TRNSYS model is coupled with MATLAB and an ANN with Bayesian optimization. Later, the multi-objective genetic algorithm (MOGA) is coupled with the neural network to perform the multi-objective optimization for economic and environmental objectives. MOO provides a Pareto frontier with the optimal solutions for different community sizes, which are then subjected to multi-criteria decision making (MCDM) to facilitate the selection according to the needs/preferences of stakeholders. For MCDM, we used TOPSIS (Technique for Order of Preference by Similarity to Ideal Solution), which ranks the solutions based on the desired criteria. To illustrate the significance of uncertainty on the optimized objectives, we performed a global sensitivity analysis (GSA) (Saltelli and Annoni, 2010).

A.1.5.1. MCDM development for SDHS evaluation

A.1.5.1.1. Indicators normalization

The indicators used for the sustainability evaluation vary in nature and value range. Before applying the MCDM, we normalize the indicators to a common range [0,1]. We used a distance-based normalization (TOPSIS) for the MCDM (Lior, 2017). The normalization method for the indicator being minimized is expressed in Eqs (A.1.18 – A.1.19), while for the indicator being maximized is expressed in Eqs. (A.1.20 – A.1.21):

$$v_{ij} = \frac{x_j^{min}}{\bar{x}_{ij}} \quad \text{(A.1.18)}$$

$$x_j^{min} = min(\vec{x}_{ij}) \quad \text{(A.1.19))}$$

$$v_{ij} = \frac{\vec{x}_{ij}}{x_j^{max}} \quad \text{(A.1.20)}$$

$$x_j^{max} = \max(\vec{x}_{ij}) \quad \text{(A.1.21)}$$

A.1.5.1.2. Indicators' weighting method

The importance of each criterion might be different for each stakeholder. There are subjective and objective methodologies to apply weighting factors (Campos-Guzmán et al., 2019): objective methods are based on mathematical models and more suited for numerical data. One of the widely used objectives is the entropy-based weighting approach, and it is easily adaptable (Bhowmik et al., 2018). Suppose, a set 'D' which represent our sustainability criteria characterized by a vector $d_j = (d_{j_1}, d_{j_2}, \dots, d_{j_m})$ in terms of normalized indicator 'i' is defined as:

$$D_j = \sum_{i=1}^{m} d_{ij_j} = 1,2, \dots, m \quad \text{(A.1.22)}$$

Then, the entropy of j^{th} indicator is given by:

$$e_j = -\frac{1}{\ln(m)} \sum_{i=1}^{m} \frac{d_{ij}}{D_j} \ln \frac{d_{ij}}{D_j} \quad \text{(A.1.23}$$

In the end, the normalized weight is calculated as:

$$w_j = \frac{1 - e_j}{\sum_{j=1}^{m} (1 - e_j)} \quad \text{(A.1.24)}$$

A.1.5.1.3. TOPSIS distance-based normalization method

The TOPSIS algorithm, developed by Hwang et al. (Hwang and Yoon, 1981), is widely used in MCDM problems. This method uses the normalized values obtained from Eqs (19-21) and assumes a distance-based criterion indicating that the ideal solution lies at the shortest distance from the positive ideal solution and the longest distance from the negative ideal solution. The calculated distances are then compared to find out the best plausible solution. The advantage of TOPSIS is that it can provide a ranking of each solution for each criterion (Sari, 2021).

To determine the rank, first, we identify the positive ideal solution (A^+) and the negative ideal solution (A^-):

$$A^+ = \left\{ \left(\underbrace{max}_{i} v_{ij} | j \in I \right), \left(\underbrace{min}_{i} v_{ij} | j \in I' \right), i = 1,2, \dots, m \right\} = \{v_1^+, v_2^+, \dots, v_m^+\} \quad \text{(A.1.25)}$$

$$A^- = \left\{ \left(\underbrace{min}_{i} v_{ij} | j \in I \right), \left(\underbrace{max}_{i} v_{ij} | j \in I' \right), i = 1,2, \dots, m \right\} = \{v_1^-, v_2^-, \dots, v_m^-\} \quad \text{(A.1.26)}$$

Here, $I = \{j = 1, 2,\ldots, n\}$ and $I' = \{j = 1, 2,\ldots, n\}$ represent the sets of economic and environmental criterion. Then, we measure the Euclidean distance for each solution from the positive and negative ideal solutions using the following equations:

$$S_i^+ = \sqrt{\sum_{j=1}^{n} \left(v_{ij} - v_j^+\right)^2}, \qquad for\ i = 1,2,\ldots,m \tag{A.1.27}$$

$$S_i^- = \sqrt{\sum_{j=1}^{n} \left(v_{ij} - v_j^-\right)^2}, \qquad for\ i = 1,2,\ldots,m \tag{A.1.28}$$

Lastly, proximity index ($C_i \in [0,1]$ for $i = 1, 2,\ldots, m$) is calculated to find the remoteness from the positive and negative ideal solutions for ranking, as:

$$C_i = \frac{S_j^-}{S_j^+ + S_j^-} \tag{A.1.29}$$

A.1.5.2. Global sensitivity analysis (GSA)

The final step of this methodology is to perform a sensitivity analysis to offer an understanding of the most sensitive system parameters. Given GSA's advantage over LSA, a Bayesian-based GSA approach (BACCO) (Qin et al., 2013) is employed. This approach can cover an extensive range of parameters with an interaction for their relative distribution under uncertainty. It also reduces the computational time compared to Monte-Carlo based GSA approach.

BACCO methodology has two main stages: (i) acting as an emulator (statistical representative model) and (ii) uncertainty analysis. The emulator is trained with the data obtained from the simulation-optimization model. This dataset covers the feasible domain of solutions in a Latin hypercube design. Once the emulator is working, it is cross-validated to check its efficiency. The second stage covers the multidimensional domain of design variables to quantify the sensitivity of the parameters. The GSA is performed with respect to EPI, NPC, RCP, and EO in terms of percentage variation of each input to estimate the impact of ten economic decision variables. These variables comprise natural gas price (C_{ng}), buying (C_{el}) and selling to the grid electricity prices (S_{el}), natural gas (i_{ng}), electricity inflation rate (i_e), investment cost (IC), operational cost (OC), replacement cost (RC), in addition to system inflation (i) and discount rates (d).

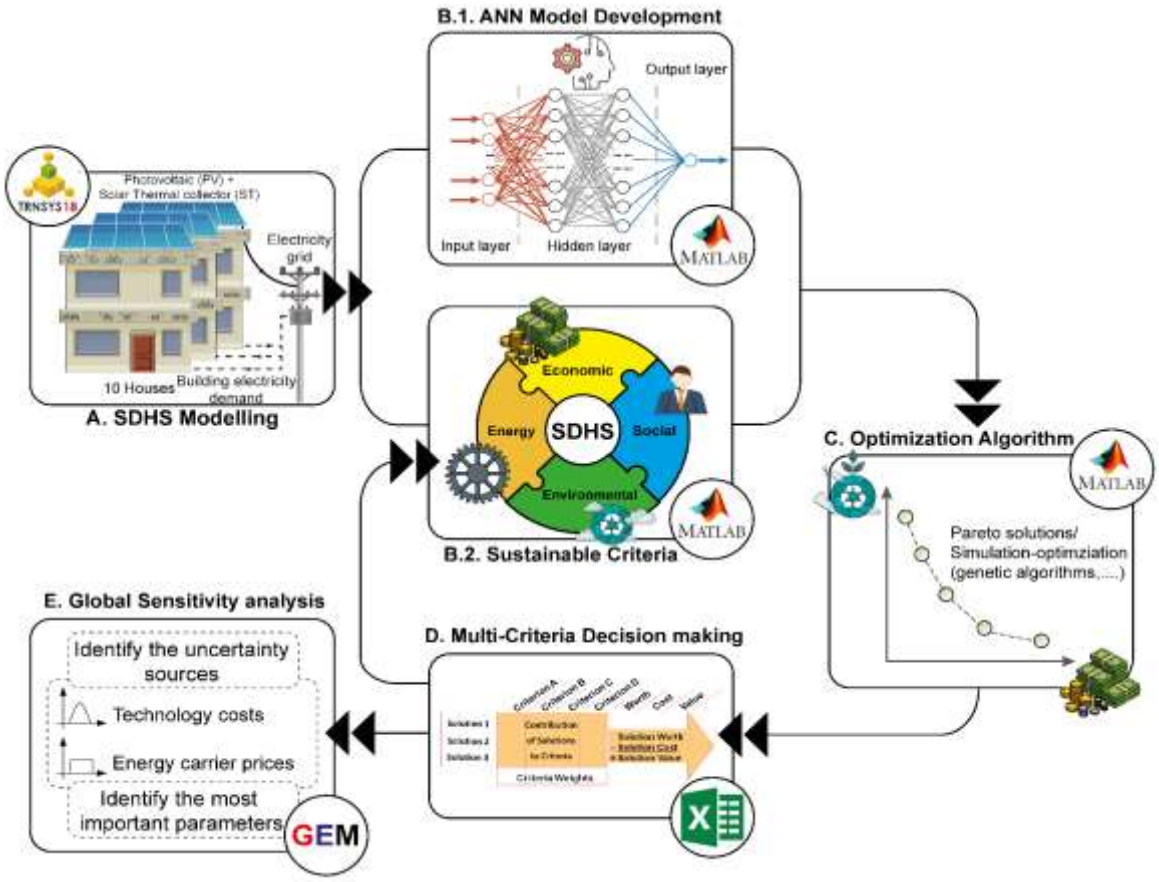

FIG. A.1.7: FRAMEWORK FOR THE HYBRID MULTI-OBJECTIVE OPTIMIZATION SYSTEM OF SDHS

A.1.6. Results and discussion

This work provides a sustainable insight into the applicability of surrogate models for the economic-environmental-social optimization of the transient SDHS model. The surrogate model was used to optimize the SDHS framework for different community sizes ranging from 10 to 500 houses under different scenarios (i.e., scenario 1: minimum cost; scenario 2: 25% less environmental damage; scenario 3:

50% less environmental damage; scenario 4: 75% less environmental damage; and scenario 5: minimum environmental damage). The wide range of the decision variables produced multiple results, which are discussed in the following sections. The first portion of the results and discussion section addresses the metamodel's fittingness for the SDHS framework optimization. The second portion sheds light on the SDHS optimization results for economic-environmental-social indicators and physical and technical constraints. In this section, optimal solutions are analyzed for all community sizes under each scenario. The third portion provides an insight into the ranking of the optimal solutions based on weighted criteria using multi-criteria-decision-making. The final portion checks the robustness of the metamodel using the global sensitivity analysis.

A.1.6.1. Surrogate model convergence results

In this work, a K-fold cross-validation strategy is adopted to fit the surrogate model. The 2048 samples (i.e., simulation results) are organized in k subsets (M.H. Abokersh et al., 2020). The ANN model is trained with k-1 subsets, while k^{th} subsets are used to test the trained model in each run. Table A.1.3 displays a summary of the ANN model performance.

TABLE A.1.3: PERFORMANCE OF ANN MODEL IN PREDICTING THE TRNSYS SIMULATION OUTPUT.

Solar circuit					SH circuit			DHW circuit		
Q_{SOL}	Q_{PV}	Q_{Usefu}	Q_{abs}	P_{elec}	Q_{SST}	$Q_{SST\ los}$	Q_{AUX_1}	Q_{DHW}	$Q_{DHW\ los}$	Q_{AUX_2}

$R^2 - Adj$	99.8 %	99.7 %	98.3 %	97.7 %	97.8 %	99.5 %	97.7 %	99.2 %	95.5 %	98.9%	99.4 %
$C.V$	1.98 %	1.87 %	3.97 %	8.87	8.16 %	2.87 %	8.54 %	8.15 %	0.49 %	2.70%	3.08 %

Results in Table A.1.3 show that the surrogate metamodel prediction agrees with TRNSYS simulation outputs where $C.V$ has good model accuracy (maximum deviation 8.87%) for any surrogate model output as the $R^2 - Adj.$ is always above 95.5% for all outputs. Hence, we can be confident about the ANN model's predictability for the proposed SDHS framework's thermal performance for the given training data range. Metamodeling offers significant reductions in computational time compared with conventional heuristic optimization techniques.

A.1.6.2. Multi-objective optimal solutions

The validated ANN-based surrogate model is employed to optimize the economic and environmental performance of the SDHS for various community sizes and under different scenarios (i.e., scenario 1 - minimum cost, scenario 2 - 25% less environmental damage, scenario 3 - 50% less environmental damage, scenario 4 - 75% less environmental damage and scenario 5 - minimum environmental damage). All the scenarios are compared to the base case (decentralized heat pump) explained in section 2. The first set of optimal results for the economic criteria are shown in Fig. A.1.8. Economic criterion (NPC) is simplified to €/m^2 of the building. Base case has NPC at 66.6 €/m^2 which is constant for all the scenarios. For the smallest community size (10 houses), the optimal solution for scenario 1 (minimum cost) has an economic

performance analogous to the base case (70.1 €/m^2). The economic performance for 10 houses community size decreases with the decrease in environmental damage factor of SDHS as the NPC for scenario 5 (minimum environmental damage) is 125 €/m^2. However, as the community sizes increase from 10 to 25, 50, 100 and 500 houses, the economic performance increases significantly and proportionally. For 25 houses community sizes, the economic performance is improved for scenarios 1, 2, 3 and 4 by 32%, 28%, 23% and 12%, respectively, over the base case. While scenario 5 has an unfavourable performance for 25 community size compared to the base case as the base case outperforms the former by 22%. For 50 houses community size, the optimal SDHS solution surpasses the base case's economic performance for scenario 5 (minimum environmental damage) and has an NPC of 64.7 €/m^2. For community sizes higher than 50 houses, the proposed SDHS has economic and environmental solutions over the base case for every scenario considered here. The best economic solution is obtained for the minimum cost scenario in 500 houses community (21 €/m^2). For scenario 4 and scenario 5, the economic performance is similar at a value of NPC equal to 30.7 €/m^2.

The environmental damage factor (Fig. A.1.8) shows that all optimal solutions have a better environmental performance compared to the base case, which has RCP value of 10.1 Pt/m^2 while the least environmental friendly optimal solution is the minimum cost (scenario 1) for 10 houses community size which has a RCP value 3.2 Pt/m^2, which improves by 300% the environmental performance compared with the base case. Therefore, all the optimal solutions perform extremely well for environmental criterion against the base case. Like the economic performance, the

environmental performance of the SDHS improves as we move to bigger community sizes since it is possible to cover the energy demand by a higher percentage of renewable energy. The case of 500 houses community gives the best environmental performance for scenarios 4 and 5 with RCP value of 2.1 Pt/m^2 which shows an impressive 400% improvement compared with the base case's economic performance. Thus, the use of ANN model's enables to find optimal solutions which improved environmental and economic performance compared to the base case.

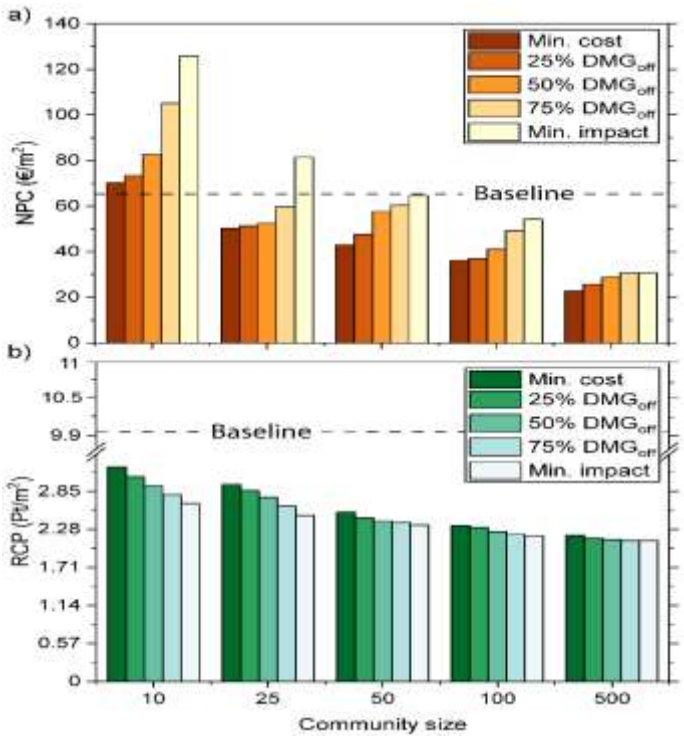

FIG. A.1.8. OPTIMAL SOLUTIONS OF SDHS FOR VARIOUS COMMUNITY SIZES UNDER DIFFERENT SCENARIOS WHERE (A) THE ECONOMIC CRITERIA, WHEREAS (B) THE ENVIRONMENTAL CRITERIA.

To arrive at the optimal solutions described above and depicted in Fig. A.1.8, the metamodel considers multiple decision variables for different scenarios and community sizes. The optimal design and sizing of the SDHS also become an important consideration to achieve the desired economic and environmental performances. An in-depth analysis of the optimal solutions obtained provides us with a guideline for the SDHS system design and sizing. SDHS was divided into three circuits, namely: (i) Space heating circuit; (ii) Solar field circuit; and (iii) Domestic hot water circuit. Each circuit consists of specific components to serve specific purposes in the SDHS network. These decision variables vary due to multiple scenarios and provide a guideline for optimal system design. This range of the decision variables for optimal solutions is shown in *Fig. A.*1.9. Each diagram has lower wick (representing minimum cost scenario), a center body (representing the scenario 2, 3 and 4) and the upper wick (representing minimum environmental damage scenario).

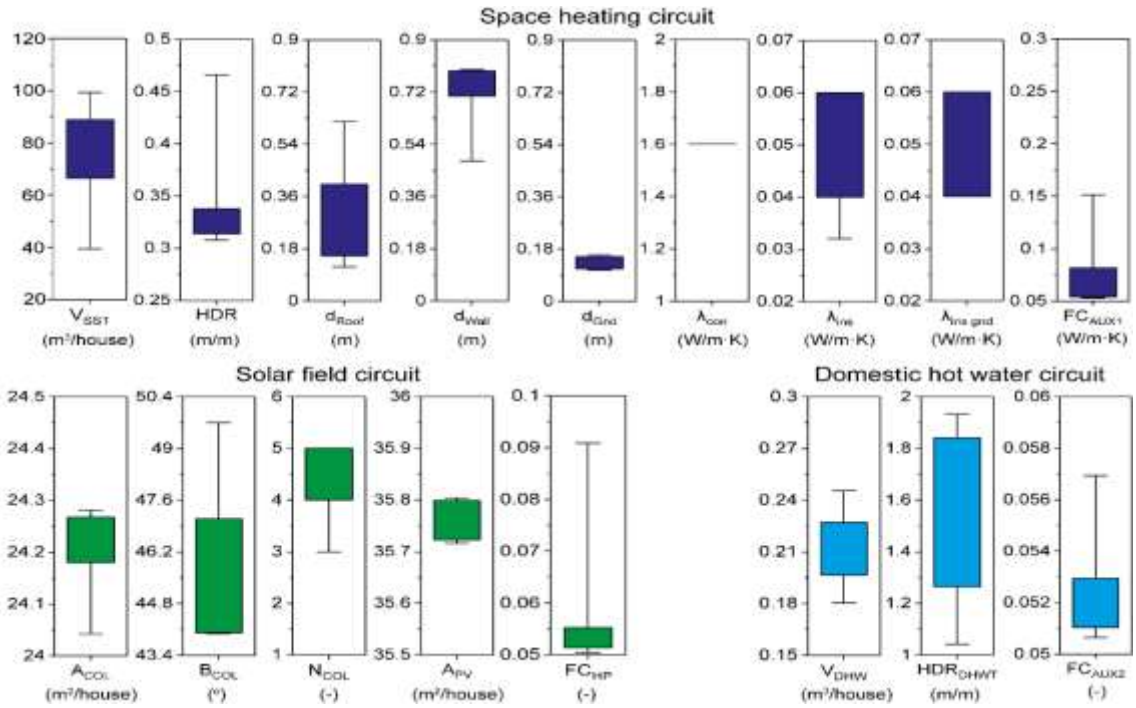

FIG. A.1.9. GUIDELINE FOR KEY PARAMETERS VALUES TO DESIGN OPTIMAL SDHS SOLUTION UNDER VARIOUS SCENARIOS.

To facilitate a comprehensive sustainable analysis of the optimal SDHS solutions, a breakdown of the key performance indicators mentioned in section 3 is shown in Fig. A.1.10. The performance indicators are divided into 4 main categories: (i) Energy; (ii) Economical; (iii) Environmental; and (iv) Social. All scenario solutions perform better for the smallest community size of 10 houses than the base case for energy indicators. The performance of energy indicators improves from minimum cost scenario to minimize environmental damage scenario in general for all the community sizes, although the gradient for improvement from scenario 1 to scenario 5 is high for 10 houses community size. A comparison between scenario 1 and the base case for 10 houses shows 2.5 folds improved EPI performance (building

energy performance grade = A+) for the optimal solution against the base case (building energy performance grade = D). In contrast, the optimal solution of scenario 5 has 4 times improved EPI performance over the base case to achieve a building energy performance grade A++. For social indicator, the 10-houses community size has 350% improved performance for all the scenarios. As we move towards bigger community sizes, EPI's performance increases from 0.56 to 0.16, giving us a significant improvement range from 3 to 10 times in the energy performance over the base case for different scenarios. The building energy performance is reflected by the solar thermal fraction, which can increase from 81% on a community of 10 houses up to 95% on a community size of 500 houses. On the other hand, the installed PV system provides extra electricity of around 70% for all community sizes to be sold to the electricity grid, which can support the PEB state. Furthermore, the increment in solar energy usage with increasing the community size is reflected in the reduction of natural gas usage where it diminishes from 23% at the scenario 1 community size of 10 houses to only 5.6% under the same scenario at community size of 500 houses.

For economic indicators, optimal solutions have a better scope in the long term because of the PBT indicator. In contrast, the base case is depreciative and has no payback, while optimal solutions have a payback and, therefore, provide a better option for long term planning. However, as we move to bigger community sizes, from 25 to 500 houses, economic indicators overcome the base case, and we find that for 50 houses community size, even the most environment-friendly solution has better economic performance than that of the base case with the payback period of 26 years. Furthermore, with the movement toward a bigger community size of 500, the PBT

can be reduced to 13.6years. The environmental indicator has shown an improved performance for all the community sizes under all scenarios, where the environmental performance is improved from 11.7 years at community size of 10 houses to 8.4 years at community size of 500 houses. Similarly, the social indicator shows improved performance for the optimal solutions over the base case, ranging from 1.3 times for 10 houses community size to 4 folds for 500 houses community size.

A.1.6.3. Optimal solutions ranking based on MCDM

The large set of optimal solutions obtained from the ANN model under different scenarios for different community sizes provide stakeholders with multiple options to choose from. To facilitate the stakeholders' decision-making, a ranking system is developed using multi-criteria decision making (MCDM). The criteria considered for this ranking system are energy, economic, environmental, social and a hybrid considering all the criteria. A summary of the indicators used for each criterion alongside their weight is shown in Table A.1.4. A weighted entropy TOPSIS approach described in section A.1.5.1 is used to rank the solutions under various scenarios.

The ranking of optimal solutions for different community sizes under the considered five scenarios is shown in Table A.1.5. The balance scenario (i.e., 50% DMG_{off}) gets priority for 10, 25 and 100 houses community size while it turns out 2nd ranked for 50 houses community and 3rd for 500 houses community. For 50 houses community size 25% DMG_{off} is best ranked while for 500 houses community 75% DMG_{off} is the first solution. It is worth noting that in 500 houses community, more

environment-friendly solutions (i.e., scenario 4 and 5) make the top ranks by a clear margin and stand out.

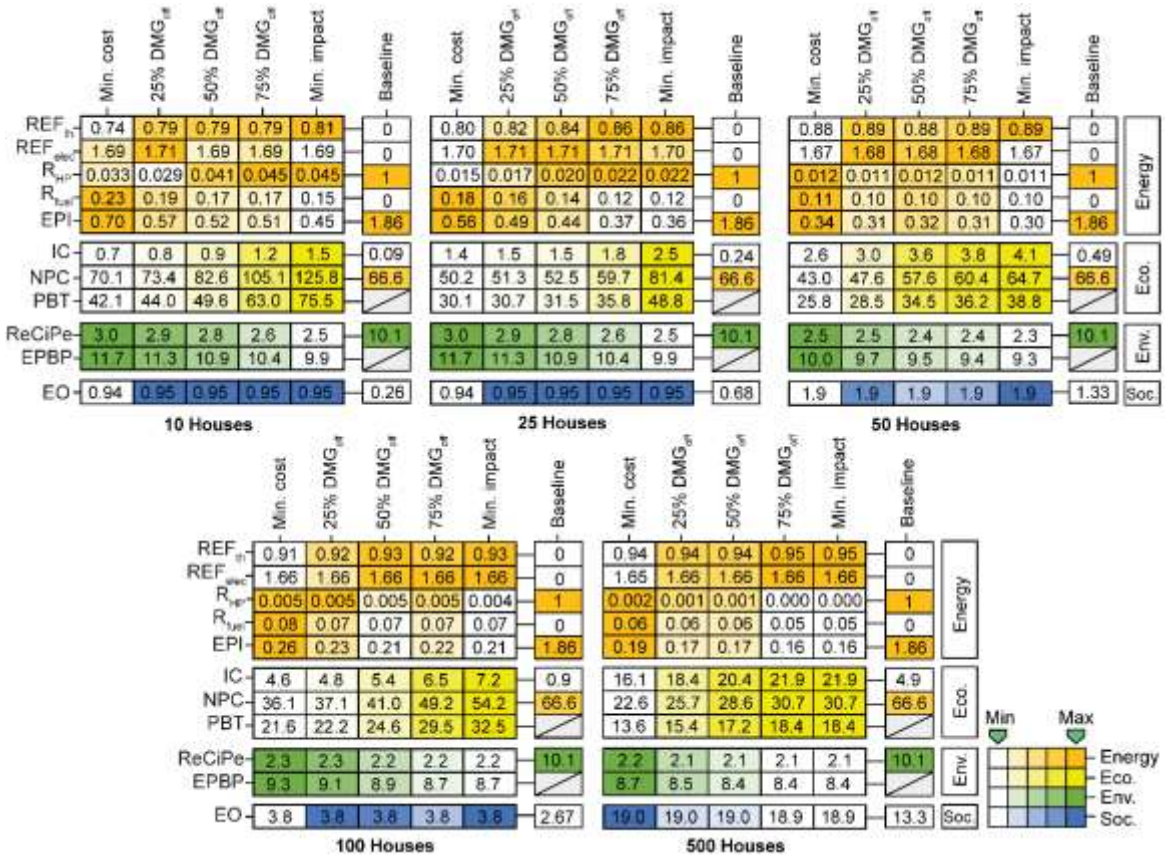

FIG. A.1.10. KEY PERFORMANCE INDICATORS FOR BEST RANKED OPTIMAL SOLUTIONS AND BASE CASES UNDER DIFFERENT COMMUNITY SIZES.

Table A.1.4. Weighted indicators to apply TOPSIS for MCDM.

	Indicators	Weights
Energy	$(W_{REF_{th}}, W_{REF_{elec}}, W_{R_{HP}}, W_{R_{fuel}}, W_{EPI})$	(1.2%, 0%, 38.2%, 30.3%, 30.3%)

Economic	$(W_{IC}, W_{NPC}, W_{PBT})$	(43%, 28.5%, 28.5%)
Environmental	(W_{ReCiPe}, W_{ADSR})	(50%, 50%)
Social	(W_{EO})	(100%)
Hybrid system	$(W_{Energy}, W_{Economic}, W_{Environmental}, W_{Social})$	(28.8%, 67.8%, 3.2%, 0.2%)

Table A.1.5. Ranking of optimal solutions based on community size and scenario.

Community size	10 houses		25 houses		50 houses		100 houses		500 houses	
Scenario	P_i	Rank	P_i	Rank	P_i	Rank	P_i	Rank	P_i	Rank
Min. cost	0.73	3	0.71	4	0.77	3	0.76	3	0.64	5
25% DMG_{off}	0.75	2	0.73	3	0.80	1	0.77	2	0.71	4
50% DMG_{off}	0.76	1	0.76	1	0.77	2	0.79	1	0.73	3
75% DMG_{off}	0.70	4	0.75	2	0.75	4	0.75	4	1.00	1
Min. impact	0.65	5	0.65	5	0.72	5	0.71	5	0.99	2

A.1.6.3.1. Technical analysis

To analyze optimal solutions' thermal and energy performance, the technical analysis has been performed for optimal solutions. The thermal energy is used for space heating and hot water demands. As shown in Fig. A.1.11, the plots depict the energy demand and energy supplied (Q_{cov}) by the solar collectors (thermal and PV) for all the community sizes throughout the year. Space heating demand (kWh/m^2) is high for the winter months (November, December, January and February). For November, December, and January, the proposed SDHS system can provide 100% of the thermal energy to satisfy the demand in every community size. The SH demand is not met by Q_{cov} in the months of February and March for 10, 25 and 50 houses communities and the excess demand in these cases is satisfied by the auxiliary unit. The plot also shows that as the community size increases the Q_{cov} is able to cover more SH demand and for community size of 100 houses and above, the SDHS can satisfy SH demand fully on its suggesting of reduction in environmental damage at the SDHS for bigger community sizes.

The DHW demand exists throughout the year, unlike SH demand. The DHW demand has 20% to 50% increase in the months of winter and Q_{cov} needs to be supplemented with auxiliary units to meet this extra demand for DHW. Q_{cov} shows a very small increasing gradient with the increase in community sizes, as shown in Fig. A.1.11. The electricity demand also has a similar nature as the SH and DHW demand over the year. Electricity demand is higher in October- March than the EC_{RE} produced by PV panels for the all the community sizes. Therefore, the excess electricity

demand is met by grid electricity through smart metering. In April-August, PV collectors' electricity is higher than the demand. This extra production of electricity is supplied to the grid through smart metering to earn credits. These results show the transition not only to the NZEB concept, but it can serve the transformation from LCB to PEB for community sizes with more than 100 houses.

A.1.6.3.2. Economic analysis

The economic performance of optimal solutions is further analysed by breaking down the NPC into its various components. Fig. A.1.12 shows the cost distribution of SDHS components for the top-ranked solutions for every community size, mentioned in section 6.2, the analysis of the cost components for the base case has a very low capital cost (6.2%) and replacement cost (7.8%) while the operational cost is extremely high (86%) which makes the base case a depreciating project as each operational costs adds to the cost of the project. On the other hand, for optimal solutions, the project's capital cost varies from 46.6% to 56.1%, operational cost varies from 13.2% to 1.6%, and replacement cost varies from 40.4% to 42.3%. The capital cost percentage of the optimal solutions increases as the community size increases because bigger community sizes corresponding to scenario 4 and scenario 5 (less environmental damage) have more renewable energy technology and a high capital cost.

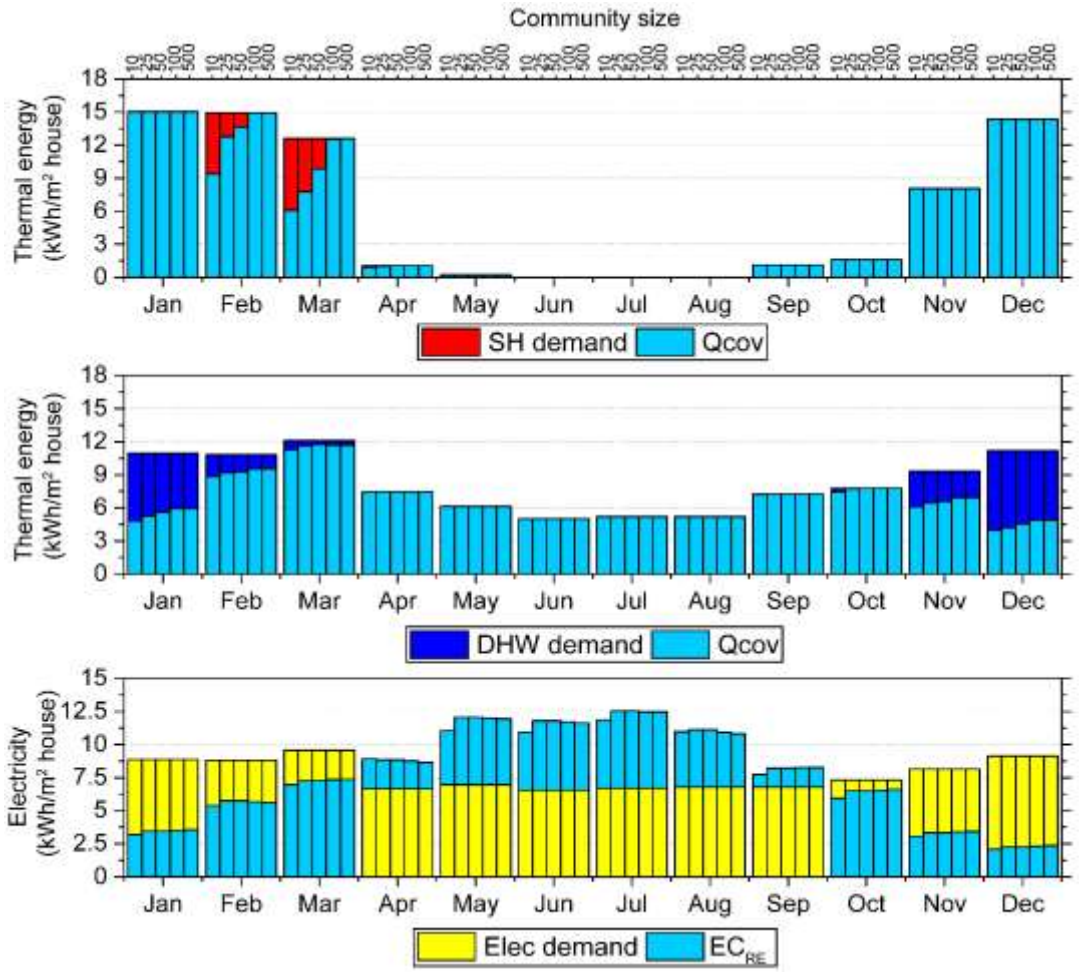

FIG. A.1.11. ENERGY DEMAND AND SUPPLY (PER M^2) FOR ALL COMMUNITY SIZES THROUGHOUT THE YEAR. THE FIGURE CONSISTS OF TWO LAYERS WHERE THE DEMAND PROFILES ARE PLOTS IN THE BACK LAYER, WHEREAS THE RENEWABLE COVERAGES ARE PLOTTED AT THE FRONT LAYER

The operational cost of the SDHS system reduces as we approach bigger community sizes, while the SDHS solution also provides more than 40% of the NPC as replacement costs which suggest that the depreciation of the SDHS project is reduced by at least 500%. Finally, with the increment in the community size, the total

SDHS cost dramatically increases, especially moving toward more green solutions requiring extra investments. Thus, the SDHS for the community of 10 houses has a total life cost of €1.98 M, and it increases up to €36.8 M for the community size of 500 houses.

A.1.6.3.3. Environmental analysis

The environmental indicator is an important part of this study. Therefore, a detailed analysis of optimal SDHS solutions is performed to see each ranked optimal solution environmental impact. Fig. A.1.13 shows the distribution of environmental damage caused by each component of the SDHS solutions compared to the base case below for the same community size. RCP points measure the environmental damage of each component. For the base case, the main cause of environmental damage is the electricity consumption from the grid. For 10 houses and 100 houses community sizes, under 50% DMG_{off} scenario, the environmental damage is almost 10 times lower than for the corresponding base cases while it is comparable for 25 houses community size under the same scenario. For 25% DMG_{off} and 75% DMG_{off} scenario, environmental damage is more than 10 times lower compared to the base cases for corresponding community sizes.

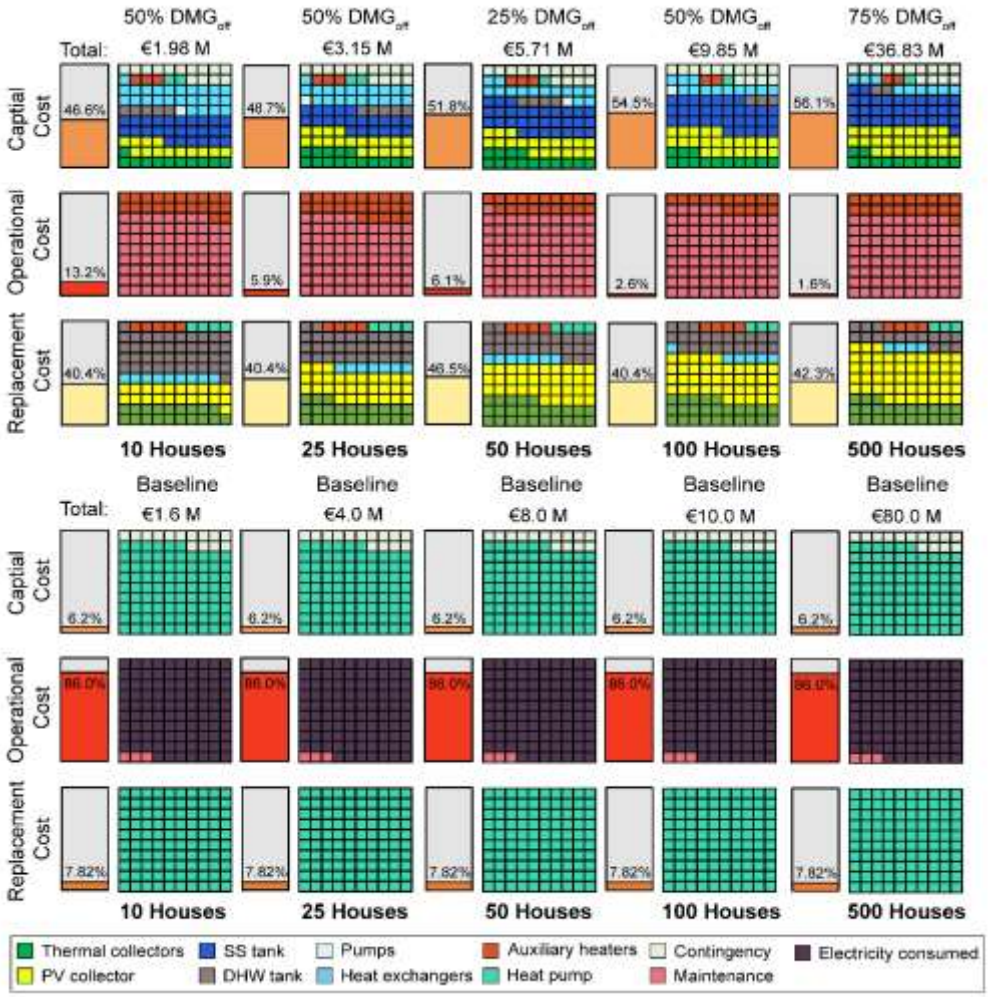

Fig. A.1.12. Cost analysis of optimal solutions for different community sizes compared to base case for respective community sizes

Component wise environmental analysis of SDHS solutions provides us with a better understanding of the damage caused by each system. Fig. A.1.13 entails that as we increase the community size, environmental damage due to the consumption of natural gas reduces significantly; for example, in the optimal SDHS system for 10 houses, the environmental damage caused by natural gas consumption is 38% of the

total damage while that in case of 500 houses is just 17%. The percentage of environmental damage due to solar collectors (PV + thermal) is the major constituent (49 % to 67%) for environmental impact for all SDHS solutions. A third major contributor to environmental damage in optimal solutions is SST, which constitutes 4% to 6% of total damage. Other components for environmental damage are auxiliary units (1% - 2%), heat exchangers (2%), DHW tank (2% - 3%) and pumps (1%).

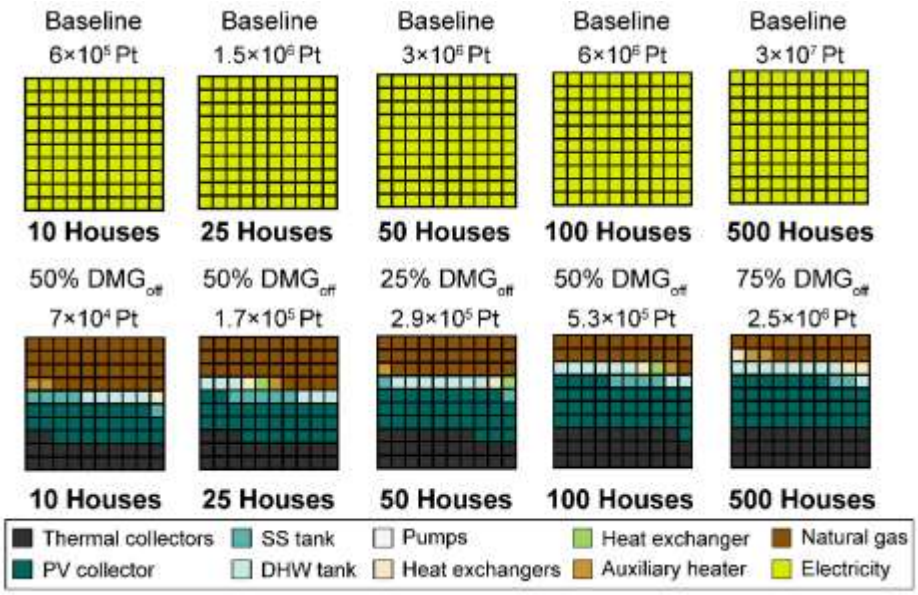

FIG. A.1.13. COMPARISON OF RESULTS OF ENVIRONMENTAL ANALYSIS UNDER DIFFERENT OPTIMAL SCENARIOS FOR VARIOUS COMMUNITY SIZES.

Following the above analysis, on-site constructed SST has a major influence on economic indicators. Therefore, a deeper analysis of the SST is performed where Fig. A.1.14 represents the optimized values for the different SST parameters for each optimal solution. We conclude that $U_{overall}$ = 0.14 W/m^2 is a maximum value for the optimal solution of the largest community size, whereas SST of SDHS for 25 houses

community has the lowest $U_{overall}$ = 0.10 W/m^2. Optimal configurations of SST hare listed in *Fig. A*.1.14, the variation in the parameter values is not consistent with the increase in V_{SST} and community size where the d_{Roof} is around 0.34 m for community size of 10 house and it reduces to 0.12 m, and the d_{Wall} reduces from 0.79 m to 0.6 m. On the other hand, the d_{Gnd} stayed around 0.13 ± 0.02 m. For the SST construction material, the UHPC with λ_{con} = 1.6 W/m·K has a superiority over other construction materials due to its techno-economic and environmental benefits. Regarding the insulation materials, most of the optimal solutions insulate the SST ground using foam glass gravel with thermal conductivity of 0.06 W/m·K. In contrast, the SST walls use the foam glass only at the community size of 25 houses, and other community sizes introduce extruded polystyrene due to its low price. The optimal size of SST for 500 houses community size solution has the most efficient and economical values of design parameters where the SST uses mineral wool in both walls and ground. Thermal performance and the SST's efficiency for the selected optimal solutions are plotted in Fig. A.1.15, where we see an increase in the SST efficiency performance of optimal solutions from 68% at 10 houses up to 89.7% at a community size of 500 houses.

In addition to analyzing the SDHS optimal solutions at different community size, the capability of the methodological optimization framework based on a robust ANN in handling the Heuristics optimization is illustrated through comparing the computational expenses of the optimization process with the SDHS optimization problem mentioned by Tulus et al. (Tulus et al., 2019).

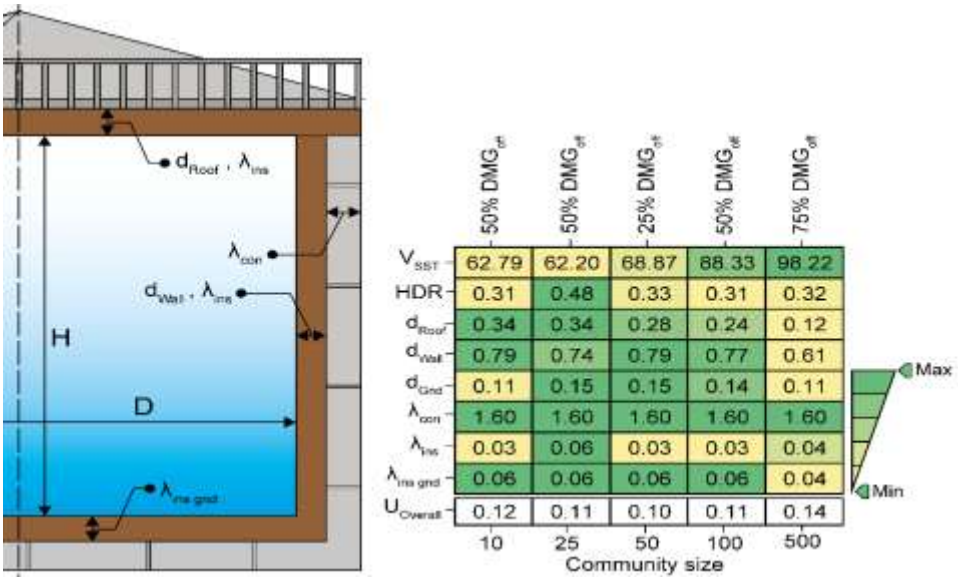

FIG. A.1.14. DESIGN PARAMETERS OF SST FOR VARIOUS COMMUNITY SIZE AND OPTIMAL SOLUTION SCENARIOS.

In this study, the average computation time for the anchor points was 15,700 CPU seconds and 47,000 CPU seconds for intermediate Pareto solutions using an Intel® Xeon® E5-2620 v4 2.10 GHz processor with 32.0 GB RAM. In this new framework, the average computational time for developing the full Pareto frontier is only around 600 CPU seconds using the same machine. This huge reduction is due to replacing the TRSNYS model with a robust ANN model and combining it in a MOO framework.

A.1.6.4 GSA results

To understand the influence of critical parameters on the objective function, a global sensitivity analysis is performed. The analysis implies BACOO for its low computational cost. Here we have taken 10 houses community size minimum cost-

optimal solution as the reference case to study the effects of parameters on the objective function. The reason to select the mentioned case for GSA is to have the closest economic performance to the base case.

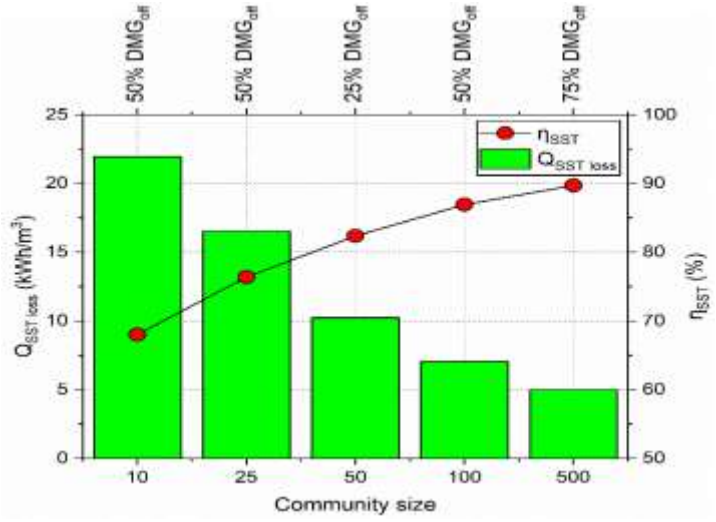

FIG. A.1.15. THE ANNUAL THERMAL PERFORMANCE OF SST WITH INCREASED COMMUNITY SIZES FOR OPTIMAL SOLUTIONS

The parameters for BACOO analysis for GSA (as explained in section A.1.5.2) includes prices of natural gas, electricity, inflation rate for gas and electricity, investment cost, replacement cost, operational cost and discount rate. The effect of these parameters is shown in Fig. A.1.16 on energy performance (Fig. A.1.16a), economic performance (Fig. A.1.16b), environmental performance (Fig. A.1.16c) and on social performance (Fig. A.1.16d). Fig. A.1.16a shows that the energy performance presented by the EPI, which is highly affected by the cost of natural gas and electricity followed by inflation in electricity price, selling cost of electricity to the grid. The main factors affecting the economic performance presented by NPC are

the operational cost, price of natural gas and investment cost. An interesting observation was in the case of environmental performance where the inflation seemed to affect it greatly, and the other costs (investment, operational and replacement) have a tiny impact on the environment performance under uncertainty (Fig. A.1.16c). Similarly, in Fig. A.1.16d, GSA for social performance indicated that variables like cost of natural gas and electricity have an extreme impact on social performance followed by operational cost, inflation in electricity price and discount rate. Hence, GSA's results cumulatively suggest that natural gas and electricity prices, operational cost, and inflation rates are the most critical factors to ensure the proposed SDHS system's expected performance.

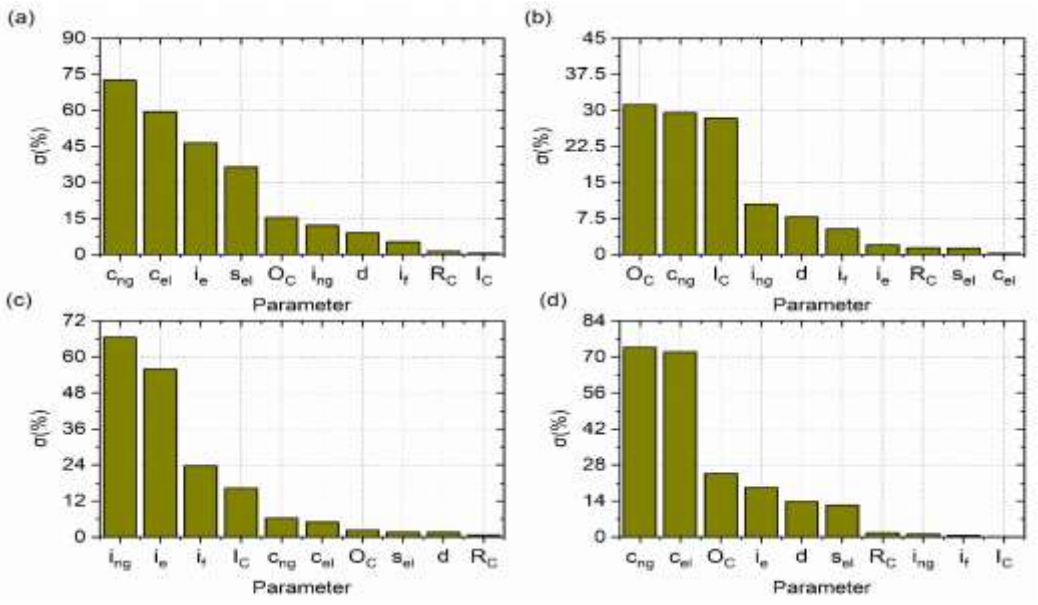

FIG. A.1.16. RESULTS OF THE GLOBAL SENSITIVITY ANALYSIS FOLLOWING THE BACOO METHOD TO INDICATE THE INFLUENCE OF CRITICAL PARAMETERS ON (A) ENERGY INDICATOR; (B) ECONOMIC INDICATOR; (C) ENVIRONMENTAL INDICATOR;

AND (D) SOCIAL INDICATOR FOR MINIMUM COST SOLUTION OF 10 HOUSES COMMUNITY SIZE.

A.1.7. Conclusion

This paper presents an investigation for the sustainable potential of solar assisted district heating system (SDHS) for retrofitted residential communities with different sizes located in Emmen, Netherlands, to achieve Nearly Zero Energy Building (NZEB). The work tends to optimize the performance of SDHS under energy, economic, environmental, and social criteria to facilitate the stakeholders) in the transition from low-carbon buildings (LCBs) to positive energy buildings (PEBs). A machine learning algorithm linked to TRSNYS is developed to simulate the SDHS thermal performance in this context. A multi-objective optimization model is established to minimize the life cycle cost and environmental impact, maximizing green energy use and social benefits. This ensures the system performance and implementation of the smart energy metering system for connecting to the grid. To estimate the SDHS performance from the perspective of sizing, different community sizes (10, 25, 50, 100, 500) were considered under five scenarios representing the effect of cost and environmental damage. A multi-criteria decision-making approach based on TOPSIS (Technique for Order of Preference by Similarity to Ideal Solution) incorporating global sensitivity analysis (GSA) is proposed to help the stakeholders to see beyond the life cycle cost (LCC) and life cycle assessment (LCA) based on selection criteria to choose the most appropriate scenario optimal solution for the

desired community size and interpret the effect of various economic parameters on the sustainable performance of SDHS. The summary of the findings is the following:

- Compared to the existing base case (decentralized heat pump), the minimum cost-optimal SDHS solution for 10 houses community size increases by 5.5 %, which failed to improve economic potential. However, the environmental performance improved 3.5 times, with 38% more social benefits.
- As the community size increases, more cost-effective and environment-friendly SDHS systems are found. The most environment-friendly optimal SDHS solution for 500 community size is 50% more cost-effective: 450% more environment friendly and has 150% more social benefits compared to the 500 houses community size using the decentralized heat pump.
- The technical analysis of the optimal solution suggests that with the proposed SDHS system, it is possible to achieve a NZEB status for any community size with a solar fraction up to 95% at 500 houses. However, it is possible to achieve PEB status only for community size higher than 50 houses due to its economic feasibility supported by 25 years of a payback period.
- Economic analysis of the optimal solutions suggests that seasonal storage tank has the biggest impact on the project cost of the SDHS model. In contrast, the environmental analysis shows that PV solar collectors constitute for the greatest part of the environmental impact caused by any optimal SDHS solution.

- Global sensitivity analysis suggests that cumulatively a change in natural gas prices has the highest effect on the SDHS model's economic, environmental, and social performances.
- The adopted methodology has also resulted in providing a guideline for the SDHS system sizing with the optimal size range of SDHS system components.

This work concludes that SDHS provides an attractive renewable energy sources option for cost-effective transitioning to NZEB for medium to long term residential projects. Although the initial investment cost is high, SDHS is comparatively cost-effective in terms of the net present cost. Moreover, our proposed SDHS framework is in line with the 4th generation district heating, which allows for the transition of existing buildings from LCBs to PEBs.

Acknowledgements

The work is funded by the Spanish government RTI2018-093849-B-C33 (MCIU/AEI/FEDER, UE). This work is supported by the Ministerio de Ciencia, Innovación y Universidades – Agencia Estatal de Investigación (AEI) (RED2018-102431-T). This project has received funding from the European Union's Horizon 2020 research and innovation programme under the Marie Skłodowska-Curie grant agreement No. 713679 and from the Universitat Rovira i Virgili (URV). In addition, this work was part of the Dutch project TKI Optimaal and co-funded by TKI Urban

Energy from the Surcharge for Top Consortia for Knowledge and Innovation (TKIs) of the Ministry of Economic Affairs of the Netherlands.

A.1.8 Nomenclature

$Cap_{heating}$	Energy supplied by heat pump (MW)
C_{el}	Buying the grid electricity price (€/MWh)
C_{ng}	Natural gas price (€/MWh)
d	Discount rate (%)
DAM_d	Endpoint score for environmental damage category (-)
EC_{RE}	Electricity generated by PV array (MWh)
EG_S	Electricity purchased from the grid (MWh)
EO	Employment opportunity (-)
IC	Capital cost of the SDHS (€)
i_{ng}	Natural gas inflation rate (%)
i_e	Electricity inflation rate (%)
i	Inflation rate (%)
LCC	Life cycle cost (€)
NPC	Net present cost (€/m^2)
OC	Operational cost of SDHS (€)
PBT	Payback time (years)

Q_{AUX}	Total thermal energy demand supplied by auxiliary units (MWh)
$\dot{Q}_{AUX_1}$	Thermal power supplied by auxiliary heater 1 (MW)
$\dot{Q}_{AUX_2}$	Thermal power supplied by auxiliary heater 2 (MW)
$Q_{DHW\ load}$	Total thermal energy demand for hot water (MWh)
$Q_{electric\ load}$	Total electricity demand (MWh)
$Q_{SH\ load}$	Total thermal energy demand for space heating (MWh)
Q_{total}	Total energy consumption (MWh)
R_{fuel}	The ratio of total energy supplied by fossil fuels (-)
RC	The replacement cost of SDHS (€)
RC_{roof}	Thermal resistance of the roof (m^2·K/W)
RC_{floor}	Thermal resistance of the floor(m^2·K/W)
RC_{facade}	Thermal resistance of the façade (m^2·K/W)
RCP	Normalized indicator metric for environmental damage (Pt./ m^2)
REF_{elec}	Renewable energy fraction for electrical energy (-)
REF_{th}	Renewable energy fraction for thermal energy (-)
R_{HP}	The ratio of total energy supplied by the heat pump (-)
S_{el}	Selling to the grid electricity price (€/MWh)

Abbreviations

ANN	Artificial neural network
DH	District Heating
DHWT	Domestic hot water tank
EPBP	Energy performance building parameter
EPI	Energy performance indicator
4GDH	4th generation district heating
GHG	Greenhouse gas emissions
GSA	Global sensitivity analysis
HP	Heat pump
LCB	Low carbon buildings
LCIA	Life Cycle Inventory Analysis
MCDM	Multi-criteria decision making
NZEB	Nearly-zero energy building
PEB	Positive energy building
PV	Photovoltaic
SDHS	Solar assisted district heating system
SH	Space heating
SST	Seasonal storage tank

A.1.9 References

A Multiobjective Simplex Method, 2005. , in: Multicriteria Optimization. Springer-Verlag, pp. 171–196. https://doi.org/10.1007/3-540-27659-9_7

Abokersh, Mohamed Hany, Kangkana Saikia, Luisa F cabeza, Dieter Boer, M.V., 2020. Flexible heat pump integration to improve sustainable transition toward 4th generation district heating. Energy Convers. Manag.

Abokersh, M., Vallès, M., F. Cabeza, L., Boer, D., 2020. A Multicriteria Approach to Evaluate Solar Assisted District Heating in the German Market, in: 14th International Conference on Energy Sustainability. ASME. https://doi.org/10.1115/ES2020-1668

Abokersh, Mohamed Hany, Vallès, M., Cabeza, L.F., Boer, D., 2020. A framework for the optimal integration of solar assisted district heating in different urban sized communities: A robust machine learning approach incorporating global sensitivity analysis. Appl. Energy 267, 114903. https://doi.org/10.1016/j.apenergy.2020.114903

Abokersh, M.H., Vallès, M., Jiménez, L., Boer, D., 2020. Cost-Effective Processes of Solar District Heating System Based on Optimal Artificial Neural Network, Computer Aided Chemical Engineering. https://doi.org/10.1016/B978-0-12-823377-1.50068-9

Al Dakheel, J., Del Pero, C., Aste, N., Leonforte, F., 2020. Smart buildings features and key performance indicators: A review. Sustain. Cities Soc. https://doi.org/10.1016/j.scs.2020.102328

Alajmi, A., Wright, J., 2014. Selecting the most efficient genetic algorithm sets in solving unconstrained building optimization problem. Int. J. Sustain. Built Environ. 3, 18–26. https://doi.org/10.1016/j.ijsbe.2014.07.003

Ayoub, M., 2020. A review on machine learning algorithms to predict daylighting inside buildings. Sol. Energy 202, 249–275. https://doi.org/10.1016/j.solener.2020.03.104

Barone, G., Buonomano, A., Forzano, C., Giuzio, G.F., Palombo, A., 2020. Passive and active performance assessment of building integrated hybrid solar photovoltaic/thermal collector prototypes: Energy, comfort, and economic analyses. Energy 209, 118435. https://doi.org/10.1016/j.energy.2020.118435

Bauer, D., Marx, R., Nußbicker-Lux, J., Ochs, F., Heidemann, W., Müller-Steinhagen, H., 2010. German central solar heating plants with seasonal heat storage. Sol. Energy 84, 612–623. https://doi.org/10.1016/j.solener.2009.05.013

Behzadi, A., Arabkoohsar, A., 2020. Feasibility study of a smart building energy system comprising solar PV/T panels and a heat storage unit. Energy 210, 118528. https://doi.org/10.1016/j.energy.2020.118528

Behzadi, A., Arabkoohsar, A., Yang, Y., 2020. Optimization and dynamic techno-economic analysis of a novel PVT-based smart building energy system. Appl. Therm. Eng. 181, 115926. https://doi.org/10.1016/j.applthermaleng.2020.115926

Bengio, Y., Lodi, A., Prouvost, A., 2020. Machine learning for combinatorial optimization: A methodological tour d'horizon. Eur. J. Oper. Res. https://doi.org/10.1016/j.ejor.2020.07.063

Bhowmik, C., Gangwar, S., Bhowmik, S., Ray, A., 2018. Selection of energy-efficient material: An entropy–TOPSIS approach, Advances in Intelligent Systems and Computing. https://doi.org/10.1007/978-981-10-5699-4_4

Cameron, L., Van Der Zwaan, B., 2015. Employment factors for wind and solar energy technologies: A literature review. Renew. Sustain. Energy Rev. https://doi.org/10.1016/j.rser.2015.01.001

Campos-Guzmán, V., García-Cáscales, M.S., Espinosa, N., Urbina, A., 2019. Life Cycle Analysis with Multi-Criteria Decision Making: A review of approaches for the sustainability evaluation of renewable energy technologies. Renew. Sustain. Energy Rev. https://doi.org/10.1016/j.rser.2019.01.031

Cao, X., Dai, X., Liu, J., 2016. Building energy-consumption status worldwide and the state-of-the-art technologies for zero-energy buildings during the past decade. Energy Build. 128, 198–213. https://doi.org/10.1016/j.enbuild.2016.06.089

Chang, Y., Wei, Y., 2021. The utilization of renewable energy for low-carbon buildings, in: Renewable-Energy-Driven Future. Elsevier, pp. 289–309. https://doi.org/10.1016/B978-0-12-820539-6.00009-1

Chen, Y., Wang, J., Lund, P.D., 2020. Sustainability evaluation and sensitivity analysis of district heating systems coupled to geothermal and solar resources. Energy Convers. Manag. 220, 113084. https://doi.org/10.1016/j.enconman.2020.113084

Commission, E., 2020. 2 Energy efficiency state of non-profit housing stock in the Netherlands 61–82.

Dawood, S., Crosbie, T., Dawood, N., Lord, R., 2013. Designing low carbon buildings: A framework to reduce energy consumption and embed the use of renewables. Sustain. Cities Soc. 8, 63–71. https://doi.org/10.1016/j.scs.2013.01.005

Ely Lecture, R.T., Nicholas Stern, B., Anderson, D., Bowen, A., Catovsky, S., Diamond, P., Dietz, S., Edenhofer, O., Fankhauser, S., Floater, G., Garbett, S.-L., Garnaut, R., Guesnerie, R., Heal, G., Hawellek, D., Henry, C., Hepburn, C., Joskow, P., Landau, J.-P., Mirrlees, J., Moniz, E., Pacala, S., Patmore, N., Pope, V., Ralston, L., Romani, M., Schellnhuber, J., Skellern, M., Socolow, R., Weitzman, M., 2008. The Economics of Climate Change, American Economic Review: Papers & Proceedings.

Fathi, Soheil, Srinivasan, R., Fenner, A., Fathi, Sahand, 2020. Machine learning applications in urban building energy performance forecasting: A systematic review. Renew. Sustain. Energy Rev. https://doi.org/10.1016/j.rser.2020.110287

Ghosh, A., 2020. Potential of building integrated and attached/applied photovoltaic (BIPV/BAPV) for adaptive less energy-hungry building's skin: A comprehensive Review. J. Clean. Prod. 276, 123343. https://doi.org/10.1016/j.jclepro.2020.123343

Gondal, I.A., 2020. Prospects of Shallow geothermal systems in HVAC for NZEB.

Energy Built Environ. https://doi.org/10.1016/j.enbenv.2020.09.007

Gonzalo Guillén-Gosálbez, José Antonio Caballero, and L.J., 2007. Application of life cycle assessment to the structural optimization of process flowsheets. Comput. Aided Chem. Eng. 24, 1163–1168. https://doi.org/10.1016/S1570-7946(07)80218-5

Grillone, B., Danov, S., Sumper, A., Cipriano, J., Mor, G., 2020. A review of deterministic and data-driven methods to quantify energy efficiency savings and to predict retrofitting scenarios in buildings. Renew. Sustain. Energy Rev. https://doi.org/10.1016/j.rser.2020.110027

Gursel, A.P., Ostertag, C., 2017. Comparative life-cycle impact assessment of concrete manufacturing in Singapore. Int. J. Life Cycle Assess. 22, 237–255. https://doi.org/10.1007/s11367-016-1149-y

Hadorn, J., 1990. Guide to Seasonal Heat Storage. SIA, Swiss Association of Engineers and Architects. Zurich.

Hamburg, A., Kuusk, K., Mikola, A., Kalamees, T., 2020. Realisation of energy performance targets of an old apartment building renovated to nZEB. Energy 194, 116874. https://doi.org/10.1016/j.energy.2019.116874

Han, H., Zhang, Z., Cui, X., Meng, Q., 2020. Ensemble learning with member optimization for fault diagnosis of a building energy system. Energy Build. 226, 110351. https://doi.org/10.1016/j.enbuild.2020.110351

Hany, M., Spiekman, M., Vijlbrief, O., Goch, T.A.J. Van, Vall, M., Boer, D., 2021.

A real-time diagnostic tool for evaluating the thermal performance of nearly zero energy buildings 281. https://doi.org/10.1016/j.apenergy.2020.116091

Hong, T., Lee, M., Koo, C., Jeong, K., Kim, J., 2017. Development of a method for estimating the rooftop solar photovoltaic (PV) potential by analyzing the available rooftop area using Hillshade analysis. Appl. Energy 194, 320–332. https://doi.org/10.1016/j.apenergy.2016.07.001

Hong, T., Wang, Z., Luo, X., Zhang, W., 2020. State-of-the-art on research and applications of machine learning in the building life cycle. Energy Build. https://doi.org/10.1016/j.enbuild.2020.109831

Huijbregts, M.A.J., Steinmann, Z.J.N., Elshout, P.M.F., Stam, G., Verones, F., Vieira, M., Zijp, M., Hollander, A., van Zelm, R., 2017. ReCiPe2016: a harmonised life cycle impact assessment method at midpoint and endpoint level. Int. J. Life Cycle Assess. 22, 138–147. https://doi.org/10.1007/s11367-016-1246-y

Hwang, C.-L., Yoon, K., 1981. Methods for Multiple Attribute Decision Making. pp. 58–191. https://doi.org/10.1007/978-3-642-48318-9_3

Jeong, J., Hong, T., Kim, J., Chae, M., Ji, C., 2018. Multi-criteria analysis of a self-consumption strategy for building sectors focused on ground source heat pump systems. J. Clean. Prod. 186, 68–80. https://doi.org/10.1016/j.jclepro.2018.03.121

Klein, S.A. et al., 2004. TRNSYS Version. 18, Solar Energy Laboratory, University

of Wisconsin-Madison, Website: <http://sel.me.wisc.edu/ trnsys>.

Kuhn, T.E., Erban, C., Heinrich, M., Eisenlohr, J., Ensslen, F., Neuhaus, D.H., 2020. Review of Technological Design Options for Building Integrated Photovoltaics (BIPV). Energy Build. 110381. https://doi.org/10.1016/j.enbuild.2020.110381

Laguna Salvad, L., Villeneuve, E., Masson, D., 2019. Decision making in near zero energy building refurbishment: A technology alternatives ranking tool. IFAC-PapersOnLine 52, 313–318. https://doi.org/10.1016/j.ifacol.2019.11.196

Lai, X., Liu, J., Shi, Q., Georgiev, G., Wu, G., 2017. Driving forces for low carbon technology innovation in the building industry: A critical review. Renew. Sustain. Energy Rev. https://doi.org/10.1016/j.rser.2017.02.044

Li, G., Xuan, Q., Akram, M.W., Golizadeh Akhlaghi, Y., Liu, H., Shittu, S., 2020. Building integrated solar concentrating systems: A review. Appl. Energy. https://doi.org/10.1016/j.apenergy.2019.114288

Li, H., Nord, N., 2018. Transition to the 4th generation district heating - Possibilities, bottlenecks, and challenges, in: Energy Procedia. https://doi.org/10.1016/j.egypro.2018.08.213

Li, H., Wang, S., 2019. Coordinated optimal design of zero/low energy buildings and their energy systems based on multi-stage design optimization. Energy 189, 116202. https://doi.org/10.1016/j.energy.2019.116202

Lior, N., 2017. Sustainability as the quantitative norm for water desalination

impacts. https://doi.org/10.1016/j.desal.2016.08.008

Lund, H., Duic, N., Østergaard, P.A., Mathiesen, B.V., 2018. Future district heating systems and technologies: On the role of smart energy systems and 4th generation district heating. Energy 165, 614–619. https://doi.org/10.1016/j.energy.2018.09.115

Luo, T., Tan, Y., Langston, C., Xue, X., 2019. Mapping the knowledge roadmap of low carbon building: A scientometric analysis. Energy Build. https://doi.org/10.1016/j.enbuild.2019.03.050

Magrini, A., Lentini, G., Cuman, S., Bodrato, A., Marenco, L., 2020. From nearly zero energy buildings (NZEB) to positive energy buildings (PEB): The next challenge - The most recent European trends with some notes on the energy analysis of a forerunner PEB example. Dev. Built Environ. 3, 100019. https://doi.org/10.1016/j.dibe.2020.100019

Majcen, D., Itard, L.C.M., Visscher, H., 2013. Theoretical vs. actual energy consumption of labelled dwellings in the Netherlands: Discrepancies and policy implications. Energy Policy 54, 125–136. https://doi.org/10.1016/j.enpol.2012.11.008

Marszal, A.J., Heiselberg, P., Lund Jensen, R., Nørgaard, J., 2012. On-site or off-site renewable energy supply options? Life cycle cost analysis of a Net Zero Energy Building in Denmark. Renew. Energy 44, 154–165. https://doi.org/10.1016/j.renene.2012.01.079

Mavromatidis, G., Orehounig, K., Carmeliet, J., 2018. Uncertainty and global sensitivity analysis for the optimal design of distributed energy systems. Appl. Energy 214, 219–238. https://doi.org/10.1016/j.apenergy.2018.01.062

MH Abokersh, M Vallès, LF Cabeza, D.B., 2020. Challenges Associated With The Construction And Operation Of Seasonal Storage For A Small Solar District Heating System: A Multi-Objective Optimization Approach, in: 14th International Renewable Energy Storage Conference 2020 (IRES 2020). IRES 2020, pp. 150–160. https://doi.org/10.2991/ahe.k.210202.023

Mishra, M., 2020. Machine learning techniques for structural health monitoring of heritage buildings: A state-of-the-art review and case studies. J. Cult. Herit. https://doi.org/10.1016/j.culher.2020.09.005

Mokhtara, C., Negrou, B., Settou, N., Gouareh, A., Settou, B., 2019. Pathways to plus-energy buildings in Algeria: Design optimization method based on GIS and multi-criteria decision-making, in: Energy Procedia. Elsevier Ltd, pp. 171–180. https://doi.org/10.1016/j.egypro.2019.04.019

Nearly Zero Energy Building Standard | Business & Public Sector | SEAI [WWW Document], n.d. URL https://www.seai.ie/business-and-public-sector/standards/nearly-zero-energy-building-standard/ (accessed 10.8.20).

Nö, K., Niedenfü Hr, S., Beyß Id, M., Wiechert Id, W., 2018. A Pareto approach to resolve the conflict between information gain and experimental costs: Multiple-criteria design of carbon labeling experiments. https://doi.org/10.1371/journal.pcbi.1006533

Pinamonti, M., Baggio, P., 2020. Energy and economic optimization of solar-assisted heat pump systems with storage technologies for heating and cooling in residential buildings. Renew. Energy 157, 90–99. https://doi.org/10.1016/j.renene.2020.04.121

Qin, X., Wang, H., Li, Yu'e, Li, Yong, McConkey, B., Lemke, R., Li, C., Brandt, K., Gao, Q., Wan, Y., Liu, S., Liu, Y., Xu, C., 2013. A long-term sensitivity analysis of the denitrification and decomposition model. Environ. Model. Softw. 43, 26–36. https://doi.org/10.1016/j.envsoft.2013.01.005

Rehman, H. ur, Hirvonen, J., Sirén, K., 2018. Performance comparison between optimized design of a centralized and semi-decentralized community size solar district heating system. Appl. Energy 229, 1072–1094. https://doi.org/10.1016/j.apenergy.2018.08.064

Rehman, H. ur, Korvola, T., Abdurafikov, R., Laakko, T., Hasan, A., Reda, F., 2020. Data analysis of a monitored building using machine learning and optimization of integrated photovoltaic panel, battery and electric vehicles in a Central European climatic condition. Energy Convers. Manag. 221, 113206. https://doi.org/10.1016/j.enconman.2020.113206

Saltelli, A., Annoni, P., 2010. How to avoid a perfunctory sensitivity analysis. Environ. Model. Softw. 25, 1508–1517. https://doi.org/10.1016/j.envsoft.2010.04.012

Sari, F., 2021. Forest fire susceptibility mapping via multi-criteria decision analysis techniques for Mugla, Turkey: A comparative analysis of VIKOR and

TOPSIS. For. Ecol. Manage. 480, 118644. https://doi.org/10.1016/j.foreco.2020.118644

Seyedzadeh, S., Pour Rahimian, F., Oliver, S., Rodriguez, S., Glesk, I., 2020. Machine learning modelling for predicting non-domestic buildings energy performance: A model to support deep energy retrofit decision-making. Appl. Energy 279, 115908. https://doi.org/10.1016/j.apenergy.2020.115908

Song, J., Oh, S.D., Song, S.J., 2019. Effect of increased building-integrated renewable energy on building energy portfolio and energy flows in an urban district of Korea. Energy 189, 116132. https://doi.org/10.1016/j.energy.2019.116132

Sun, H., Burton, H. V., Huang, H., 2020. Machine Learning Applications for Building Structural Design and Performance Assessment: State-of-the-Art Review. J. Build. Eng. 33, 101816. https://doi.org/10.1016/j.jobe.2020.101816

Sun, Y., Huang, P., Huang, G., 2015. A multi-criteria system design optimization for net zero energy buildings under uncertainties. Energy Build. 97, 196–204. https://doi.org/10.1016/j.enbuild.2015.04.008

Susan, S., Wardhani, D., 2020. Building integrated photovoltaic as GREENSHIP'S on site renewable energy tool. Results Eng. 7, 100153. https://doi.org/10.1016/j.rineng.2020.100153

Tulus, V., Abokersh, M.H., Cabeza, L.F., Vallès, M., Jiménez, L., Boer, D., 2019. Economic and environmental potential for solar assisted central heating plants

in the EU residential sector: Contribution to the 2030 climate and energy EU agenda. Appl. Energy 318–339. https://doi.org/10.1016/j.apenergy.2018.11.094

Tulus, V., Boer, D., Cabeza, L.F., Jiménez, L., Guillén-Gosálbez, G., n.d. Enhanced thermal energy supply via central solar heating plants with seasonal storage: A multi-objective optimization approach. https://doi.org/10.1016/j.apenergy.2016.08.037

You, C., Kim, J., 2020. Optimal design and global sensitivity analysis of a 100% renewable energy sources based smart energy network for electrified and hydrogen cities. Energy Convers. Manag. 223, 113252. https://doi.org/10.1016/j.enconman.2020.113252

Zhang, Y., Zhang, X., Huang, P., Sun, Y., 2020. Global sensitivity analysis for key parameters identification of net-zero energy buildings for grid interaction optimization. Appl. Energy 279, 115820. https://doi.org/10.1016/j.apenergy.2020.115820

Zhou, Y., Zheng, S., Liu, Z., Wen, T., Ding, Z., Yan, J., Zhang, G., 2020. Passive and active phase change materials integrated building energy systems with advanced machine-learning based climate-adaptive designs, intelligent operations, uncertainty-based analysis and optimisations: A state-of-the-art review. Renew. Sustain. Energy Rev. https://doi.org/10.1016/j.rser.2020.109889

Annex 2. Economic analysis

A.2.1. The components of the of net present cost

The overall initial cost of investment consists of several items such as the cost of the equipment purchase, installation, and transportation, including the cost of any contingencies and it can be expressed as follows (Turton, 2008; Tulus et al., 2016):

$$IC = (1 + \alpha_{CF}) \sum (PEC_k . FBM_k) \qquad \forall k \qquad \text{(A.2.1)}$$

where PEC_k represents the purchase cost of equipment unit k, while the bare module factor FBM_k is responsible for the installation and transportation expense of unit k. α_{CF} denotes the contingency factor. The cost component PEC_k can be updated from the initial value in the base year A to the year of installation B based on the Chemical Engineering Plant Cost Index (CEPCI, 2023) using the following equation:

$$PEC_k = {PEC_k}^{year\ A} \frac{{CEPCI}^{year\ B}}{{CEPCI}^{year\ A}} \qquad \forall k \qquad \text{(A.2.2)}$$

The initial cost of purchasing unit k in year A (PEC^{yearA}) can be estimated for various equipment units using Eqs. (A.2.3) to (A.2.7).

$${PEC_k}^{year\ A} = \alpha_k \left({CAP_k}^{\beta_k}\right) \qquad \forall k = COL, PV, DHW, AUX \qquad \text{(A.2.3)}$$

$${PEC_k}^{year\ A} = \alpha_k \left({CAP_k}^{\beta_k}\right) CAP_k \qquad \forall k = HP \qquad \text{(A.2.4)}$$

$${PEC_k}^{year\ A} = {CAP_k}^{\beta_k} . 10^{[\alpha_k (log_{10} CAP_k)^{\beta_k}]} \qquad \forall k = HE_1, HE_2, HE_3 \qquad \text{(A.2.5)}$$

$$PEC_k{}^{year\ A} = \alpha_k \ln\left(\frac{CAP_k}{1000}\right) + \beta_k \qquad \forall k = P_1, P_2, P_3, P_4 \qquad \text{(A.2.6)}$$

$$PEC_k{}^{year\ A} = INS_{SST} + CON_{SST} \qquad \forall k = SST \qquad \text{(A.2.7)}$$

$$\text{Where, } INS_{SST} = \alpha_k\left(CAP_k{}^{\beta_k}\right) \qquad \forall k = XPS, MW, FG \qquad \text{(A.2.7.1)}$$

$$CON_{SST} = \alpha_k\left(CAP_k{}^{\beta_k}\right) \qquad \forall k = NC, HPC \qquad \text{(A.2.7.2)}$$

$$CON_{SST} = \alpha_k e^{\left(\frac{\beta_k}{10^5} CAP_k\right)} \qquad \forall k = UHPC \qquad \text{(A.2.7.3)}$$

Here α_k and β_k are the equipment cost parameters, CAP_k is responsible for the design variables of equipment unit k. The design variables are the area of the solar collector (A_{COL}), the volume of the fully stratified storage tanks ($VSST$, $VDHWT$), types of insulation materials used for the SST (XPS, MW, FG) which includes extruded polystyrene, mineral wool, and foam glass gravel, respectively, types of the SST construction material (NC, HPC, $UHPC$) comprising of normal concrete, high-performance concrete, and ultra-high performance concrete, respectively, area of heat transfer for the heat exchangers (A_{HE1}, A_{HE2}, A_{HE3}), and the mass flow rates of discharge for the pumps ($\dot{m}_1$, $\dot{m}_2$, $\dot{m}_3$, $\dot{m}_4$).The total operating cost (O_c) is the discounted summation of all annual operating costs and can be expressed as follows:

$$O_C = C_M PWF_M + C_P PWF_P + C_{AUX} PWF_{AUX} \qquad \text{(A.2.8)}$$

where the C_M indicate the annual maintenance, C_P is the electricity cost due to the recirculation pumps, and heat pump. While C_{AUX} is the energy cost of the auxiliary heaters (natural gas boilers). The term PWF reflects the present worth factor which is calculated for the specific cost of operation considering the inflation rate (i) and

the rate of interest (r) over the lifetime of the proposed system. The cost of replacing several equipment units of the proposed SDHS can be estimated as shown below:

$$RC = PVF_n \sum_k (PEC_k . FBM_k) \quad \text{(A.2.9)}$$

Here PVF_n is the present value factor of the future cash flows in the year n. The equipment which will incur a replacement cost in our study due to a high rate of depreciation over the system's lifespan are the solar collectors, storage tank used for DHW, heat pump, heat exchangers, and auxiliary heaters.

A.2.2 Eco-environmental input parameters

The initial cost parameters are outlined in Table A.2.1. On the other hand, the annual maintenance costs are estimated to be 1.5% of its investment cost. Based on the EUROSTAT database ("Database - Eurostat," n.d.), the natural gas for household prices is 0.0444, whereas the electricity buying price is 0.1359 Euro/kWh and selling price is 0.11 Euro/kWh. In addition, an inflation rate of 5.9% and 5% is selected for the natural gas and electricity, respectively. An inflation rate of 2.3% is selected for the proposed system, whereas the discount rate is 3.5%. On the other hand, the LCA input parameters are extracted from the Ecoinvent database ("ecoinvent Database - ecoinvent," n.d.). This database categorizes the damage associated with the SDHS equipment based on the Recipe 2016approach, a summary of the impact of different components in the SDHS is shown in Table A.2.2.

Table A.2.1: The economic parameters for the initial cost of the heat pump integrated into SDHS

Unit	Options	α_k	β_k	CAP_k	Base year	Ref.	FBM_k
Solar collector		974.2	0.833	Aperture area (m^2)	2007	[3]	1
Photovoltaic panels		300	1	Aperture area (m^2)	2016		1
Heat pump		2053.8	-0.348	Thermal power (kW)	2014	[4]	1
DHWT		3955	0.65	Volume (m^3)	2007	[5]	1
Auxiliary heater		225	0.746	Duty (kW)	2001	[1]	2.1
Heat exchanger		3.133	0.331	Exchange area (m^2)	2001	[1]	3.29
Pump (P1, P2)		389	283.2	Mass flow rate (kg/h)	2009	[6]	3.24
Pump (P3, P4)		389	717	Mass flow rate (kg/h)	2009	[6]	3.24
SST insulation	XPS	561.09	0.397	Material thickness (m)	2017	[7]	1
	MW	1902.7	0.942	Material thickness (m)	2018	[8]	1
	FG	311.41	0.968	Material thickness (m)	2014	[9]	1
SST construction	NC	4178.1	-0.394	Volume (m^3)	2000		1
	HPC	2575	-0.363	Volume (m^3)	2004	[10]	1
	$UHPC$	90.83	-3	Volume (m^3)	2004		1

Table A.2.2: The environmental impact of heat pump integrated SDHS equipment based on ReCiPe 2016

Unit	Option	Impact factor (ReCiPe 2016)
Solar collector		32.5 Pt/m^2
Photovoltaic panels		26.3 Pt/m^2
Heat pump		22.3 Pt/kW
DHWT		173.1 Pt/m^3
Auxiliary boiler		1.57·103 Pt/kW
Heat exchanger		2.515 Pt/m^2
Pump		62.8 Pt/kW
SST insulation	XPS	0.773 Pt/kg
	MW	0.0016 Pt/kg
	FG	0.266 Pt/kg
SST construction	NC	0.008 Pt/kg
	HPC	0.002 Pt/kg
	$UHPC$	0.0206 Pt/kg
Natural gas		0.0245 Pt/kWh
Electricity		0.0380 Pt/kWh

A.2.3 Nomenclature

CAP_k	design variable of equipment unit k
$CEPCI_{year\ A}$	chemical engineering plant cost index in the base year
$CEPCI_{year\ B}$	chemical engineering plant cost index in the installation year
Con_{SST}	purchase cost of the construction material of the seasonal storage tank (€)

I_C	Initial investment cost (€)
C_{AUX}	energy cost of the auxiliary heater (€)
C_M	annual cost of equipment unit k(€)
O_C	Operational and maintainance cost (€)
C_P	annual operational cost of pump and heat pump (€)
RC	replacement cost (€)
FBM_k	bare module factor of equipment unit k
i	annual inflation rate (%)
Ins_{SST}	purchase cost of the seasonal storage tank insulation material (€)
PEC_k	purchase cost of equipment unit k(€)
PWF_n	present worth factor of periodic future cash flows (-)
PVF_n	present value factor of single future cash flow at the beginning of nth time period (-)
r	interest rate (%)
$VDHWT$	Volume of domestic storage tank (m^3/MWh·a)
$VSST$	Volume of seasonal storage tank (m^3/MWh·a)

Greek symbols

α_{CF}	factor of contingency charges and fees
α_k	purchase cost coefficient of equipment unit k

β_k	purchase cost exponent of equipment unit k

Abbreviations

AUX	Auxiliary heater (fuelled by natural gas)
COL	solar collector field
DHW	Domestic Hot Water
DHWT	Domestic Hot Water Tank
FG	Foam Glass gravel
HE	Heat Exchanger
HP	Heat Pump
HPC	High-Performance Concrete
MW	Mineral Wool
NC	Normal Concrete
P	Centrifugal pump
SST	Seasonal Storage Tank
UHPC	Ultra-High-Performance Concrete
XPS	Extruded Polystyrene

Indices

k	equipment unit

A.2.5 References

Database - Eurostat [WWW Document], n.d. URL https://ec.europa.eu/eurostat/data/database (accessed 5.5.23).

ecoinvent Database - ecoinvent [WWW Document], n.d. URL https://ecoinvent.org/the-ecoinvent-database/ (accessed 5.5.23).

Tulus, V., Boer, D., Cabeza, L.F., Jiménez, L., Guillén-Gosálbez, G., 2016. Enhanced thermal energy supply via central solar heating plants with seasonal storage: A multi-objective optimization approach. Appl. Energy 181, 549–561. https://doi.org/10.1016/j.apenergy.2016.08.037

Turton R, Bailie RC, Whiting WB, Shaeiwitz JA, Bhattacharyya D. Analysis, synthesis, and design of chemical processes. 3rd ed. Prentice Hall; 2008.

Chemical Engineering Plant Cost Index (CEPCI): Economic Indicator. ChemEng J; 2023. <http://www.chemengonline.com/pci-home> (accessed 5.5.2023].

Annex 3. Supplementary data

Table A.3.1. Summary of economic variables considered under 100 scenarios.

Scenarios	Profit (€)	ECOST (€)	LAR disc (€)	E liq (€)
1	480,047	220,556	12,789	169,412
2	478,941	222,682	12,789	170,519
3	482,080	222,682	12,790	167,379
4	509,922	221,932	12,790	139,537
5	508,466	223,074	12,790	140,994
6	495,292	222,031	12,790	154,168
7	490,453	222,772	12,790	159,006
8	477,039	222,117	12,790	172,421
9	465,359	222,389	12,790	184,101
10	463,713	222,759	12,790	185,747
11	484,500	222,738	24,204	176,374
12	484,500	221,891	24,204	176,374
13	486,428	221,439	24,204	174,446
14	500,262	212,152	12,790	149,198

15	500,262	222,110	12,790	149,198
16	488,141	210,661	12,790	161,319
17	496,819	222,744	12,790	152,641
18	497,541	222,507	12,790	151,919
19	497,541	211,643	12,790	151,919
20	497,727	221,111	12,790	151,733
21	497,727	223,280	12,790	151,733
22	494,229	221,809	12,790	155,231
23	486,864	222,863	12,790	162,596
24	483,451	225,461	12,790	166,009
25	491,419	211,164	12,790	158,040
26	473,657	223,072	12,790	175,803
27	478,917	221,871	12,790	170,543
28	476,337	222,415	12,790	173,123
29	459,886	212,731	12,790	189,574
30	470,088	222,517	12,790	179,372
31	480,272	212,571	12,790	169,188

32	477,393	220,953	12,790	172,067
33	489,557	222,767	12,790	159,903
34	480,272	222,960	12,790	169,188
35	480,549	222,313	12,790	168,911
36	476,349	222,317	12,790	173,111
37	491,160	222,171	12,790	158,300
38	477,176	211,356	12,790	172,284
39	488,769	222,733	12,790	160,691
40	475,778	221,856	12,790	173,682
41	474,173	221,990	12,790	175,287
42	488,402	221,802	12,790	161,057
43	470,872	223,117	12,790	178,587
44	468,589	220,755	12,790	180,870
45	478,509	222,380	12,790	170,951
46	479,707	211,222	12,790	169,753
47	478,805	222,537	12,790	170,655
48	477,674	222,331	12,790	171,786

49	477,259	212,130	12,790	172,201
50	478,436	211,599	12,790	171,024
51	471,908	212,163	12,790	177,552
52	475,109	222,691	12,790	174,351
53	470,862	211,607	12,790	178,598
54	470,095	223,175	12,790	179,365
55	469,825	222,499	12,790	179,635
56	479,728	210,669	12,790	169,732
57	476,953	221,503	12,790	172,507
58	467,430	222,389	12,790	182,030
59	475,885	210,869	12,790	173,574
60	471,211	221,498	24,204	189,664
61	476,773	212,128	12,790	172,687
62	478,655	222,681	12,790	170,805
63	479,945	221,851	12,790	169,515
64	478,005	211,631	12,790	171,454
65	463,300	223,102	12,790	186,160

66	467,349	221,503	12,790	182,111
67	465,163	222,576	12,790	184,297
68	479,176	222,011	12,790	170,283
69	478,417	222,813	12,790	171,043
70	477,593	212,930	12,790	171,867
71	475,573	222,705	12,790	173,887
72	476,938	222,328	12,790	172,521
73	474,851	222,534	12,790	174,609
74	476,290	222,379	12,790	173,170
75	476,925	225,467	12,790	172,534
76	475,406	223,155	12,790	174,054
77	476,067	213,502	12,790	173,392
78	474,602	222,347	12,790	174,858
79	474,683	222,602	12,790	174,777
80	470,381	212,180	24,204	190,493
81	471,756	222,757	12,790	177,704
82	469,243	221,833	12,790	180,217

83	471,186	221,751	12,790	178,274
84	469,882	222,508	12,790	179,578
85	471,572	211,171	12,790	177,887
86	470,275	211,376	12,790	179,185
87	469,702	222,857	12,790	179,758
88	469,227	221,740	12,790	180,233
89	468,519	221,811	12,784	180,936
90	466,393	222,037	12,790	183,066
91	452,918	212,584	12,790	196,542
92	452,886	223,363	12,790	196,574
93	457,832	211,029	12,790	191,628
94	462,301	212,674	12,790	187,159
95	478,134	222,737	12,790	171,326
96	475,293	212,212	12,790	174,167
97	476,167	222,588	12,790	173,293
98	458,400	222,706	12,790	191,060
99	466,525	222,132	12,790	182,935

100	40,645	222,706	12,790	208,815

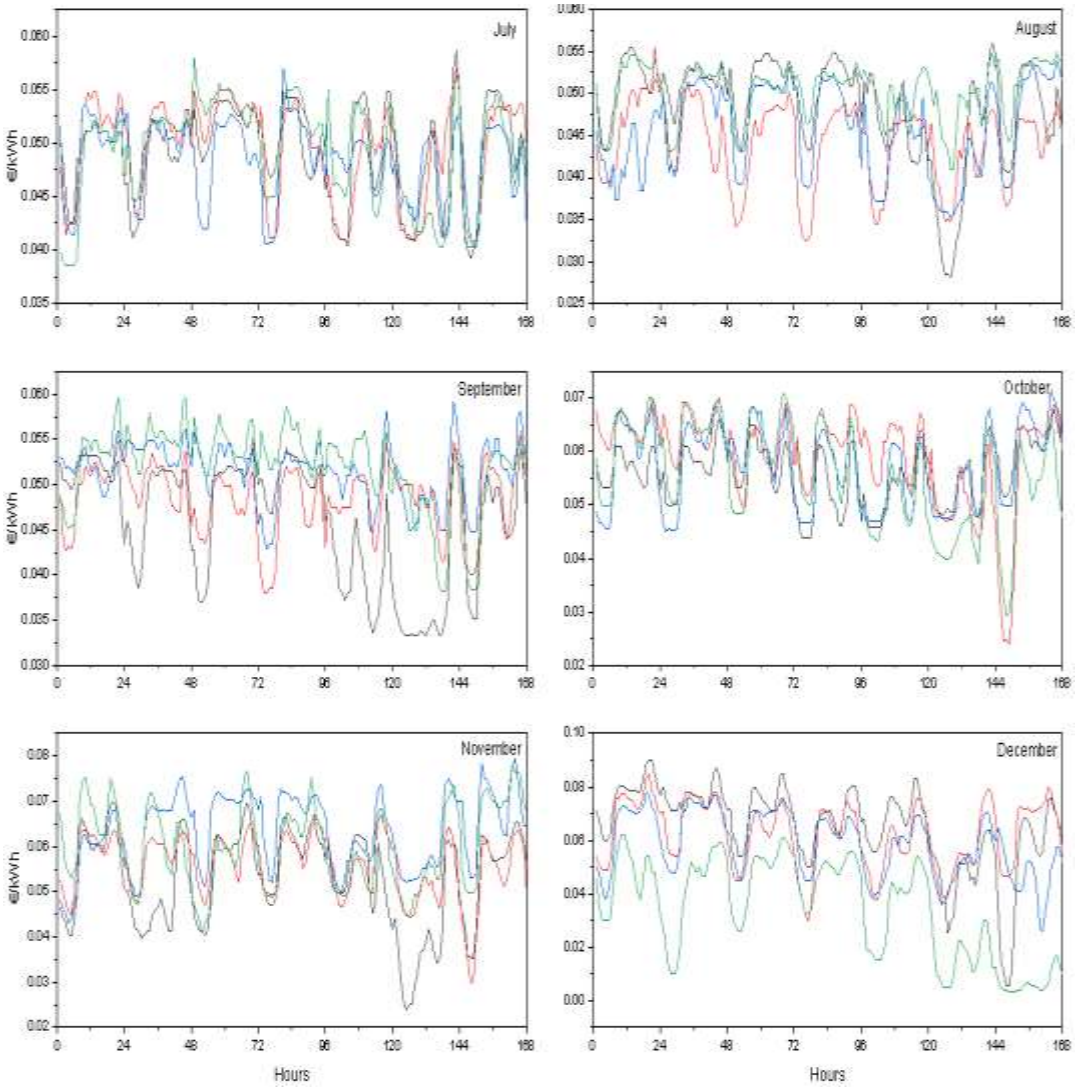

Figure A.3.1 Hourly electricity price data for weeks one to four from July to December (color scheme as in figure 2.3.4)

UNIVERSITAT
ROVIRA i VIRGILI